SIMULTANEOUS ANALYTE QUANTIFICATION IN LOW VOLUME SAMPLES USING A MICROFLUIDIC DEVICE

by

MEHDI GHODBANE

A dissertation submitted to the

Graduate School-New Brunswick

Rutgers, The State University of New Jersey

In partial fulfillment of the requirements

For the degree of

Doctor of Philosophy

Graduate Program in Biomedical Engineering

Written under the direction of

Martin L. Yarmush

And Approved by

_____

_____

_____

_____

_____

New Brunswick, New Jersey

January 2015

ABSTRACT OF THE DISSERTATION

SIMULTANEOUS ANALYTE QUANTIFICATION IN LOW VOLUME SAMPLES USING A MICROFLUIDIC DEVICE

By: MEHDI GHODBANE

Dissertation Director:

Martin L. Yarmush

Immunoassays are one of the most widely performed assays in clinical and research settings due to their sensitivity, specificity, and ability to measure wide ranges of analytes. Recently, immunoassay technology has greatly improved due to the development of multiplex platforms, capable of measuring multiple analytes in a single sample. However, immunoassays are costly, time-consuming, and require relatively large sample volumes that inhibit their use in specific applications. Performing immunoassays using microfluidic devices has been shown to significantly reduce assay time, cost, and sample and reagent consumption. However, previous immunoassay devices possess drawbacks that prevent their broad use, including: low sensitivity, limited dynamic range, inability to change the analyte specificity, specialized reagent requirements, inability to produce quantitative data, and low sample throughput. Therefore, the objective of this dissertation was to develop a microfluidic immunoassay device overcoming the aforementioned limitations.

A proof-of-concept device was developed capable of performing 8 parallel immunoassays on commercially available antibody conjugated microbeads. This eliminates the need for specialized reagents while allowing any analyte, for which antibodies are available, to be measured. Furthermore, we developed the first experimentally validated computational fluid dynamic model of antibody antigen binding in microchannels. Design of experiments (DOE) and multi-objective optimization techniques were used in conjunction with the model to optimize an IL-6 immunoassay with a sensitivity of 358 fM using only 1.35 μL of sample volume. The device design was then scaled-up to allow 32 samples to be processed simultaneously. With the expanded device, we demonstrated high-sensitivity, a large dynamic range, and quantification of 6 cytokines (Il-1b, Il-6, IL-10, IL-13, MCP-1, and TNF-a). Finally, we measured *in vitro* experimental supernatants in parallel using the microdevice and a conventional benchtop assay. The microdevice provided comparable results while reducing sample volume from 50 to 4.2 μL. In summary, we demonstrated a low-volume, highly sensitive assay with a large dynamic range capable of processing large numbers of samples using commercially available reagents. Due to these advantages, the technology in this work has far-reaching *in vitro, in vivo,* and clinical applications.

Dedication

To my family, my mother, father, brother and wonderful wife. Nothing I have ever accomplished, including this dissertation, would be possible if not for their everlasting love and support throughout my life.

Acknowledgements

I would like to take this opportunity to recognize everyone who made this dissertation possible. First, I would like to thank my thesis advisor, Dr. Martin L. Yarmush MD, PhD. None of the work in this dissertation would be possible if he did not accept me into his laboratory and provide the continued support and straightforward criticism necessary to push me to be a better scientist. Although he runs two labs at different institutions and manages a large number of students, post-doctoral researchers, and projects, his door has always been open. In addition, Dr. Rene Schloss has an integral part of my development. Her patience and continuous guidance not only helped me to succeed, but also provided me the confidence early in my graduate studies to allow the project to gain momentum. She has been involved in every aspect of this project and has always helped me focus on potential solutions in lieu of current problems. Dr. Tim Maguire has also been a vital part of this project. A person with endless positivity and energy, Dr. Maguire was able to keep me motivated through the most difficult periods in my doctoral studies. I am lucky to have been able to work in a laboratory with three individuals supporting my growth as a scientist.

I was also fortunate to have two excellent collaborators/committee members, without which this project could not have been possible. Dr. Rohit Ramachandran was a critical part of the computational platform and modeling studies contained in this thesis. Without his guidance and the help of his lab members, that work may have not been published. He has also been a pleasure to work with, as all of our interactions have been professional and incredibly

productive. Dr. Jeffrey Zahn is another collaborator who had a great deal of input into this project. His extensive, in-depth knowledge of microfluidics, terrific attention to detail, and willingness to delve into the technical aspects of the projects were crucial in my success. He has provided valuable guidance from the very start of this project, and was especially vital in preparing and critiquing the publications.

I would like to thank several previous students who provided guidance specific to this project. Dr. Larry Sasso provided me the basic training required to fabricate devices. Dr. Bhaskar Mitra shared with me his mastery of microfabrication, and most importantly taught me never to shy away from trying out new ideas. Dr. Jeffrey Barminko showed me how constant hard work is necessary in research to succeed, and was always available to discuss any ideas or issues I had. Dr. Nir Nativ trained me when I first joined the lab, and showed me how to be extremely critical and meticulous in my research.

Members of Dr. Zahn's lab, Jean Lo, Jack Zheng, Joe Fantuzzo, Nathalia, Garcia, Dr. Mercedes Morales, and Dr. Larry Sasso were a great resource in discussing fabrication and equipment issues. Dr. Kellie Anderson, Dr. Sara Salahi, Dana Barrasso, and Anwesha Chaudhury, were kind enough to share their expertise of computational modeling and optimization with me. Henry Yu, Anthony Kulesa, Alyssa Kosmides, and Kyle Zablocki were very talented undergraduates that had a significant impact on this research. These colleagues were an invaluable part of this thesis.

I would like to thank my friends from other labs, Ana Rodriguez, Alex Brunfeldt, Michael Koucky, Najeeb Chowdhury, Dr. Aaron Carlson, Dr. Shirley Masand, Dr. Ian Gaudet, Dr. Aina Andrianarijaona, Dr. Shannon Smith, George Dorfman, Sebastian Vega, Emmanuel Ekwueme, Karthryn Drzewiecki, Sagar Singh, Jay Patel, Dan Lewis, Corina White, Paulina Krzyszczyk, Sally Stras, Michelle Sempkowski, Laura Higgins, Ana Gomez, Trevan Locke, Brittany Taylor, Antoinette Nelson, Justin Rice, Dan Browe, Connie Yu, Margot Zevon, and Kamau Pierre. I would like to thank my lab members (Yarmush and Berthiaume lab), past and present. Dr. Francois Berthiaume, Dr. JP Dolle, Dr. Kevin Nikitczuk, Dr. Jeffrey Barminko, Dr. Nir Nativ, Dr. Rohit Jindal, Andrea Gray, Dr. Serom Lee, Agnes Yeboah, Ileana Marrero-Berrios, Renea Faulknor, Dr. Melissa Pryzborowski, Gabriel Yarmush, Max Balter, and Alvin Chen. These people have been my colleagues and friends for several years, and I am incredibly lucky to have been able to perform my graduate studies alongside such a great group of scientists. Through the difficult times of my PhD, it has always been a pleasure to wake up everyday go to the lab because of these people.

Last but not least, I would like to thank my family. My brother Salim, now in the second year of his PhD, is my best friend (and my best man). He has known me my entire life, and now we can share the PhD experience. We are 5 years apart, and have never been in school together at any level until now. It is pretty special that we had this last year together in graduate school. My parents, Samir and Rachida Ghodbane, are the most important people in my life. They

have always pushed me to succeed, especially when I was younger and did not understand the value of education. My parents were born in North Africa and won scholarships to study in France, where they met. My father then did his PhD at Georgetown, and while he could not speak a word of English when he started, he was able to earn his doctorate in Physical Chemistry in only 4 years. Through their tireless hard work and love, they were able to provide my brother and me every opportunity in the world. In addition, they have always been there for me helping me through a countless number of difficult situations. Their support and love has been unwavering my entire life, and they have been nothing but perfect role models that I respect, admire, and love profoundly. I am extremely grateful to have such wonderful parents, and this dissertation would never have happened without them.

Finally, I have to thank my wonderful wife, Laura. I have known her since we were playing violins together in 5th grade. She is always there for me, and supported me throughout my graduate studies, moving to North Jersey and putting my needs first while I completed my PhD. Laura is a beautiful, kind, intelligent woman who I cannot imagine living without. I love her more than words can describe.

This dissertation was done with the support of a huge group of very special people. I will always remember this time and appreciate what everyone has done for me. In addition, I would like to thank the the National Institute of Health Rutgers Biotechnology Training Program (T32GM008339), and the

National Science Foundation Integrated Science and Engineering of Stem Cells Program (DGE0801620) for funding support.

Table of Contents

List of Tables

List of Illustrations

Chapter 1: Introduction

The Immunoassay

The immunoassay is one of the most common biochemical tests performed in both clinical and research settings[1]. This technique takes advantage of several properties of antibody-antigen interactions. The first is a result of the structure of antibodies, Y-shaped proteins consisting of two identical light chains and two identical heavy chains. Each chain contains constant regions, and variable chains. Subtle variations in the constant region define the five different classes of antibodies (or immunoglobulins) that exist, IgM, IgD, IgG, IgG, IgA, and IgE[2]. Changes in amino acid residues in the variable regions result in specificity (i.e. the ability to recognize and bind) to different molecules[3]. The enormous number of possible combinations of amino acids in the binding site results in antibodies with specificity for a large number of naturally occurring and synthetic molecules. Second, the specificity of antibodies-antigen interactions permits the detection of antigens at very low concentrations. Finally, extremely strong non-covalent binding allows the antibody-antigen complex to withstand further processing steps[4]. Due to these properties, immunoassays are highly sensitive and specific assays that can be used to measure any analyte for which antibodies are available, including biomarkers, hormones, lipoproteins, antibodies, viruses, small molecules, and bacteria[5]. Thus, immunoassays have found a wide variety of applications in medical diagnostics, proteomics, pharmaceutical and biological research with an estimated global market of $7.7 Billion (in 2010)[6].

Many immunoassays for protein analysis are based on the principal of the sandwich immunoassay, requiring two antibodies to bind to the same antigen. A popular format is a heterogeneous immunoassay, where capture antibodies are immobilized on a solid surface such as a well plate. Antigen-antibody binding occurs on the solid supports, and unbound antigens are easily washed away. Once antigens are bound, detection antibodies specific for an epitope (i.e. amino acid sequence in the antigen recognized by the antibody) different from the capture antibody are introduced[4]. These detection antibodies are usually biotinylated, allowing a streptavidin bound molecule to bind to the antibody-antigen complex in a subsequent step. In the enzyme linked immunosorbent assay (ELISA) streptavidin is conjugated to an enzyme. A substrate solution is added which is catalyzed to a colorimetric or fluorescent product. Alternatively, a fluorophore can be conjugated to streptavidin. Depending on if the product is colorimetric or fluorescent, absorbance or fluorescence measurements are used to quantify the amount of protein present in the sample, respectively[7-8].

While immunoassays are highly specific and sensitive with broad applications, they have several limitations. First, highly trained operators are required. In addition, the procedure is labor intensive, involving many wash steps. Furthermore, immunoassays are very expensive due to the complex procedures required to generate and purify high affinity antibodies[9]. In addition, incubation times are long since analyte molecules must diffuse great distances to react with the antibodies[8]. Finally, immunoassays typically required 50-100 µL of sample volume, which can be a significant drawback in certain applications.

Multiplexing Immunoassays

In many cases, more than one analyte is of interest. For example, recent advances in biomarker research has increased desire to measure panels of molecules in a single patient sample[10]. However, common immunoassays only interrogate a single analyte in a given assay. Therefore, analysis of a several analytes requires parallel assays to be performed. This results in a linear increase in the cost, sample volume, and workload necessary to perform the analysis. Multiplex assays (i.e. measuring multiple analytes in a single sample) can streamline analysis and greatly decrease the sample volume required. Therefore, multiplexing technologies have been developed in recent years and represent an important trend in the evolution of the immunoassay in the future[11].

One of the most widely used multiplex immunoassay platforms is the Luminex xMAP system. This technology works on the principle of optically encoded beads. Microspheres with a diameter of 5.6 or 6.5 μm are internally labeled with specific concentrations of red and infrared (IR) dyes. Ten concentrations of each type of dye are used, therefore creating 100 possible subpopulations of beads[12]. These dye concentrations correspond to the capture antibody on the surface of the beads allowing up to 100 proteins to be quantified in a single sample[13]. Sandwich immunoassays are performed on the surface of the beads. At the completion of the assay they are analyzed using a Bio-plex Analyzer, a specialized flow cytometer developed for this application. The detection system measures red, (IR), and green fluorescence intensities for each bead individually. The red versus IR fluorescence intensity is plotted and beads

with the same capture antibody cluster together, identifying the analyte specificity of each bead and thus facilitating multiplexing. Each group of beads is gated and the green fluorescence intensity is used to quantify the concentration of a specific analyte[14]. An overview of the technology is shown in Figure 1.1. This assay is marked by excellent dynamic range (i.e. 5-6 orders of magnitude), has a relatively fast assay time compared to ELISA, and undergoes strict quality control standards. It has also become very popular, as it has been used in 7000 publications to date[12]. However this technology has the same drawbacks as single analyte immunoassays, including a long assay time, laborious procedure, need for trained technicians, high cost, and large sample requirement.

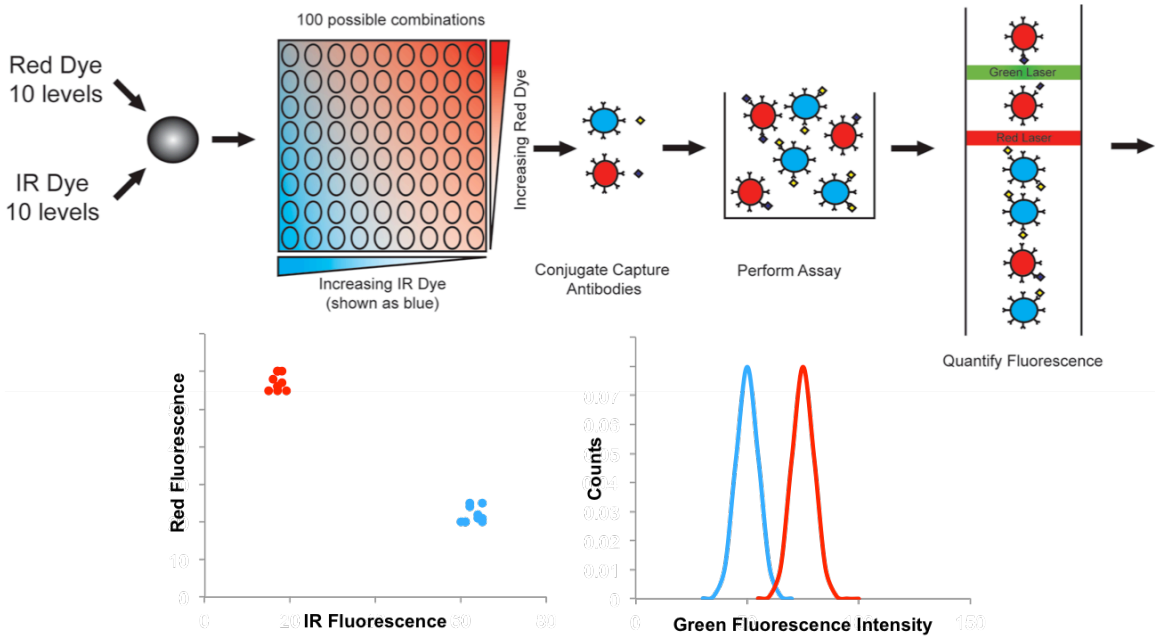

Figure 1.1: Overview of the Luminex xMap System.

(Top) Microbeads are encoded with varying concentrations of red and IR dye with 100 possible combinations. Beads with a specific dye concentrations are conjugated to capture antibodies specific to antibodies of choice. In this figure,

the blue beads are specific for the yellow analyte and the red beads are specific for the purple protein. The beads are simultaneously incubated with a sample containing both analytes. After labeling with secondary antibodies and a fluorescent tag, the beads are read by a Bio-Plex 200 analyzer. The red laser quantifies the red and IR intensity which are plotted relative to each other (bottom left). Each cluster represented the optical signature of the respective beads. The green laser quantifies the amount of each protein present on each bead (bottom right). The median fluorescence is use to represent the amount of protein present in the sample.

Microfluidic Bead Based Immunoassays

Microfluidic technology has the potential to alleviate the aforementioned drawbacks of immunoassays. Microfluidic devices are amendable to automation, allowing for high-throughput and highly reproducible assays[13, 15]. This would eliminate the need for highly trained operators and alleviate the labor involved in performing the assay. In addition, several inherent advantages exist when performing this assay at the microscale. First, the surface area to volume ratio is greatly increased. Additionally, since diffusion time is proportional to the square of the distance a molecule must travel[16], performing the assay in a reduced volume provides a large reduction in diffusion time. These two advantages have been shown to drastically reduce incubation times at high antigen concentrations. These benefits are augmented when performing bead-based immunoassays, i.e. antibodies are immobilized on the surface of microbeads rather than on microtiter

plates or microchannel walls. For example, Sato et al. used 45 μm beads and decreased the time required to saturate binding of 10 μg/mL IgA from 18 hours to less than 20 minutes, a 90-fold reduction[17]. Further decreasing the bead diameter would amplify this advantage, as would be the case using the abovementioned Luminex beads. A comparison of the surface area to volume ratio and relative diffusion time in the different assay formats is shown in Table 1.1.

Antibody Immobilization Surface	Surface Area to Volume ratio (cm^{-1})	Diffusion Time Reduction Compared to 96 well plate
96 well plate	7 cm^{-1}	1
100 x 100 x 200 μm channel	250 cm^{-1}	~1/225
11 45 μm diameter beads	350 cm^{-1}	~1/5600
3650 6.5 μm diameter microspheres	2420 cm^{-1}	~1/1.33×10^{6}

Table 1.1: Comparison of Surface Area to Volume Ratio and Diffusion Time between different antibody immobilization surfaces.

Surface area to volume calculations: 96 well plate: entire surface of the well in contact with solution (diameter=6.5 mm, height=1.5mm). Channel walls: surface area of the dimensions listed above. Beads: Surface area of each bead multiplied by the number of beads. For the last three rows, volume of the channels was used since the listed number of beads takes up that volume. Diffusion time calculations: Calculated by the ratio of the longest possible distance between a molecule and an antibody. Well Plate: height of the solution

was used (1.5mm). Channel Walls: Half of the largest dimension (100μm) 45 Beads: Taken from[17] 6.5 um beads: Estimated from half of the radius of the bead

Bead based microfluidic assays provide advantages in addition to decreased diffusional distances and increased surface area to volume ratios. First, they help promote mixing[13], a common problem in microfluidics due to the small Reynolds number resulting from the small dimensions of microfluidic channels[18]. One study showed that a packed bed of microbeads provides rapid and efficient mixing across relatively large distances in microfluidic channels[19]. Moreover, microbeads have been shown to amplify fluorescence signals in microchannels[20]. Finally, millions of beads can be conjugated to antibodies in a single batch, providing increased inter-assay reproducibility compared to individually producing antibody arrays or adsorbing antibodies onto the surface of a well plate[21].

In addition to the advantages provided by the physics of the micoscale, miniaturization naturally decreases both sample and reagent usage. Due to the high cost of immunoassay reagents, assay cost is greatly reduced compared to conventional benchtop immunoassays[15]. In some applications, limited sample volumes allow microfluidic immunoassays to perform measurements on scarce samples unable to be analyzed using conventional techniques[22].

The many advantages of microfluidic bead based immunoassays in conjunction with the Luminex xMap reagents discussed in the previous section provides a possible approach to analyzing panels of proteins in very small

sample volumes. In the following section, specific applications that would benefit from sample and/or cost reduction of multiplex immunoassays are discussed.

Applications of Low Volume Multiplex Microfluidic Bead Based Immunoassays

Single analyte immunoassays are currently the norm in both research and clinical settings, with multiplex assays slowly gaining popularity. Single analyte immunoassays, namely ELISA, require 50-100 µL of sample volume. In addition, only one analyte can be measured in this assay. The Luminex based multiplex immunoassay is commercially available and allows up to 100 proteins to be simultaneously quantified. However, 25-50 µL are required per sample and also suffer from being very expensive. While these assays have proven incredibly useful, reduction of sample consumption to less than 5 µL and the associated cost savings would benefit to numerous applications, spanning *in vitro, in vivo* and clinical scenarios.

In Vitro Applications

Typical *in vitro* experiments are performed in well plates, allowing for parallel cultures under different experimental conditions. The working volume of a 96 well plate is 75-200 µL, and 100 µL of media is typically used in many laboratories including ours. . With this volume of media, the sample required for ELISA only allows for one analyte to be quantified per well in duplicate. Using a multiplex immunoassay, many analytes can be measured using the entire media volume. Therefore, studies aiming to investigate temporal profiles must dedicate

a well to each time point of interest. This quickly increases the number of cells and culture reagents needed resulting in the investigation of only a small number of time points.

If the sample volume needed to measure multiple proteins was reduced to less than 5 μL, temporal profiles could be generated using single wells. Small volumes could be extracted over time from individual wells dedicated to an experimental condition. The media could be replaced upon sampling, resulting in virtually unlimited time points generated from a single well. To illustrate this benefit, imagine a study with 4 time points of interest (e.g. day 1, 2, 3, 4) with experimental duplicates. Using a 96 well plate, only 12 experimental conditions (including controls) can be included on a plate due to the volume requirements of conventional immunoassays. With a reduced sample volume, a single 96 well plate could be used to investigate 48 experimental conditions. In addition, temporal profiles with as many time points as desired could be generated, yielding an increased understanding of the dynamic behavior of the culture system. This ability would be very well suited to high-throughput screening studies. One example from our laboratory is a study attempting to elucidate the effect of a panel of different molecules on directing cell secretion using design of experiments (DOE) techniques[23].

The advantages of low-volume analysis can further be extended to scaled down culture systems. While 96 well plates are typically used for the highest possible throughput in academic research, 384 and 1536 well plate formats are widely available from a variety of manufacturers. However, small working

volumes prohibit analysis using immunoassay methods. For example, scaling down a 96 well plate culture using 100 µL of media per well to a 384 or 1536 well plate while keeping the media height constant would translate to 17.4 and 6.5 µL of media per well, respectively. These media volumes are too small to analyze using ELISA or multiplex immunoassay methods. However, a reduced sample volume of less than 5 µL would allow for quantification of panels of analytes from each well. In addition, this greatly reduces the cells required in the culture system. At a typical cell seeding density used in our lab of 5,000 cells/cm^2, this would translate to 1609 cells/well in a 96 well plate[24]. In 384 and 1536 well plate formats, the cells are reduced to 280 and 105 per well, respectively. This represents a reduction of the required cells and media by 83% for the 384 well plate and 94% for the 1536 well plate. A comparison of the 3 different well plate formats is included in Table 1.2. Thus, significant cost savings would arise not only from the decreased assay cost, but also from the reduction of cells, media, and stimuli (small molecules, growth factors, proteins, etc.) required in the experimental system. In addition, experimental throughput would be increased from the decrease in time required to expand sufficient cells to perform experiments.

Plate format	96 Well	384 well	1536
Well Diameter (mm)	6.4	2.67	1.63
Well Surface Area (cm^2)	3.2	0.56×10^{-2}	2.1×10^{-2}
Cells/well	1609	280	105
Media Volume (µL)	100	17.4	6.5
Cell and Volume Reduction Relative to 96 Well Plate (%)		83	94

Table 1.2: Comparison of 96, 384, and 1536 well plate formats.
Cells per well is calculated by using the same cell seeding density of 5000 cells/cm^2. The media volume is calculated by keeping the media height identical relative to 100 µL/well for the 96 well plate format

In Vivo Applications

The low volume of a certain biological samples that can be extracted from animal models has hindered *in vivo* studies in several areas of research. A few examples are discussed in this section.

Cerebrospinal Fluid Studies in Rodent Models

Cerebrospinal fluid (CSF) is constantly produced in the third and fourth ventricles of the brain by the choroid plexus. It is a clear fluid with similar constitution as plasma with the exception of lower protein levels[25]. Pulsatile flow carries CSF throughout the central nervous system from the ventricles to the subarachnoid space into the spinal canal. CSF is reabsorbed into the blood at various sites in the CNS[26].

CSF has several important functions critical to the central nervous system. First, CSF provides buoyancy to the brain and provides mechanical protection to the central nervous system (CNS). In addition, CSF removes metabolic waste and provides nutrients to the CNS[25]. Finally, CSF flow allows for the transport of hormones and neurotransmitters to different parts of the CNS[27].

Several properties of CSF make it an attractive bodily fluid to analyze when studying the CNS. First, CSF is in constant contact with the CNS and reflects pathological and metabolic changes. It is also relatively easy to obtain and is routinely collected in clinical settings. In addition, CSF is constantly replenished allowing repeatedly sampling[25]. It has already shown utility in the clinic for the diagnosis of meningitis, *coccidiodies immitis* fungal infection, and multiple sclerosis[28].

Due to these characteristics, studies have attempted to identify CSF biomarkers for neurological disorders such as Parkinson's disease[29], Alzheimer's disease (AD)[30], ALS, and CNS tumors[31]. In the case of AD, the search for biomarkers in blood has not yet provided any viable candidates. However, CSF biomarkers are increasingly being used in the clinic along with computerized tomography (CT) or magnetic resonance imaging (MRI) as diagnostic tools. In addition, biomarkers could provide utility in clinical trials with regards to the diagnosis of AD prior to the onset of dementia and assessing the efficacy of therapeutics[32].

In humans, the total volume of CSF is 150 mL[27], with the volume of spinal CSF measured to be 80 mL[33]. This equates to approximately half of the total

CSF residing in the spinal cord. However, a rat possesses only 250 µL of CSF[34], and produces approximately 100 µL/hr[35]. Assuming the volumetric distribution is consistent between species, a rat only has 125 µL of CSF in the spinal cord. This small volume of available CSF is the main barrier in performing studies in animal models, which would allow for larger sample number and more controlled studies compared to human trials. Taking 100 µL samples required for ELISA or multiplex immunoassay analysis would deplete 80% of the CSF in the rat spinal cord. Due to the fact that the CNS is already in a state of trauma, it is likely that removing such a large volume of CSF will lead to additional complications. In addition, CSF samples taken in the clinic represent a much smaller percentage of total CSF volume. In a clinical trial that revealed post-SCI biomarkers indicative of injury severity, only 3-4 mL were drawn[36]. Since a gradient of protein concentrations exists along the length of the spinal cord[31], it would be prudent to extract a sample of relative volume in animal studies as clinical relevance is the ultimate goal. Therefore, samples should be limited to approximately 2.5% of total CSF volume, or approximately 7 µL. Unfortunately, conventional protein analysis techniques do not allow for analysis of samples of that size.

Due to the volume limitations of rat CSF, animal studies of experimental Parkinson's disease drugs have been performed in larger mammals such as monkeys or dogs[35]. This requires more sophisticated veterinary facilities and staff, presents ethical issues, and results in a high cost. An assay with a low sample volume would allow these studies to be performed in rats, circumventing

these issues. In addition, more animals could be studied while using much less experimental drug compound per animal.

The search for reliable spinal cord injury (SCI) biomarkers is another area of CNS research that has been impeded due to the low available volume of rat CSF. Ideally, studies looking for biomarkers of SCI would be performed in humans. Indeed, previous studies have been performed and identified several potential CSF biomarkers for SCI[36-38]. However, human studies have several drawbacks. Obviously, the severity and location of injury between patients in human clinical trials cannot be controlled. This is problematic, as studies done in rats have shown that the severity of an injury has a clear effect on the levels of detectable inflammatory markers. For example, Yang et al. showed that concentrations of pro-inflammatory cytokines Il-1β, TNF-α, and IL-6 were significantly increased in a severe rat model of spinal cord injury. However, in a milder injury model, increases were not detected[39]. Second, the relatively low prevalence of SCI in addition to the very small window of enrollment in a clinical study makes it very difficult to recruit an adequate number of patients[40]. An alternative would be to perform these experiments in a primate model. However, experimenting on primates is expensive and raises ethical issues, limiting the number of animals in any given experiment[41]. Therefore, rats are the most common animals used to study SCI.

There is currently a very large body of literature studying the inflammatory cascade following SCI in rodent models[39, 42-51]. Logically, these studies would be the starting point in identifying inflammatory biomarkers following spinal cord

injury. While these studies provide candidate molecules, they are limited in several ways. First, the vast majority of these studies analyze gene expression on injured spinal tissue, while very few measure protein concentrations. While this provides insight into molecular mechanisms mediating inflammation, changes in gene expression do not necessarily indicate changing protein concentrations[39]. Consequently, the use of spinal tissue leads to additional disadvantages. Since acquiring tissue to perform analysis is destructive, an animal must be sacrificed for each data point. This limitation, in conjunction with the variation in spontaneous recovery between animals[41], results in experiments requiring large numbers of animals in order to reach statistical significance. Therefore the number of time points that can be analyzed becomes practically limited. Moreover, each study typically focuses on a small number of analytes, usually focusing on well-studied cytokines such as IL-1β, TNF-α, and IL-6. While these proteins are undoubtedly important to the progression of post-SCI inflammation, there are surely many others involved[44, 49, 52-53]. Finally, the results of these studies provide some contradictory evidence. For example, Yang et al. reported that TNF-α cytokine expression peaks at 1 hour post injury and quickly drops by 6 hours[39]. Conversely, Lee et al. reported that TNF-α expression remains elevated at almost identical levels from 1-24 hours post injury[45]. Although both models used Sprague-Dawley rats, the injury models were different. Variations in inflammatory profiles are also observed when different species, i.e. mouse versus rat, or different strains, i.e. Sprague-Dawley versus Lewis rats, are used [54].

Taken together, these limitations suggest that our temporal understanding of inflammatory markers when compiled from several studies may not be indicative of the actual cascade occurring in any given model. In order to be able to confidently study the progression of inflammation and identify possible biomarkers, these limitations must be overcome. One possible solution would be to study CSF, rather than tissue, in rats. This would allow us to reduce the number of animals necessary to carry out these studies and study temporal inflammation in individual animals, eliminating confounding animal variability and reducing the number of animals needed. In addition, the study of CSF would allow for clinical translation, as it has been shown that CSF can be acquired over time in patients with SCI[55].

Very few reports have been published that have attempted to measure cytokines in rat CSF following SCI. The first studies attempting to do this only looked at one protein. Wang et al. only detected TNF-α in one animal (n=56) over the first 72 hours following injury[56] while Harrington et al. were able to measure TNF-α for 6 hours following injury[57]. Once again, the species used and injury model differed, making direct comparison impossible. Finally, Pegg et al. were able to measure IL-1β for 7 days following injury[58]. Together, these studies measuring single proteins provided very little information about cytokines in rat CSF following SCI.

A more recent study took advantage of advances in multiplexing technology. Light et al. analyzed CSF following SCI in a rat model and used antibody array technology to measure 34 proteins[10]. Their analysis revealed a significant

increase in MMP-8 12 days after spinal cord injury, the only time point in the study. Together, these studies demonstrate that cytokines can be measured in rat CSF and multiplex analysis may facilitate the discovery of inflammatory biomarkers.

Although a small number of studies have successfully analyzed CSF in rats, the temporal progression of inflammatory cytokines in CSF remains unknown. Very few time points have been studied, and only one study measured proteins other than TNF-α and IL-β. Since these are down regulated 24 hours post-injury[39, 47, 51], they are most likely not good candidates as markers for the progression of inflammation. In general, the void in rat CSF analysis is most likely due to technical issues in obtaining sufficient CSF. Studies in rats have only been performed with CSF extracted from the cisterna magna, reportedly obtaining 50-100 μL of sample[10, 34-35, 58-59]. While this method has been proven to be effective, it may not be ideal for studying SCI. As discussed previously, CSF is formed in the ventricles in the brain. It then flows to the subarachnoid space in the cisterna magna prior to flowing into the spinal cord[26]. Since the cisterna magna is one of the first structures CSF comes in contact with, sampling CSF in the cisterna magna may not be indicative of the state of the injured spinal cord. In addition, the total protein concentration is 2.5 times higher in the lumbar cistern when compared to the ventricles[31]. These two factors suggest that CSF from the lumbar region is a better candidate for assessing spinal cord damage than CSF from the cisterna magna. In addition, lumbar puncture is routinely performed in the clinic, so studies looking for biomarkers should ideally use the

same method of CSF extraction. As discussed above, this would equate to about 2.5% of the total CSF volume, or 7 µL in rats. Therefore, CSF analysis in rat models of SCI represents another *in vivo* application that would greatly benefit from an assay capable of measuring a panel of proteins in a sample volume of 5 µL or less.

Synovial Fluid

Synovial joints such as the knee are found throughout the body and are responsible for mobility in the skeletal system. These joints are surrounded by synovial fluid, a viscous fluid responsible for lubricating synovial joints throughout the body. Under normal conditions, the fluid is composed of hyaluronic acid, phospholipids, proteins, and cholesterols. However, the composition of synovial fluid changes under inflammatory conditions such as osteoarthritis and rheumatoid arthritis[60]. Therefore, this fluid has been long studied to determine its composition and properties[61], elucidate mechanisms of inflammation[62], and attempt to identify potential biomarkers[63]. Studies in humans have identified cytokines such as TNF-α, IL-1β, and IL6 as potential targets for drugs. However, human synovial fluid cannot be used to characterize early stage inflammation, as patients typically do not report to the clinic until after symptoms have appeared. In addition, anti-inflammatory drugs are administered to alleviate pain and swelling, altering the temporal inflammatory response. Thus, mechanisms of early onset are unknown. Therefore, animal models are required to investigate early inflammatory events and drug effects in controlled studies[64]. Several animal models are available including mouse, rat, horse, rabbit, guinea pig, and

dog, each with its associated advantages and disadvantages. The lowest cost and easiest to manage are rodent models, but are limited by the volume synovial fluid that can be extracted[65]. Even studies performed in larger animals such as rabbits require the pooling of samples to obtain sufficient volumes for analysis[61]. Therefore, techniques have been developed in animal models including lavage with saline[66], perfusion of the joint[64], and Whatman Paper Recovery[67] which all result in the dilution of the synovial fluid to increase the extracted volume. Therefore, a low volume multiplex immunoassay would allow for analysis of synovial fluid from rodent models. In addition, pure synovial fluid is directly extracted and analyzed in human studies[68]. Consequently, analysis of pure synovial fluid in animal models would represent a clinically translatable sample. This would allow for the study of the inflammatory cascade and potential identification of biomarkers for osteoarthritis and rheumatoid arthritis using a low cost and easily managed animal model.

Clinical Applications

In addition to the research applications discussed above, a low volume multiplex immunoassay device also has potential uses in clinical settings. First, the cost savings due to the decreased reagent usage has the potential to greatly reduce the cost of diagnostic procedures. In addition, the low sample consumption can be exploited and used analyze precious or scarce samples. For example, the small available CSF volume of pediatric and neonatal patients makes obtaining sufficient sample from analysis challenging[22]. Finally, biomarker discovery studies require the analysis of many proteins in large numbers of

samples. Therefore, an assay with high-throughput, low-cost, multiplexing capabilities is perfectly suited to biomarker discovery studies[69].

Previous Microfluidic Multiplexing Immunoassays

A miniaturized multiplexing immunoassay with low-cost and sample consumption has wide ranging applications in both research and clinical settings. Therefore, a great deal of research has attempted to create such an assay. This section explores these technologies, discussing their operating principle, advantages, and limitations.

One multiplexing platform is based on DNA encoded antibody libraries (DEAL)[70]. With this approach, oligonucleotides are first patterned on glass slides. The complimentary oligonucleotide is then conjugated to an antibody off-chip, and the DNA conjugated antibodies are then incubated with the DNA spots. Self-assembly localizes the antibody to its corresponding DNA spot on the glass slide, allowing the location of each antibody to be known. To facilitate multiplexing, this is done in parallel with a selected group of oligonucleotide-conjugated antibodies and their anti-sense DNA strands. Once localized, a sandwich immunoassay is performed in the device and the fluorescence is read on an array scanner[70]. This approach was applied to multiplexing in whole blood. One design consisted of reagent reservoirs upstream of the DEAL array. Reagents are added to reservoirs, and filter paper is then inserted into the outlet. Capillary action self-propels the fluid through the device, sequentially flowing the reagents over the DEAL array. This device allowed the detection of 11 cytokines simultaneously[71]. Another embodiment of this technology utilized a

peroxide reservoir with a platinum-silver pin as a catalyst. When the pin is pushed into the hydrogen peroxide reservoir, it catalyzes the conversion of hydrogen peroxide to water and oxygen. The oxygen expands significantly, building pressure in the fluidic channels, driving fluid flow. This device successfully detected 10 proteins spiked into whole blood in 2 μL samples[72]. This approach has several advantages; fluid flow is self propelled, multiplex in small sample volumes, and perform assays in 40 minutes. However, there are several limitations, such as the need to pattern glass slides with DNA, limited flow rate control, an additional assay step to pattern capture antibodies, a small dynamic range, and the inability to process multiple samples on a single chip.

Additional multiplexing devices have utilized surface patterned antibodies for performing immunoassays. Bernard et al. developed a “Micromosaic Immunoasay” for multiplexing immunoglobulin G (IgG)[73]. A microfluidic network of straight parallel channels in placed onto a glass slide, and antigen solution then fills the channels. The antigens adsorb onto the surface in strips on the surface of the slide. The channels are removed and non-specific binding is blocked. After drying, the microfluidic network is placed on the slide perpendicular to the antigen strips, and fluorescently tagged IgG solutions fill the channels. The IgGs to bind to their specific antigens in known locations and the slide is imaged with a fluorescent microscope. This approach was demonstrated to have a sensitivity of 40 pM using IgGs from different species. While implementation is straightforward, this assay suffers from an addition assay step

to immobilize capture antibodies, low sensitivity, and a small dynamic range compared to bench top multiplex immunoassays.

A similar concept was used by Chin et al. to detect antibodies for infectious diseases[74]. The device consists of a single channel with four meandering detection zones, each patterned with an antigen (i.e. HIV, syphilis, etc.). A piece of tubing is loaded with the assay reagents and samples separated by air bubbles. Reagents are then introduced in the following order: wash buffer, sample, wash buffer, gold-labeled antibodies, wash buffer, water, silver ions. The antibodies in the samples bind to their respective antigens, and gold-labeled antibodies bind to the captured antibodies. The silver ions are then reduced onto the surface of the gold particles, allowing for signal amplification, and the absorbance of the silver film is measured. This simple device is low-cost and could be used in resource-limited settings. However, only one sample can be processed at once and the output is positive or negative, not quantitative.

Another device performed parallel ELISAs for separate analytes on a single sample, using a catalase instead of an enzyme[75]. Once the immunoassay sandwich is formed, the chip can “slide” so the assay chamber connects with hydrogen peroxide and ink reservoirs. The catalase catalyzes the conversion of hydrogen peroxide to oxygen and water, which causes the ink to expand into a microfluidic channel. Therefore, the displacement of the ink is proportional to the amount of analyte in the sample. The output is a “bar graph” of ink, which requires no sophisticated detection equipment. With this approach, a 30-plex

assay using only 10 µL of fluid was demonstrated. However, this approach only processes one sample at once and has a relatively low sensitivity of 5 ng/mL.

Compact disc (CD) based devices ("Lab-on-a-disc") drive fluid flow using the centrifugal force generated when the CD is spun. ELISA was first reported using this approach[76] which has since been adapted to multiplex assays[77]. Separate chambers containing polystyrene beads conjugated to different capture antibodies are contained on a single disc. The samples and reagents are contained in separate reservoirs sequestered by ferrowax microvalves that can be opened using a laser. After the reagents are sequentially introduced and the immunoassay sandwich is formed, substrate is added and absorbance is read on chip to quantify 3 analytes. While this device can perform the assay in only 20 minutes, the limit of detection of 240 pg/mL is relatively high, a large sample volume of 200 µL is required, and only two samples can be processed at once.

Garcia-Cordero and Maerkl developed a method for patterning capture antibodies using a button-membrane approach[78]. When a circular "button valve" is pressurized, a PDMS membrane expands and presses onto a glass slide. Antibody solutions are introduced into the channels, and adsorption is blocked where the PDMS is in contact with the glass. Using this patterning approach, a massively parallel immunoassasy device was developed. Glass slides were patterned with 384 with a 5 nL sample spots using a microarray robot then dried. A microfluidic network containing microvalves is then bonded to the glass slide. The sample spots are isolated using the valves, and 4 capture antibodies spots are patterned directly adjacent to each sample. The samples are rehydrated and

then allowed to incubate with the capture antibodies. The remaining immunoassay reagents are introduced sequentially under flow, and the spots are read using a microarray scanner. With this approach, 4 analytes in 384 5 nL samples are simultaneously assayed with a high sensitivity of 100 fM for some analytes[79]. However, this approach suffers from a limited dynamic range due to the optical reading, requires a microarray robot in order to spot the samples, and has a low sensitivity of 1 pM for some analytes.

Another approach to developing microscale multiplex immunoassays has involved using the Luminex microspheres mentioned previously. Diercks et al. developed a device that trapped the beads in a microchannel[1]. Samples are then re-circulated over the beads in order to minimize the necessary sample volume. The reagents are then sequentially added and the signal is measured using a fluorescent microscope. This device can simultaneously measure 4 proteins in a sample volume of just 5 nL. However, the device requires on-chip pumping at very low flow rates, and the dynamic range is limited to 2 orders of magnitude due to microscopic analysis.

Another group using Luminex beads overcame this limitation by analyzing the beads off-chip using a Bio-Plex analyzer. Yu et al. inserted a filter into capillary tubing in order to trap the beads while allowing for fluid flow. They were able to measure seven proteins in 1 μL of tissue lysates[80]. However, the number of samples that can be run simultaneously is limited to the number of syringe pumps. In addition, since the device does not facilitate parallel processing, standards cannot be run and therefore quantitative data is not obtained.

Electrochemical detection is another method employed to perform multiplex immunoassays. One embodiment used a single stranded DNA molecule conjugated to a redox reporter anchored to an electrode[81]. The complimentary DNA with a conjugated peptide epitope is introduced and the DNA hybridizes. In this configuration, electron transfer can occur. If a protein binds to the epitope, electron transfer is impeded causing a change in current. This method only requires a few minutes to complete the assay, but has a very low sensitivity (nM) and requires 200 μL of sample.

Another group used a purification module attached to a nanowire[82]. Capture antibodies are attached to the surface of a chip using a photocleavable crosslinker. The sample is introduced and the analyte binds to the capture antibodies. After washing, ultraviolet light (UV) cleaves the antibody antigen complex from the surface which then flows over a nanowire containing the detection antibody. The binding of the protein-capture antibody complex to the detection antibody on the nanowire causes a change in current that allows for sample quantification. This device can perform an assay on 10 μL of sample in only 20 minutes, but only processes two samples and has a low sensitivity (ng/mL).

The advantages and disadvantages of the devices described in this section are summarized in Table 1.3. Examination of previous literature reveals that all previous devices suffer from one or more of the following limitations: sample consumption (>5 μL), a low sensitivity (>fM), small dynamic range (<2 orders of magnitude), the inability to easily change the analytes being measured,

the need to synthesize specialized reagents that are not commercially available, the inability to provide quantitative data, and/or the inability to process large numbers of samples simultaneously.

	Small sample volumes	High Sensitivity	Dynamic range	Analyte Flexibility	Commercially Available Reagents	Quantitative	Parallel Processing
Commercial Luminex Assay	✗	✔	✔	✔	✔	✔	✔
DEAL[71-72, 83]	✔	✔	✗	✔	✗	✔	✗
Capillary Trap Device[80]	✔	✔	✔	✔	✔	✗	✗
CD Immunoassay[77]	✗	✗	✗	✔	✔	✔	✗
Recirculating Flow Device[1]	✔	✗	✗	✔	✔	✔	✔
Button Valve Immunoassay[79]	✔	✔	✗	✗	✗	✔	✔
V Chip Elisa[75]	✗	✗	✔	✗	✔	✔	✗
Silver Film Device[74]	✔	✔	✗	✔	✗	✗	✗
DNA redox device[81]	✗	✗	✗	✔	✗	✗	✗
Nanowire Device[82]	✔	✗	✗	✔	✗	✔	✗

Table 1.3: Overview of currently available multiplexing technologies.
No current method possesses all of the characteristics listed. Small sample volume is defined as less than 5 uL. High sensitivity is defined as a limit of detection in the 100s of pM range. A device must have a working range of at least 3 orders of magnitude to be considered as having a large dynamic range. Analyte flexibility denotes the ability to change the analytes being measured without changing the device design. Commercially available reagents signifies that no reagents need to be synthesized by the user. Parallel processing signifies the ability of a device to process at least 8 samples simultaneously.

Thesis Objective

The limitations discussed prevent a single device to be broadly applied to diverse applications. Therefore, the objective of this thesis is to design a device overcoming these limitations. These design criteria for the device are as follows:

1. Low sample consumption < 5 μL
2. High sensitivity (fM)
3. Large Dynamic Range (3+ orders of magnitude)
4. The ability to easily change analytes using a single device design
5. The ability to perform assays using commercially available reagents
6. The ability to produce quantitative data
7. The ability to process multiple samples simultaneously (i.e. parallel processing)

Thesis Summary

To accomplish these goals, we developed a microfluidic immunoassay device capable of utilizing commercially available Luminex microbeads. These beads can be purchased pre-conjugated to a variety of antibodies. In addition, the beads can be conjugated to any antibody using a commercially available kit. The use of these widely available reagents allow the device to measure any analyte for which antibody pairs are available without the need for specialized reagent synthesis. In addition, we benefit from the advantages afforded by performing bead-based immunoassays.

The design and development of the microfluidic based multiplexing immunoassay device is described in this dissertation. Chapter 2 outlines the

development of an 8-channel proof-of-concept device. This chapter discusses the design and fabrication of the device, as well as optimization of the assay parameters. Due to experimental difficulties and variability inherent with microfluidic research, a computational fluid dynamics (CFD) model predicting antibody-antigen binding kinetics in microfluidic channels is developed and validated. We then utilize this model in conjunction with DOE and multi-objective optimization techniques to minimize the amount of sample volume required to perform a highly sensitive immunoassay. Finally, the optimal parameters determined from the computational platform are used to demonstrate detection of 358 fM of IL-6 using only 1.35 μL of sample volume.

Chapter 3 describes the expansion of the proof-of concept design to a device capable multiplexing of 6 analytes in 32-samples simultaneously. The limit of detection and dynamic range of each analyte is determined, demonstrating high sensitivity and a large dynamic range for all 6 analytes. Finally, the utility of the device is demonstrated by analyzing samples from an *in vitro* culture system. The samples are analyzed using a conventional Luminex multiplex immunoassay and the microdevice in parallel, using 50 and only 4.2 μL of sample, respectively. A strong agreement between the two assay formats is shown. Therefore, we successfully demonstrate a low volume, parallelized, quantitative, highly sensitive multiplex immunoassay assay with a large dynamic range using commercially available reagents. These characteristics allow this device to be potentially applied to a variety of *in vitro, in vivo*, and clinical applications.

A detailed fabrication and operation procedure for the device is detailed in Chapter 4. The purpose of this section is to elaborate on our published methods with sufficient detail for straightforward reproduction of the results presented in this thesis. Each step of the fabrication process is explained, and issues that required extensive troubleshooting are emphasized. In addition, a protocol is included for each step. Finally, the operating procedure of the device is described in great depth.

Chapter 5 summarizes the findings of this dissertation and discusses the limitations of this technology relative to currently existing devices. Furthermore, additional device optimization that we believe is required to take the device from proof-of-concept stage to a commercial assay is suggested. Finally, a potentially commercially viable platform based on the device developed in this work is described.

References

1. Diercks, A.; Ozinsky, A.; Hansen, C.; Spotts, J.; Rodriguez, D.; Aderem, A., A microfluidic device for multiplexed protein detection in nano-liter volumes. *Analytical Biochemistry* **2009,** *386* (1), 30-35.
2. Janeway, C. A.; Travers, P.; Walport, M.; Shlomchik, M. J., *Immunobiology: the immune system in health and disease*. Churchill Livingstone: 2001; Vol. 2.
3. Lodish, H., Berk, Arnold, Kaiser, Chris A., Krieger, Monty, Bretscher, Anthony, Ploegh, Hidde, Matsudaira, Paul, *Molecular Cell Biology*. 6 ed.; W.H. Freeman and Company: New York, 2008.
4. Wild, D., *The immunoassay handbook*. Elsevier Ltd.: San Diego, 2005.
5. Henares, T. G.; Mizutani, F.; Hisamoto, H., Current development in microfluidic immunosensing chip. *Anal. Chim. Acta* **2008,** *611* (1), 17-30.
6. Report Reveals Growth Opportunities in the Immunoassay Market. http://www.genengnews.com/gen-news-highlights/report-reveals-growth-opportunities-in-the-immunoassay-market/81243609/?kwrd=In Vitro Diagnostics.
7. Lim, C. T.; Zhang, Y., Bead-based microfluidic immunoassays: The next generation. *Biosensors and Bioelectronics* **2007,** *22* (7), 1197-1204.

8. Ng, A. H. C.; Uddayasankar, U.; Wheeler, A. R., Immunoassays in microfluidic systems. *Anal. Bioanal. Chem.* **2010,** *397* (3), 991-1007.
9. Roque, A. C. A.; Lowe, C. R.; Taipa, M. Â., Antibodies and genetically engineered related molecules: production and purification. *Biotechnology progress* **2004,** *20* (3), 639-654.
10. Light, M.; Minor, K. H.; DeWitt, P.; Jasper, K. H.; Davies, S. J. A., Multiplex array proteomics detects increased MMP-8 in CSF after spinal cord injury. *Journal of Neuroinflammation* **2012,** *9* (1), 122.
11. Zheng, W. H., L Multiplexed Immunoassays. In *Advances in Immunoassay Technology*, Chiu, N., Ed. InTech: 2012.
12. Houser, B., Bio-Rad's Bio-Plex(R) suspension array system, xMAP technology overview. *Archives of physiology and biochemistry* **2012,** *118* (4), 192-6.
13. Derveaux, S.; Stubbe, B. G.; Braeckmans, K.; Roelant, C.; Sato, K.; Demeester, J.; Smedt, S. C., Synergism between particle-based multiplexing and microfluidics technologies may bring diagnostics closer to the patient. *Anal. Bioanal. Chem.* **2008,** *391* (7), 2453-2467.
14. Dunbar, S. A., Applications of LuminexÆ xMAP(TM) technology for rapid, high-throughput multiplexed nucleic acid detection. *Clinica Chimica Acta* **2006,** *363* (1-2), 71-82.
15. Bange, A.; Halsall, H.; Heineman, W., Microfluidic immunosensor systems. *Biosensors and Bioelectronics* **2005,** *20* (12), 2488-2503.
16. Bird, R. B.; Stewart, W. E.; Lightfoot, E. N., *Transport phenomena*. Wiley: 2006.
17. Sato, K.; Tokeshi, M.; Odake, T.; Kimura, H.; Ooi, T.; Nakao, M.; Kitamori, T., Integration of an immunosorbent assay system: Analysis of secretory human immunoglobulin A on polystyrene beads in a microchip. *Anal. Chem.* **2000,** *72* (6), 1144-1147.
18. Beebe, D. J.; Mensing, G. A.; Walker, G. M., Physics and Applications of Microfluidics in Biology. *Annual Review of Biomedical Engineering* **2002,** *4* (1), 261-286.
19. Seong, G. H.; Crooks, R. M., Efficient mixing and reactions within microfluidic channels using microbead-supported catalysts. *Journal of the American Chemical Society* **2002,** *124* (45), 13360-13361.
20. Shin, K. S.; Lee, S. W.; Han, K. C.; Kim, S. K.; Yang, E. K.; Park, J. H.; Ju, B. K.; Kang, J. Y.; Kim, T. S., Amplification of fluorescence with packed beads to enhance the sensitivity of miniaturized detection in microfluidic chip. *Biosensors and Bioelectronics* **2007,** *22* (9), 2261-2267.
21. Wilson, R.; Cossins, A. R.; Spiller, D. G., Encoded microcarriers for high-throughput multiplexed detection. *Angew. Chem.-Int. Edit.* **2006,** *45* (37), 6104-6117.
22. Phillips, T. M., Rapid analysis of inflammatory cytokines in cerebrospinal fluid using chip-based immunoaffinity electrophoresis. *Electrophoresis* **2004,** *25* (1011), 1652-1659.

23. Barminko, J. A.; Nativ, N. I.; Schloss, R.; Yarmush, M. L., Fractional factorial design to investigate stromal cell regulation of macrophage plasticity. *Biotechnology and Bioengineering* **2014**.
24. Barminko, J.; Kim, J. H.; Otsuka, S.; Gray, A.; Schloss, R.; Grumet, M.; Yarmush, M. L., Encapsulated mesenchymal stromal cells for in vivo transplantation. *Biotechnology and Bioengineering* **2011**, n/a-n/a.
25. Brown, P.; Davies, S.; Speake, T.; Millar, I., Molecular mechanisms of cerebrospinal fluid production. *Neuroscience* **2004,** *129* (4), 955-968.
26. Duncan, J.; Klinge, P.; Brinker, T.; Stopa, E.; Silverberg, G., Multiplicity of cerebrospinal fluid functions: New challenges in health and disease\ %U http://www.cerebrospinalfluidresearch.com/content/5/1/10. *Cerebrospinal Fluid Research*\ **2008,** *5*\ (1\ %M doi:10.1186/1743-8454-5-10\), 10\.
27. Zhang, J., Proteomics of human cerebrospinal fluid - the good, the bad, and the ugly. *Proteomics Clin Appl* **2007,** *1* (8), 805-19.
28. Dugdale, D., Sheth, KM. Cerebrospinal Fluid (CSF) Collection. http://www.nlm.nih.gov/medlineplus/ency/article/003428.htm (accessed Jan-23).
29. Eller, M.; Williams, D. R., Biological fluid biomarkers in neurodegenerative parkinsonism. *Nature Reviews Neurology* **2009,** *5* (10), 561-570.
30. Mattsson, N.; Zetterberg, H.; Hansson, O.; Andreasen, N.; Parnetti, L.; Jonsson, M.; Herukka, S.-K.; van der Flier, W. M.; Blankenstein, M. A.; Ewers, M., CSF biomarkers and incipient Alzheimer disease in patients with mild cognitive impairment. *Jama* **2009,** *302* (4), 385-393.
31. Hühmer, A. F.; Biringer, R. G.; Amato, H.; Fonteh, A. N.; Harrington, M. G., Protein analysis in human cerebrospinal fluid: Physiological aspects, current progress and future challenges. *Disease markers* **2006,** *22* (1), 3-26.
32. Blennow, K.; Hampel, H.; Weiner, M.; Zetterberg, H., Cerebrospinal fluid and plasma biomarkers in Alzheimer disease. *Nature Reviews Neurology* **2010,** *6* (3), 131-144.
33. Edsbagge, M.; Starck, G.; Zetterberg, H.; Ziegelitz, D.; Wikkelso, C., Spinal cerebrospinal fluid volume in healthy elderly individuals. *Clinical Anatomy* **2011,** *24* (6), 733-740.
34. Jimenez Hamann, M. C.; Tsai, E. C.; Tator, C. H.; Shoichet, M. S., Novel intrathecal delivery system for treatment of spinal cord injury. *Experimental Neurology* **2003,** *182* (2), 300-309.
35. Shapiro, J. S.; Stiteler, M.; Wu, G.; Price, E. A.; Simon, A. J.; Sankaranarayanan, S., Cisterna magna cannulated repeated CSF sampling rat model-effects of a gamma-secretase inhibitor on Aβ levels. *Journal of Neuroscience Methods* **2011,** *205*, 36-44.
36. Kwon, B. K.; Stammers, A. M. T.; Belanger, L. M.; Bernardo, A.; Chan, D.; Bishop, C. M.; Slobogean, G. P.; Zhang, H. B.; Umedaly, H.; Giffin, M.; Street, J.; Boyd, M. C.; Paquette, S. J.; Fisher, C. G.; Dvorak, M. F., Cerebrospinal Fluid Inflammatory Cytokines and Biomarkers of Injury Severity in Acute Human Spinal Cord Injury. *J. Neurotrauma* **2010,** *27* (4), 669-682.
37. Kwon, B. K.; Casha, S.; Hurlbert, R. J.; Yong, V. W., Inflammatory and structural biomarkers in acute traumatic spinal cord injury. *Clin. Chem. Lab. Med.* **2011,** *49* (3), 425-433.

38. Tsai, M.; Wei, C.; Lee, D.; Tseng, Y.; Shih, Y.; Lee, Y.; Chang, S.; Leu, S., Inflammatory mediators of cerebrospinal fluid from patients with spinal cord injury ☆. *Surg. Neurol.* **2008,** *70*, S19-S24.
39. Yang, L.; Jones, N. R.; Blumbergs, P. C.; Van Den Heuvel, C.; Moore, E. J.; Manavis, J.; Sarvestani, G. T.; Ghabriel, M. N., Severity-dependent expression of pro-inflammatory cytokines in traumatic spinal cord injury in the rat. *Journal of Clinical Neuroscience* **2005,** *12* (3), 276-284.
40. Lee, R. S.; Noonan, V. K.; Batke, J.; Ghag, A.; Paquette, S. J.; Boyd, M. C.; Fisher, C. G.; Street, J.; Dvorak, M. F.; Kwon, B. K., Feasibility of patient recruitment into clinical trials of experimental treatments for acute spinal cord injury. *Journal of Clinical Neuroscience* **2012**.
41. Filli, L.; Schwab, M. E., The rocky road to translation in spinal cord repair. *Annals of Neurology*.
42. Beck, K. D.; Nguyen, H. X.; Galvan, M. D.; Salazar, D. e. L.; Woodruff, T. M.; Anderson, A. J., Quantitative analysis of cellular inflammation after traumatic spinal cord injury: evidence for a multiphasic inflammatory response in the acute to chronic environment. *Brain* **2010,** *133* (2), 433-447.
43. Donnelly, D. J.; Popovich, P. G., Inflammation and its role in neuroprotection, axonal regeneration and functional recovery after spinal cord injury. *Experimental Neurology* **2008,** *209* (2), 378-388.
44. Hausmann, O. N., Post-traumatic inflammation following spinal cord injury. *Spinal Cord* **2003,** *41* (7), 369-378.
45. Lee, Y. L.; Shih, K.; Bao, P.; Ghirnikar, R. S.; Eng, L. F., Cytokine chemokine expression in contused rat spinal cord. *Neurochemistry International* **2000,** *36* (4,Äì5), 417-425.
46. Nakamura, M., Differences in cytokine gene expression profile between acute and secondary injury in adult rat spinal cord. *Experimental Neurology* **2003,** *184* (1), 313-325.
47. Pineau, I.; Lacroix, S., Proinflammatory cytokine synthesis in the injured mouse spinal cord: Multiphasic expression pattern and identification of the cell types involved. *The Journal of Comparative Neurology* **2007,** *500* (2), 267-285.
48. Pineau, I.; Sun, L.; Bastien, D.; Lacroix, S., Astrocytes initiate inflammation in the injured mouse spinal cord by promoting the entry of neutrophils and inflammatory monocytes in an IL-1 receptor/MyD88-dependent fashion. *Brain, Behavior, and Immunity* **2010,** *24* (4), 540-553.
49. Silver, J.; Miller, J. H., Regeneration beyond the glial scar. *Nat Rev Neurosci* **2004,** *5* (2), 146-156.
50. Stammers, A. T.; Liu, J.; Kwon, B. K., Expression of inflammatory cytokines following acute spinal cord injury in a rodent model. *J Neurosci Res* **2012,** *90* (4), 782-790.
51. Streit, W. J.; Semple-Rowland, S. L.; Hurley, S. D.; Miller, R. C.; Popovich, P. G.; Stokes, B. T., Cytokine mRNA Profiles in Contused Spinal Cord and Axotomized Facial Nucleus Suggest a Beneficial Role for Inflammation and Gliosis. *Experimental Neurology* **1998,** *152* (1), 74-87.

52. Jones, T. B.; McDaniel, E. E.; Popovich, P. G., Inflammatory-mediated injury and repair in the traumatically injured spinal cord. *Curr Pharm Des* **2005,** *11* (10), 1223-36.
53. McTigue, D. M.; Tani, M.; Krivacic, K.; Chernosky, A.; Kelner, G. S.; Maciejewski, D.; Maki, R.; Ransohoff, R. M.; Stokes, B. T., Selective chemokine mRNA accumulation in the rat spinal cord after contusion injury. *J Neurosci Res* **1998,** *53* (3), 368-376.
54. Donnelly, D.; Popovich, P., Inflammation and its role in neuroprotection, axonal regeneration and functional recovery after spinal cord injury. *Experimental Neurology* **2008,** *209* (2), 378-388.
55. Kwon, B. K.; Curt, A.; Belanger, L. M.; Bernardo, A.; Chan, D.; Markez, J. A.; Gorelik, S.; Slobogean, G. P.; Umedaly, H.; Giffin, M., Intrathecal pressure monitoring and cerebrospinal fluid drainage in acute spinal cord injury: a prospective randomized trial. *Journal of Neurosurgery: Spine* **2009,** *10* (3), 181-193.
56. Wang, C. X.; Nuttin, B.; Heremans, H.; Dom, R.; Gybels, J., Production of tumor necrosis factor in spinal cord following traumatic injury in rats. *Journal of Neuroimmunology* **1996,** *69* (1-2), 151-156.
57. Harrington, J. F.; Messier, A. A.; Levine, A.; Szmydynger-Chodobska, J.; Chodobski, A., Shedding of Tumor Necrosis Factor Type 1 Receptor after Experimental Spinal Cord Injury. *J. Neurotrauma* **2005,** *22* (8), 919-928.
58. Pegg, C., Technique for collection of cerebrospinal fluid from the cisterna magna in rat. *Journal of Neuroscience Methods* **2010,** *187* (1), 8-12.
59. Lai, Y. L.; Smith, P. M.; Lamm, W. J.; Hildebrandt, J., Sampling and analysis of cerebrospinal fluid for chronic studies in awake rats. *J Appl Physiol* **1983,** *54* (6), 1754-1757.
60. Fam, H.; Bryant, J. T.; Kontopoulou, M., Rheological properties of synovial fluids. *Biorheology* **2007,** *44* (2), 59-74.
61. Knox, P.; Levick, J.; McDonald, J., Synovial fluid-its mass, macromolecular content and pressure in major limb joints of the rabbit. *Experimental Physiology* **1988,** *73* (1), 33-45.
62. Bondeson, J.; Wainwright, S. D.; Lauder, S.; Amos, N.; Hughes, C. E., The role of synovial macrophages and macrophage-produced cytokines in driving aggrecanases, matrix metalloproteinases, and other destructive and inflammatory responses in osteoarthritis. *Arthritis research & therapy* **2006,** *8* (6), R187.
63. Kahle, P.; Saal, J.; Schaudt, K.; Zacher, J.; Fritz, P.; Pawelec, G., Determination of cytokines in synovial fluids: correlation with diagnosis and histomorphological characteristics of synovial tissue. *Annals of the rheumatic diseases* **1992,** *51* (6), 731-734.
64. Barton, N. J.; Stevens, D. A.; Hughes, J. P.; Rossi, A. G.; Chessell, I. P.; Reeve, A. J.; McQueen, D. S., Demonstration of a novel technique to quantitatively assess inflammatory mediators and cells in rat knee joints. *J Inflamm (Lond)* **2007,** *4*, 13.
65. Little, C. B.; Smith, M. M., Animal models of osteoarthritis. *Current Rheumatology Reviews* **2008,** *4* (3), 175-182.

66. Gokce, A., How Different Methodologies of Harvesting and Analysing the Samples Affect the Test Results in Determining Joint Mediators. *Arthritis* **2013,** *2013*.
67. Seifer, D. R.; Furman, B. D.; Guilak, F.; Olson, S. A.; Brooks III, S. C.; Kraus, V. B., Novel synovial fluid recovery method allows for quantification of a marker of arthritis in mice. *Osteoarthritis and Cartilage* **2008,** *16* (12), 1532-1538.
68. Yoshihara, Y.; Nakamura, H.; Obata, K. i.; Yamada, H.; Hayakawa, T.; Fujikawa, K.; Okada, Y., Matrix metalloproteinases and tissue inhibitors of metalloproteinases in synovial fluids from patients with rheumatoid arthritis or osteoarthritis. *Annals of the Rheumatic Diseases* **2000,** *59* (6), 455-461.
69. Shoemaker, L. D.; Achrol, A. S.; Sethu, P.; Steinberg, G. K.; Chang, S. D., Clinical Neuroproteomics and Biomarkers: From Basic Research to Clinical Decision Making. *Neurosurgery* **2012,** *70* (3), 518.
70. Bailey, R. C.; Kwong, G. A.; Radu, C. G.; Witte, O. N.; Heath, J. R., DNA-encoded antibody libraries: a unified platform for multiplexed cell sorting and detection of genes and proteins. *Journal of the American Chemical Society* **2007,** *129* (7), 1959-1967.
71. Wang, J.; Ahmad, H.; Ma, C.; Shi, Q.; Vermesh, O.; Vermesh, U.; Heath, J., A self-powered, one-step chip for rapid, quantitative and multiplexed detection of proteins from pinpricks of whole blood. *Lab Chip* **2010,** *10* (22), 3157-3162.
72. Qin, L.; Vermesh, O.; Shi, Q.; Heath, J. R., Self-powered microfluidic chips for multiplexed protein assays from whole blood. *Lab Chip* **2009,** *9* (14), 2016-2020.
73. Bernard, A.; Michel, B.; Delamarche, E., Micromosaic immunoassays. *Anal. Chem.* **2001,** *73* (1), 8-12.
74. Chin, C. D.; Laksanasopin, T.; Cheung, Y. K.; Steinmiller, D.; Linder, V.; Parsa, H.; Wang, J.; Moore, H.; Rouse, R.; Umviligihozo, G., Microfluidics-based diagnostics of infectious diseases in the developing world. *Nature medicine* **2011,** *17* (8), 1015-1019.
75. Song, Y.; Zhang, Y.; Bernard, P. E.; Reuben, J. M.; Ueno, N. T.; Arlinghaus, R. B.; Zu, Y.; Qin, L., Multiplexed volumetric bar-chart chip for point-of-care diagnostics. *Nature communications* **2012,** *3*, 1283.
76. He, H.; Yuan, Y.; Wang, W.; Chiou, N.-R.; Epstein, A. J.; Lee, L. J., Design and testing of a microfluidic biochip for cytokine enzyme-linked immunosorbent assay. *Biomicrofluidics* **2009,** *3* (2), 022401.
77. Park, J.; Sunkara, V.; Kim, T.-H.; Hwang, H.; Cho, Y.-K., Lab-on-a-disc for fully integrated multiplex immunoassays. *Anal. Chem.* **2012,** *84* (5), 2133-2140.
78. Garcia-Cordero, J. L.; Maerkl, S. J., Multiplexed surface micropatterning of proteins with a pressure-modulated microfluidic button-membrane. *Chem. Commun.* **2013,** *49* (13), 1264-1266.
79. Garcia-Cordero, J. L.; Nembrini, C.; Stano, A.; Hubbell, J. A.; Maerkl, S. J., A high-throughput nanoimmunoassay chip applied to large-scale vaccine adjuvant screening. *Integrative Biology* **2013,** *5* (4), 650-658.
80. Yu, X.; Hartmann, M.; Wang, Q.; Poetz, O.; Schneiderhan-Marra, N.; Stoll, D.; Kazmaier, C.; Joos, T. O., µFBI: A Microfluidic Bead-Based Immunoassay for

Multiplexed Detection of Proteins from a µL Sample Volume. *PLoS ONE* **2010,** *5* (10), e13125.
81. White, R. J.; Kallewaard, H. M.; Hsieh, W.; Patterson, A. S.; Kasehagen, J. B.; Cash, K. J.; Uzawa, T.; Soh, H. T.; Plaxco, K. W., Wash-free, electrochemical platform for the quantitative, multiplexed detection of specific antibodies. *Anal. Chem.* **2012,** *84* (2), 1098-1103.
82. Stern, E.; Vacic, A.; Rajan, N. K.; Criscione, J. M.; Park, J.; Ilic, B. R.; Mooney, D. J.; Reed, M. A.; Fahmy, T. M., Label-free biomarker detection from whole blood. *Nature nanotechnology* **2009,** *5* (2), 138-142.
83. Fan, R.; Vermesh, O.; Srivastava, A.; Yen, B. K. H.; Qin, L.; Ahmad, H.; Kwong, G. A.; Liu, C.-C.; Gould, J.; Hood, L.; Heath, J. R., Integrated barcode chips for rapid, multiplexed analysis of proteins in microliter quantities of blood. *Nature Biotechnology* **2008,** *26* (12), 1373-1378.

Chapter 2: Development of a Low Volume, Highly Sensitive Microimmunoassay using Computational Fluid Dynamics Driven Multi-Objective Optimization

Note: This chapter is reproduced from the following publication:

Development of a Low Volume, Highly Sensitive Microimmunoassay using Computational Fluid Dynamics Driven Multi-Objective Optimization, *Microfluidics and Nanofluidics, DOI* 10.1007/s10404-014-1416-9, June 2014

Mehdi Ghodbane[1], Anthony Kulesa[1], Henry H. Yu[1], Tim J. Maguire[1], Rene R. Schloss[1], Rohit Ramachandran[2], Jeffrey D. Zahn[1], and Martin L. Yarmush[1, 3, *]

[1]Department of Biomedical Engineering, Rutgers, The State University of New Jersey,

599 Taylor Road, Piscataway, New Jersey 08854, USA

[2]Department of Chemical and Biochemical Engineering, Rutgers, The State University of New Jersey, 98 Brett Road, Piscataway, NJ 08854, USA

[3]Center for Engineering in Medicine/Surgical Services, Massachusetts General Hospital, 51 Blossom Street, Boston, MA, 02114, USA

**Corresponding author: Telephone (848) 445-6528, Fax (732) 445-3155 Email: yarmush@rci.rutgers.edu*

Introduction:

The immunoassay is one of the most common biochemical tests performed in both clinical and research settings [1]. This technique takes advantage of highly selective antibody-antigen interactions to measure any biomolecular structure or particle for which antibodies are available. These include drugs, biomarkers, hormones, cytokines, antibodies, viruses, and bacteria [2]. Immunoassays have found a broad range of applications in medical diagnostics (e.g., HIV, prostate specific antigen, pregnancy, sexually transmitted diseases, etc.), proteomics, and biological research in general [3].

Despite their widespread use, the disadvantages include high cost due to expensive antibodies and reagents, the requirement for highly trained operators, the amount of labor associated with each assay, and long incubation times due to the large distances molecules must diffuse in order to react [4]. Furthermore, the required sample volume is a limitation in certain applications [5]. Microfluidic technology has the potential to mitigate these drawbacks that plague conventional immunoassays. First, miniaturization decreases both sample and reagent usage [6] directly resulting in a significant cost reduction and facilitating analysis of scarce samples that can not be analyzed using conventional techniques [5]. The small scale also decreases diffusional distances and increases the binding surface area to sample volume ratio producing faster reactions [7]. Furthermore, microfluidic devices are easily automated, allowing for high-throughput and highly reproducible assays [6-7].

Performing microimmunoassays using packed beds of microbeads as the antibody immobilization surface affords additional advantages. This provides

rapid and efficient mixing across relatively large distances [7-8], alleviating a common problem in microfluidics due to the low Reynolds number flow regime resulting from the small dimensions of microfluidic channels [9]. These benefits were shown in a previous study, where a 90-fold reduction in assay time was observed compared to its bench-top counterpart performed in a 96-well plate[10]. Moreover, altering the capture antibody on the microbead surface can easily change the analyte specificity of the assay utilizing the same device. Finally, millions of beads can be conjugated to antibodies in a single batch, allowing highly reproducible assays between devices [11].

Previous reports have described immunoassay conditions for a specific analyte with a given number of antibodies and each application has required individual empirical optimization [1, 10, 12-15]. Unfortunately, empirical optimization is costly and time consuming as this approach requires many devices and experiments. An alternative strategy is to develop a predictive mathematical model using computational fluid dynamics (CFD) combined with antibody-antigen reaction modeling within microchannels. In addition to eliminating the need for large numbers of experiments, an improved understanding of the effects of various design and operating parameters can be used to predict immunoassay performance for a given application. Unfortunately, the limited models of antibody-antigen reactions in microfluidic systems have only studied surface based reactions and have lacked experimental validation [16-18]. Nevertheless, the work of Zimmerman et al. demonstrated that a computational model enables the

prediction of operating parameters best suited for a particular application, i.e. minimal assay time, high sensitivity, or large dynamic range [19].

In this report, a microfluidic platform to perform sandwich immunoassays utilizing antibody-conjugated microbeads is designed and tested. In addition, a predictive CFD based model of antibody-antigen interactions in a packed bed format within a microchannel is developed and experimentally validated. The model is utilized in conjunction with mathematical optimization techniques in order to aid in the development of the device as well as to understand the key factors affecting assay performance. The optimal conditions determined from the mathematical optimization are then used to demonstrate a highly sensitive, low-volume microimmunoassay with large dynamic range and a greatly reduced reagent consumption and cost. The combination of the presented device and optimization methodology can be further extended to develop an assay for any analyte for which antibodies are available. Therefore, this technology may be translated to improve many research and clinical applications which rely on high-throughput studies and/or the analysis of scarce biological samples.

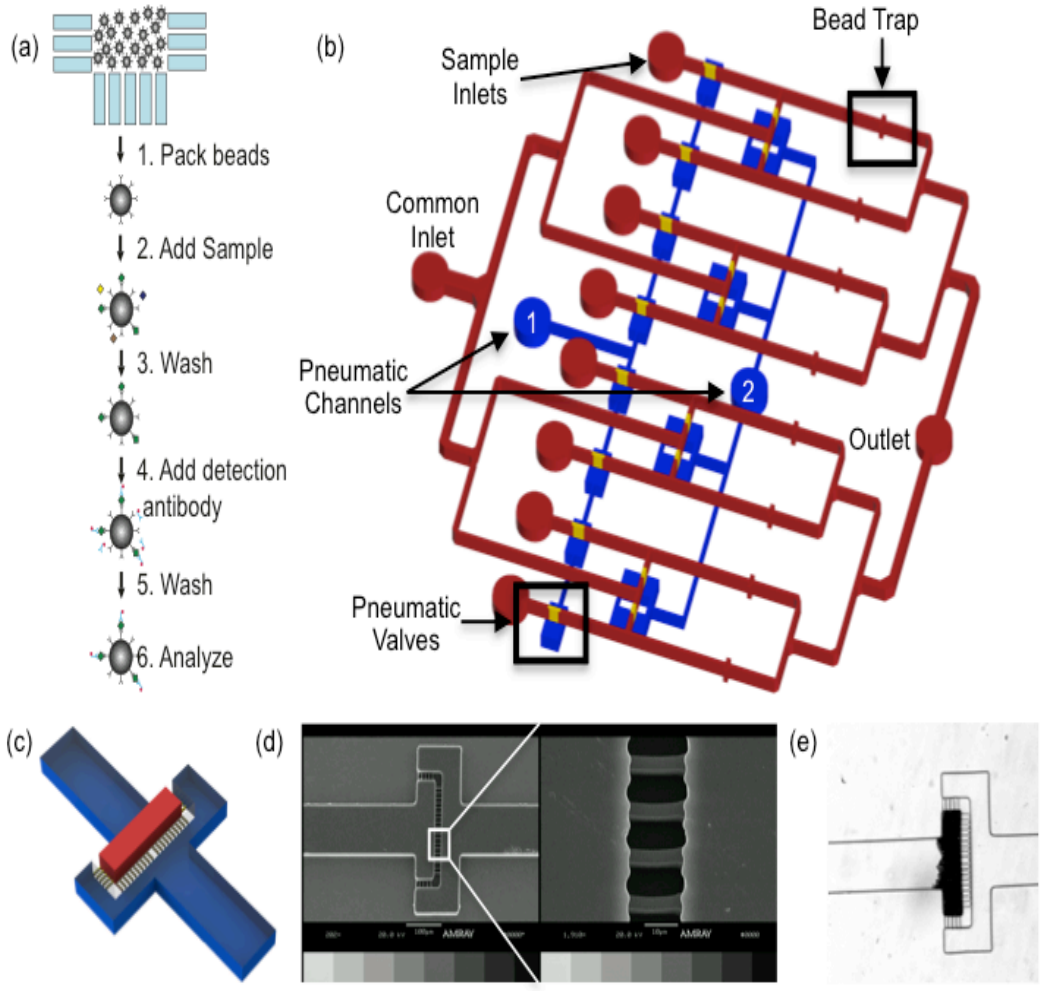

Figure 2.1: Microimmunoassay Principle.

Antibody conjugated microbeads are packed into the bead traps. Sample is then flowed over the bead beds followed by a wash step. Detection antibody is then added, the beads are washed, and the sample is ready for analysis b) Schematic representation of the microimmunoassay device. A common inlet is used for flowing all assay reagents including blocking buffer, wash buffer, antibody coated microbeads, detection antibodies, and fluorophores. Individual sample inlets allow for the simultaneous analysis of eight samples. Downstream of each

sample inlet, an array of 3 μm channels acts as a bead trap to create a packed bed that functions as a reaction chamber. A common outlet discards waste from the assay and also is used as an inlet during collection of the microbeads at the completion of the assay. Pneumatic valves are used to direct fluid flow throughout the assay. Whenever the common inlet is in use, pneumatic channel 1 is pressurized so fluid flows from the common inlet through the bead traps. During sample incubation and bead collection, pneumatic channel 2 is pressurized to prevent mixing between adjacent channels. c) 3D schematic of the bead traps. The bead bed is immobilized in the area denoted in red and the bead trap is comprised of the array of yellow features d) SEM image of the bead trap e) Brightfield micrograph of a packed bed of microbeads upstream of the bead trap

Microfluidic Device Design and Assay Operating Principle

The device is designed to perform parallel low volume sandwich immunoassays on a single chip using antibody-conjugated microbeads, allowing a single design to be used to measure any analyte with an available antibody pair. The operating principal of the microimmunoassay is shown in Figure 2.1a. Antibody conjugated microbeads are first immobilized via a mechanical trap. The sample solution then flows over the beads allowing incubation of the sample with the antibodies. A wash is performed to remove any non-specifically bound proteins, followed by labeling with a biotinylated detection antibody. Following a wash step, streptavidin-phycoerythrin flows to bind a fluorescent tag to the antibody sandwich. Subsequent to an additional wash step, the beads can be

analyzed on chip using fluorescence microscopy. Alternatively, the beads can be collected and analyzed via flow cytometry allowing for the potential for multiplexing with this device using Luminex optically encoded microbeads [20].

A schematic of the device is shown in Figure 2.1b. Pneumatic valves are incorporated into the design to divert fluid flow to desired regions of the device [21]. With this design, only two pneumatic valves are needed to facilitate eight parallel reactions, which can be easily scaled-up to process additional samples on a single chip. A common inlet is used for the introduction of assay reagents (i.e., blocking buffer, wash buffer, microbeads, detection antibodies, and fluorophores). When flow is present through the common inlet, pneumatic valve 1 is closed to divert fluid flow through the reaction zones and away from sample inlets. Individual sample inlets facilitate flowing multiple samples simultaneously as well as the collection of each individual bead population at the completion of the assay. Pneumatic valve 2 is closed during the incubation and collection steps to prevent mixing of adjacent fluid streams and bead loss through the common inlet, respectively. Downstream of each sample inlet, a bead trap immobilizes the microbeads for the duration of the assay while permitting fluid to flow through the bead bed. The bead trap consists of an array of 3 μm wide channels, considerably narrower than the diameter of the beads in our experiments, shown in Figure 2.1c. These features are 7 μm tall as we found that this is tallest we could reproducibly fabricate these features with good resolution, as shown in the scanning electron micrograph in Figure 2.1d. A picture of an immobilized packed bead bed is shown in Figure 2.1e. The bead

trap is designed to minimize flow resistance as this is a major concern with packed beds [7]. Therefore, the channel doubles in width from 100 to 200 μm at the bead trap. This halves the fluid velocity through the bed and allows the same number of beads to be packed in a bed half as long, decreasing the pressure drop resulting from the packed bed by a factor of 4 [22]. In addition, channels are oriented both parallel and orthogonal to fluid flow which has been shown to greatly reduce clogging of microbeads in microfluidic channels [23].

Mathematical Modeling and Optimization

Theoretical Background

Equations

$$\rho\left(\frac{\partial \boldsymbol{v}}{dt} + \boldsymbol{v}\cdot\nabla\boldsymbol{v}\right) = -\boldsymbol{\nabla P} + \mu\nabla^2\boldsymbol{v} + \boldsymbol{f} \quad \text{(Eq. 1)}$$

$$\nabla\cdot\boldsymbol{v} = 0 \quad \text{(Eq. 2)}$$

$$\nabla\boldsymbol{P_{bed}} = \frac{150\mu(1-\varepsilon)^2}{\varepsilon^3 D_p^2}\boldsymbol{v} \quad \text{(Eq. 3)}$$

$$0 = -\boldsymbol{\nabla P} + \mu\nabla^2\boldsymbol{v} + \frac{150\mu(1-\varepsilon)^2}{\varepsilon^3 D_p^2}\boldsymbol{v} \quad \text{(Eq. 4)}$$

$$\varepsilon V\frac{\partial C}{\partial t} = \varepsilon V(-\boldsymbol{v}\cdot\boldsymbol{\nabla} + D\boldsymbol{\nabla^2})C - \frac{(1-\varepsilon)V}{V_{Bead}}A_{Bead}\frac{d\Gamma_s}{dt} \quad \text{(Eq. 5)}$$

$$\frac{d\Gamma_s}{dt} = k_{on}C\left(\Gamma_{s_{max}} - \Gamma_s\right) - k_{off}\Gamma_s \quad \text{(Eq. 6)}$$

$$(1-\varepsilon)V\frac{A_{bead}}{V_{bead}}\frac{d\Gamma_s}{dt} = (1-\varepsilon)V\frac{A_{bead}}{V_{bead}}\left(k_{on}C\left(\frac{N_{max}}{A_{bead}} - \frac{N}{A_{bead}}\right) - k_{off}\frac{N}{A_{bead}}\right) \quad \text{(Eq. 7)}$$

$$(1-\varepsilon)V\frac{A_{Bead}}{V_{Bead}}\frac{d\Gamma_s}{dt} = (1-\varepsilon)V\left(k_{on}C\left(\Gamma_{V\,max} - \Gamma_V\right) - k_{off}\Gamma_V\right) \quad \text{(Eq. 8)}$$

$$\varepsilon V\frac{\partial C}{\partial t} = \varepsilon V(-\boldsymbol{v}\cdot\boldsymbol{\nabla} + D\boldsymbol{\nabla^2})C - (1-\varepsilon)V\left(k_{on}C\left(\Gamma_{V\,max} - \Gamma_V\right) - k_{off}\Gamma_V\right) \quad \text{(Eq. 9)}$$

The model is constructed in two parts, first, the fluid flow through the packed bed and second, the transport and surface binding of the analyte. The fluid flow is governed by the volume averaged Navier-Stokes equation (Eq. 1) and the continuity equation (Eq. 2), where ρ is the fluid density, $\boldsymbol{v}$ is the fluid velocity vector, $\boldsymbol{P}$ is pressure, μ is fluid dynamic viscosity, and $\boldsymbol{f}$ represents external forces. Within microfluidic systems, the Reynolds number is very low and flow is therefore laminar. It is assumed that the fluid is incompressible (i.e. of constant density) and fully developed at the inlet. Therefore, the left side of Eq. 1 can be assumed to be zero [22].

The presence of the packed bed is accounted for as a volume-averaged pressure drop term, $\boldsymbol{P_{bed,}}$ which reflects the average frictional loss as fluid moves through the bed. This pressure drop can be estimated using the Ergun equation for laminar flow (Eq. 3), where ε is the void fraction and D_p is the diameter of the particles that comprise the packed bed. This frictional loss term is set to zero outside the packed bed and Eq. 4 is solved in conjunction with the continuity equation for incompressible fluids (Eq. 2) to obtain the coarse grained velocity field throughout the packed bed [24]. This approach is meant to account for the overall effect of the packed bead bed on the fluid dynamics within our model. It is important to note that this volume-averaged method is not intended to represent microscopic flow profiles within the bed.

Analyte transport and binding are governed by the Convection-Diffusion equation with an added source term for the binding reaction derived from mass conservation of the analyte (Eq. 5), where V is total volume of the packed bed, C is the analyte concentration in the bulk fluid, D is the effective analyte diffusivity, Γ_s is the surface concentration of the bound analyte, and A_{Bead} and V_{Bead} are the surface area and volume per bead, respectively. The effective molecular diffusion coefficient was used in lieu of the effective dispersion coefficient as dispersion is negligible in all geometries considered in our simulations [25]. This equation considers the rate of change of the total number of molecules of the analyte, given by the volume of fluid εV and bulk concentration C, or the area of the bead surface (the bead phase volume $(1-\varepsilon)V$ scaled by the bead surface area to volume ratio A_{Bead}/V_{Bead}) and surface concentration Γ_s. Applying mass conservation shows that rate of change of the number of analyte molecules in a fluid element in the packed bed is given by the diffusive and convective transport rate of molecules in and out of the element and the rate of loss due to binding to the surface. Second order binding kinetics determines the rate of surface binding with rate constants k_{on} and k_{off} and the total density of binding sites available $\Gamma_{s\,max} - \Gamma_s$, shown in Eq. 6. Summing the convective and diffusive transport terms with the binding term yields the full reaction diffusion equation (Eq 5). The surface reaction can then be converted to a volumetric reaction by rewriting the Γ_s in the last term in Eq. 5 as a ratio of the number of moles (N) to the area of bead and multiplied by $A_{Bead}\,V_{Bead}^{-1}$, yielding Eq. 7. The A_{Bead} terms cancel, and the number of moles per bead volume can then be replaced with a volumetric

concentration, Γ_V, as shown in Eq. 8. This equation can then be inserted into Eq. 5 to produce Eq. 9. This derivation is consistent with validated chromatography models [26-27].

Constant	Biocytin-Alexafluor488	IL-6
ε	0.36[28]	
ρ (kg m^{-3})	998.2[29]	
μ (kg m^{-1} s^{-1})	0.001003[29]	
D_p (μm)	5.8*	6.5*
Γ_{max} (mol m^{-3})	0.0889*	0.013857*
k_{on} (M^{-1} s^{-1})	10^{7} [30]	10^{6} [19]
k_{off} (s^{-1})	10^{-5} [d]	10^{-3} [e]
D (m^2 s^{-1})	7.292×10^{-11} [31]	2.206×10^{-11} [31]

Table 2.1: Constants used in simulations.

*As per manufacturer specifications

Computational Methods

The simulation is restricted to the packed bed within the device as we assume negligible analyte binding occurs on the channel walls upstream of the reaction chamber. All operations pertaining to the mathematical model (i.e., generating geometries, meshing, and solving) are performed within Ansys

Workbench (Ansys, Inc, Canonsburg, PA) in different subprograms handling each individual unit operation. The first step is the construction of a simplified 3D model of the reaction chamber consisting of the bead bed and a 7 μm tall outlet region in Ansys DesignModeler. This geometry is then imported into Ansys Meshing, where it is discretized and a mesh is created. The mesh is then imported into Fluent, a computational fluid dynamics software package, where the fluid flow and transport-binding equations are solved simultaneously. The physical velocity porous formulation in Fluent is used to model the presence of random close packed beads and incorporate the pressure drop and velocity change due to the packed bed (Eq. 3) in order to solve the modified Navier-Stokes equation (Eq. 4). The transport-binding equation (Eq. 9) is solved using a user-defined function. The concentration of analyte, capture molecule, and captured analyte complex are each modeled as scalar fields defined across each cell in the mesh geometry using the user-defined scalar mode. The convection terms are provided by the fluid velocity field, and analyte diffusivity is estimated from molecular weight [31] with corrections for the tortuosity of the packed bed [32]. The consumption and production of the reaction species (e.g. the last term on the right of Eq.9) are modeled as source terms. The solution methods in Fluent are as follows: SIMPLE scheme for pressure velocity coupling, Green-Gauss Node Based gradient calculation method, Standard pressure equation solver, Second Order Upwind discretization scheme for momentum and user defined scalars, first order implicit transient formulation, and the default adaptive time stepping method [33]. The output of the model is moles of analyte bound at each time step,

calculated by a volume integral of the molar concentration of the antibody-analyte complex over the reaction volume. A text file is written containing the amount of protein bound at each time step. For the validation experiments, the constants used are for a model system of streptavidin coated beads and biocytin-Alexafluor 488 solutions. The Design of Experiments (DOE) and optimization were performed using parameters for IL-6 and typical binding constants for antibody-antigen interactions. Table 2.1 contains the values for the constants used in simulations.

Optimization Platform

An optimization software package, modeFrontier (ESTECO, Trieste, Italy), is used to sequentially iterate the simulations during the DOE and optimization runs. The workflow for the DOE and optimization studies is shown in Figure 2.2. Ranges for the length, width, and height of the reaction chamber and flow rate are defined by the user. For each simulation, the software calculates the flow velocity, minimum mesh element size, maximum mesh face size, and maximum mesh element size based on the input parameters. These calculated parameters are fed into Ansys Workbench which completes the simulation workflow described above. The output text file is read by modeFrontier at the completion of the simulation and used to calculate the amount of flow time needed to reach the limit of detection (LOD). We used the LOD of a typical flow cytometer of 750 fluorescein molecules per event as provided by the manufacturer [34]. However, our goal is to optimize the device for Luminex bead based multiplex assays that utilize phycoerythrin. To estimate the LOD using this fluorophore, we assumed

brightness at the same concentration using the same excitation source is proportional to the ratio of the product of the extinction coefficient and the quantum yield [35]. Therefore, we estimated the LOD to be 42 phycoerythrin molecules per bead. The incubation time needed to reach this threshold is multiplied by the flow rate, yielding the sample volume required to reach the detection limit.

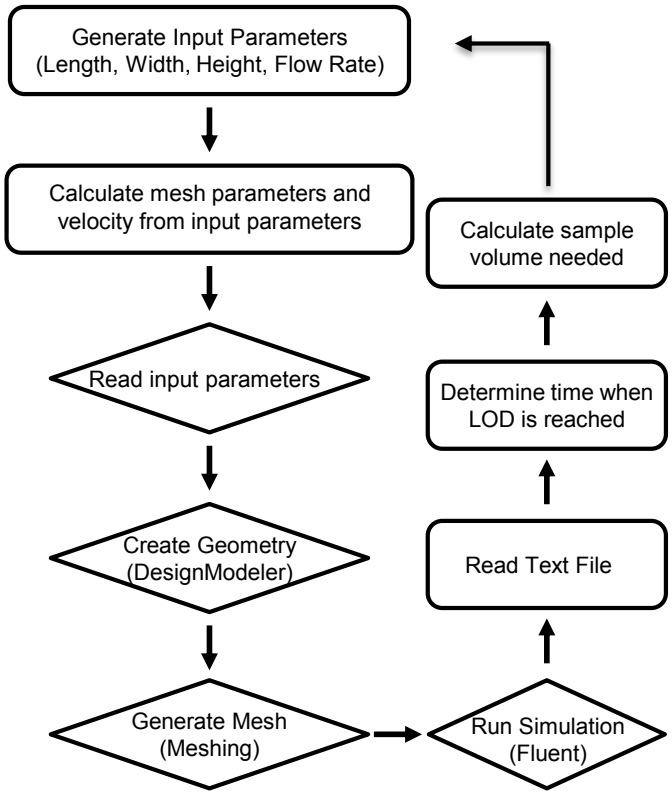

Figure 2.2: Schematic representation of the optimization workflow.

Operations in rectangles and diamonds are performed in modeFrontier and Ansys Workbench, respectively. The velocity and meshing parameters are calculated from the input parameters and fed into Ansys Workbench. The geometry is created in Ansys DesignModeler and exported to Ansys Meshing to

discretize the volume. Ansys Fluent solves the governing equation and outputs a text file containing the amount of protein bound in the bead bed at each time step calculated as a volume integral of antibody-antigen complex concentration across the reaction volume. The text file is read by modeFrontier and the data is used to determine the time at which the LOD has been reached. The sample volume is calculated from the product of incubation time required to reach the LOD and the flow rate. For DOE, the process is repeated for the next set of input parameters from the full factorial experimental design. For optimization studies, the algorithm adjusts the input parameters in an attempt to minimize the design objectives

Design of Experiments and Optimization

The goal of these studies is to determine the assay parameters that will minimize the required sample volume and incubation time. The design parameters of the proposed device are the length, width, and height of the bead bed. The height will be limited to between 25 and 41 microns, as shorter channels are highly susceptible to clogging of microbeads and fabricating taller channels becomes a more difficult and tedious fabrication process. The width (W) will be constrained between 25 and 300 μm, as our experience with this device has shown that wider channels results in uneven packing of bead beds. The length (L) of the bed will be constrained between 25 and 50 μm. Model convergence becomes an issue with a bed length of less than 25 μm, and the pressure drop across the bed becomes too large with a length over 50. Additionally, these parameters dictate the number of antibody-conjugated beads

as determined by multiplying the volume of the reaction chamber by the solid volume fraction and dividing by the volume of a single bead. Furthermore, the operating parameter of interest is the flow rate of the sample solution. The flow rate was constrained to between 5 nL/min (the slowest flow able to be generated using our syringe pump) and 100 nL/min. With these constraints, the concentration of analyte at the inlet was set to 358 fM (10 pg/mL IL-6 [36]) in an effort to optimize a highly sensitive assay.

Exploration of the effects of assay parameters within the design space was accomplished by utilizing DOE. Three levels were used for the length, width, and height, corresponding to the constraints specified above as well as a center point. For the flow rate, 15 levels were used in an effort to determine the reaction limited and transport limited operating states of the immunoassay. The experimental matrix was constructed utilizing a full factorial experimental matrix totaling 405 combinations. This relatively large number of simulations was utilized to capture any possible non-linear effects [37]. The calculation of incubation time and volume needed to reach the detection limit as well as the determination of main factor and interaction effects was performed in modeFrontier.

Multi-objective optimization was performed in modeFrontier using the Hybrid algorithm. In brief, an initial group of 10 design combinations was generated using a Uniform Latin Hypercube DOE. A child population was then created using a sequential quadratic programming (SQP) algorithm, a gradient based method using derivative approximations [38]. The combined population was then evaluated by a second generation non-dominated sorting genetic algorithm

(NSGAII) [39] that identified the optimal designs. The best designs were chosen to become the new parent population and the process was repeated for a total of 1000 simulations. Minimization of the time to perform the assay and the necessary sample volume were set as design objectives. At the conclusion of the simulations, the software determined Pareto-optimal solutions. The data was exported to Excel (Microsoft, Redmond, WA) and Matlab (Mathworks, Natick, MA) for plotting.

Experimental Methods

Device Fabrication

The device consists of two layers to facilitate the incorporation of pneumatic valves. Therefore, molds are fabricated on two separate silicon wafers, one for the fluidic network and one for the control layer using standard photolithography techniques [40]. The fluidic layer requires three separate photolithography steps. First, the beads traps are patterned using SU-8 2007 (MicroChem Corp., Newton MA) at a height of 7 μm. These features are only 3 μm wide, so the temperature was ramped during all baking steps to reduce interfacial stress and prevent delamination. In addition, the exposure dose was reduced approximately 40% compared to manufacturer recommendations to improve resolution [41]. A flood exposure was performed after development followed by a hard bake to mitigate the effect of underexposure on the mechanical integrity of the features. The valve layer is then patterned in a 36 μm layer of AZ9260 (AZ Electronic Materials) deposited in 3 sequential 12 μm spin coating steps, each followed by a baking step. Following development, the wafer

is baked above the glass transition temperature of the photoresist causing reflow, rounding the features and allowing complete closure of the channels at these locations [21, 42]. The final layer of the fluidic channel structure is fabricated using a 41 μm layer of SU-8 2025 according to manufacturer recommendations, as is the control layer on a separate wafer.

The fluidic mold is then cast in Smooth-Cast 325 Colormatch polyurethane (Smooth-On, Inc., Easton PA, 48841) as previously described [43] to prevent wearing of the silicon mold during repeated replica molding processing. The device is then fabricated using multilayer soft lithography techniques [21, 44]. Briefly, the control wafer is spin coated with a 60 μm layer [45] of (poly)dimethylsiloxane (PDMS) (Sylgard 184, Dow Corning, Midland, MI). The fluidic network is then cast with a thick layer of PDMS. The fluidic network is removed from the mold; the outlets are punched, and the devices are cleaned with scotch tape. The fluidic network is bonded to the thin layer utilizing oxygen plasma treatment followed by manual alignment using a stereomicroscope. After bonding is complete, the assembly is removed and bonded to a glass slide [46]. A schematic of the fabrication process is shown in Figure 2.3.

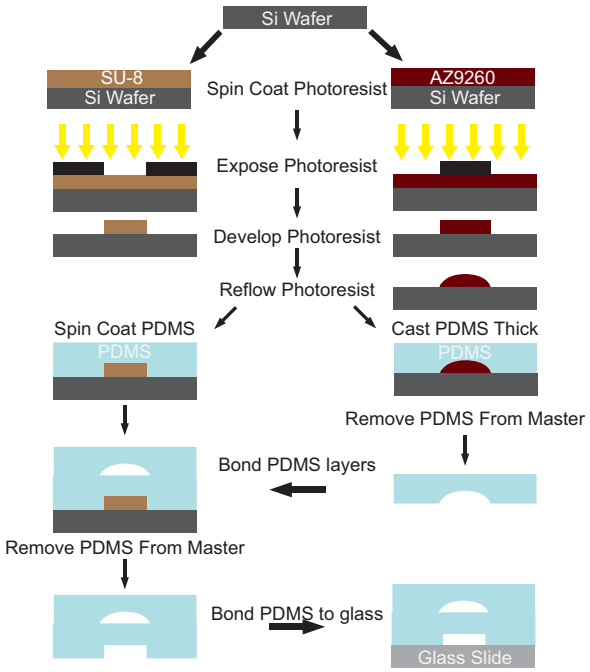

Figure 2.3: Schematic of the device fabrication procedure

Each photolithography step is represented by a single color in the device schematic in Figure 2.1b. All layers are fabricated using SU-8 with the exception of the valve seats which are made using AZ9260. Photolithography is performed using standard techniques. The AZ9260 layer is reflowed after development to create rounded channel architecture necessary for complete pneumatic valve closure. The fluidic layer and control layers are fabricated on two separate wafers. The fluidic layer is created by casting a thick layer of PDMS, while the control layer is spin-coated with PDMS yielding a thin layer. The thick layer is bonded to the thin layer, and then both layers are bonded to a glass slide

Model Validation Experiments

Devices were primed by submerging them in deionized (DI) water under vacuum overnight. Once primed, the control lines were pumped with DI water to

remove any remaining bubbles. The control channels were then connected to a compressed air tank equipped with a precision air regulator (McMaster Carr, Robbinsville, NJ, 6162K22). Prior to the assay, the channels are pressurized until closure and the pressure is not changed for the duration of the assay (typically around 40 psi). All reagents were loaded into 1 mL Luer-Lok syringes (BD Biosciences, San Jose CA, 309628) fitted with 30 gauge needles (BD Biosciences, San Jose CA, 305128) connected to Tygon microbore tubing (US Plastic Corporation, Lima OH, 56514) and infused using a syringe pump (Harvard Apparatus, Holliston, MA, 55-3333). First, the devices are flowed with 0.5% bovine serum albumin (BSA) in phosphate buffered saline (PBS) for 5 minutes at 10 μL/min to prevent analyte adsorption to the channel walls. Then, the device is flushed with PBS for 5 minutes at 10 μL/min to remove the unbound BSA.

The mathematical model was validated using a model antibody antigen binding system comprised of streptavidin coated beads (5.8 μm diameter, Bang's Laboratories, Inc., Fishers, IN, CM01N) and Alexa Fluor 488 biocytin (Molecular Probes, Eugene, OR, A12924). The microbeads were first washed in PBS by suspending 10 μl of beads in 990 μL of PBS and then resuspending in 1 mL Ficoll-Paque Plus (GE Healthcare). The bead solution was flowed into the channels at 10 μL/min until the beds were packed with the pneumatic valve 1 closed. The device was then flushed with PBS to fully pack the bead beds and remove the Ficoll-Paque from the device. Each sample inlet was then connected to a separate syringe loaded in a syringe pump with a multi syringe rack (Harvard

Apparatus, Holliston, MA, 70-2020) and samples were flowed at 500 nL/min for 3 hours over the bead bed with pneumatic valve 2 closed to prevent mixing of sample streams. For the time-lapse validation experiments, a 10 ng/mL solution of biocytin-Alexafluor 488 was made in PBS and loaded into eight separate syringes and images were taken at 3 minute intervals. For the validation experiments performed using different concentrations, 10-fold dilutions were made (10 ng/mL, 1 ng/mL, 100 pg/mL, and 10 pg/mL biocytin-AlexaFluor 488) and each concentration was loaded into two syringes to perform duplicate measurements. In both experiments, PBS was flowed at 10 µL/min for 5 minutes with pneumatic valve 1 closed immediately following incubation as a wash step. Next, all valves were opened and the sample syringes were removed, leaving only the tubing connected to the sample inlets. Another wash was performed at 10 µL/min for an additional 5 minutes to remove any residual sample from the tubing. Finally, PBS was flowed by hand through the outlet to collect the beads. The samples were then analyzed via flow cytometry.

Fluorescence Microscopy and Time Lapse Model Comparison

Fluorescent images were taken using an Olympus IX81 inverted microscope (Center Valley, PA) equipped with a XM10 digital camera and an automated stage and an EXFO X-Cite 120 fluorescent light source. Image capture and processing was performed using Olympus cellSens Dimension software. Images were captured at 3 minute intervals and processed by manually creating masks of the bead bed and a background area within the microchannel upstream of the beads. The mean fluorescence intensity of the

background was subtracted from the beads at each frame and the data was exported to Excel. The data was normalized by subtracting the minimum value of the time series and dividing by the range of fluorescence intensities. To validate the model's predictive capabilities, binding was modeled at the same flow rate and concentration and the data was normalized by dividing the amount bound at each time step by the amount bound at 3 hours.

Flow Cytometry

Beads were suspended in PBS, transferred to BD Falcon round bottom tubes (BD Biosciences, San Jose, CA, 352008), and vortexed prior to analysis. Samples were analyzed using a BD FACSCalibur and the mean fluorescence intensity of each bead population was extracted with BD CellQuest Software (BD Biosciences, San Jose, CA).

Flow Cytometry Data Analysis and Model Comparison

A standard curve using the same beads as the on-chip experiments was generated by incubating varying concentrations of biocytin-Alexafluor488 with a fixed number of microbeads in an Eppendorf tube and vortexing overnight. The beads were washed 3 times, resuspended in PBS, and analyzed via flow cytometry. Normalized fluorescence intensity was calculated by dividing the mean fluorescence of each data point by the measured fluorescence of the highest concentration. The saturation concentration was identified as the lowest concentration that resulted in the maximum measured fluorescence. Normalized concentration was then calculated by dividing each concentration by the

saturation concentration, and a plot of normalized concentration vs. normalized fluorescence was created and fitted with a 5-parameter logistic fit using Matlab.

The data from the validation experiments was then analyzed by normalizing the results from each experiment by dividing each measurement by the average of the highest concentration. The normalized data was processed using the 5-parameter logistic fit to yield normalized binding. To test the model accuracy, binding was simulated under the same flow rate and concentrations used in experiments. The predicted binding from the simulation was normalized by dividing the amount bound at 3 hours for each concentration by the concentration of binding sites on the beads as per manufacturer specifications.

On-Chip Immunoassay Experiment

On-chip immunoassay was performed using the Bio-Plex Pro Human Cytokine IL-6 antibody set, Cytokine Reagent Kit, and cytokine standards (Bio-Rad Laboratories Inc, Hercules, CA, 171304070M, 171D50001, and 171B5006M, respectively). All reagents were prepared as per manufacturer recommendations, with the standards reconstituted and diluted in 0.5% BSA in PBS. The device was operated similarly to the validation experiments described previously with some minor changes. First, Bio-Plex Pro assay buffer was used in the channel blocking and bead collection steps. In addition, Bio-plex Pro wash buffer was used instead of PBS for all wash steps. Finally, the flow rate for the sample, biotinylated detection antibody, and streptavidin-phycoerythrin incubation steps were 5, 50, and 50 nL/min and performed for 4.5, 1.5, and 0.5 hours, respectively. At the completion of the assay, the beads were collected

and transferred to a 96 well plate and analyzed using the Bio-Plex 200 system as per manufacturer recommendations. The raw event data for each bead was exported into Matlab for analysis.

Scanning Electron Microscopy

Silicon molds were cleaned using filtered compressed air and IPA, cut and taped to sample mounts. Samples were then coated using a SCD 004 Sputter Coater (Balzers Union Limited, Balzers Union Limited, Liechtenstein) loaded with a gold/palladium target and imaged using an Amray 1830I Scanning Electron Microscope (Amray, Inc., Bedford MA).

Statistical Analyses

Regression analysis was performed by plotting the normalized predicted binding versus the normalized experimental binding under the same conditions, fitting a linear regression, and calculating the R^2 value in Excel. The experimental and simulated data were also compared by a lack of fit sum of squares test. This test is performed by calculating an F-statistic (F*) which takes into account the error between the model and experimental results (lack of fit) as well as the experimental variance (pure error). The null hypothesis is no lack of fit exists between the model and experimental data. If the test statistic is greater than a critical value ($F_{critical}$) at a chosen significance level (α), the null hypothesis is rejected [37]. Since accepting the null hypothesis will allow us to conclude that the model accurately predicts our experimental system, a high significance level (α=0.25) was chosen to ensure model validity. One-way analysis of variance (ANOVA) with α=0.05 was performed using Kaleidagraph (Synergy Software,

Reading, PA). This statistical test determines whether the differences between the mean of two or more groups are statistically significant or not significant (NS), with a null hypothesis that the means of the groups are equal. In both the lack of fit sum of squares test and ANOVA, the p-value represents the probability of obtaining a test statistic at least as extreme as was observed, given that the null hypothesis is true. Full factorial experimental matrix generation, DOE data analysis, and selection of optimal designs were performed in modeFrontier.

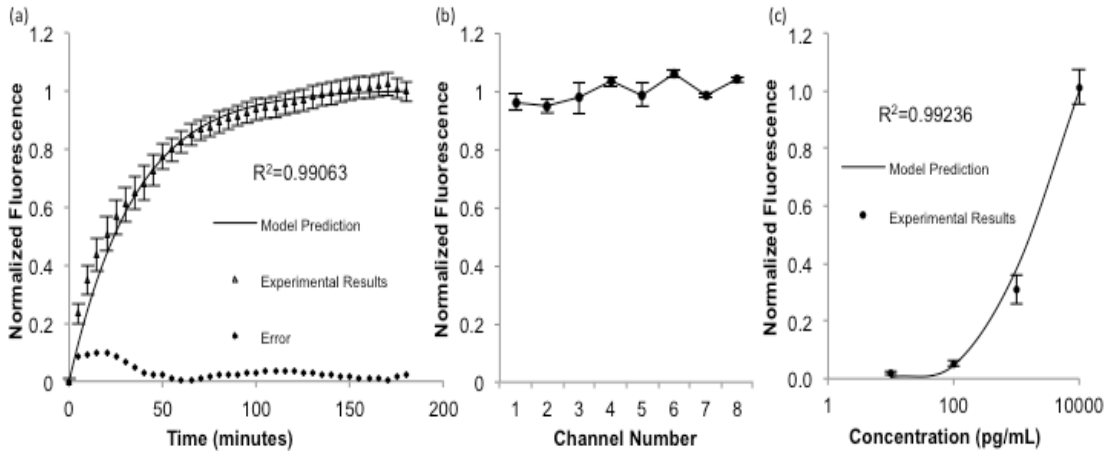

Figure 2.4: Model Validation

a) Comparison of model predictions with time lapse fluorescence data using 10 ng/mL concentrations of biocytin-Alexafluor 488 in all eight sample inlets. Error is defined as the difference between the model prediction and experimental results (n=24, R2=0.99063, p>0.25 by lack-of-fit sum of squares test) b) Beads from the time lapse experiment were collected and analyzed by flow cytometry, with no significant difference in the measured fluorescence between device channels (n=6, NS, p=0.14 by one way ANOVA) c) Different concentrations were each flowed through two sample inlets, collected, analyzed by flow cytometry,

and compared with model predictions. (n=6, R2=0.99236, p>0.25 by lack-of-fit sum of squares test). Error bars represent standard error of the mean

Results and Discussion

Model Validation

Prior to performing optimization the mathematical model was experimentally validated in order to ensure its accuracy. For the validation experiments, a model system for antibody antigen binding consisting of streptavidin coated microbeads and biocytin-AlexaFluor 488 was employed. This approach has been used in prior publications as a model system of antibody-antigen binding as it provides several advantages [47-48]. These include increased reaction speed, lower cost compared to antibody conjugated beads, and a one step reaction allowing for direct interrogation in real time using fluorescent microscopy. This allows binding curves to be experimentally constructed in order to directly compare CFD simulations to experimental results.

The first validation experiment was performed by flowing 10 ng/mL biocytin-AlexaFluor488 over a packed bed of streptavidin coated microbeads at a flow rate of 500 nL/min through all eight sample inlets simultaneously. The fluorescence intensity in the bead bed was captured over time and compared to normalized predicted binding of the mathematical model using the same inlet concentration and flow rate. The comparison of the predicted and experimental results is shown in Figure 2.4. Visual inspection of the results reveals a strong agreement between the predicted values of the mathematical model and the

observed results in the device. The error, defined as the difference between the model prediction and experimental results, is largest initially while the rate of binding is highest and decreases as the binding curve plateaus. The accuracy of the simulations is further validated through statistical analysis. Regression analysis shows a very good correlation between the data as shown in Figure 2.4a (R^2=0.99063). In addition, a lack of fit sum of squares test was performed and revealed that no significant differences exist between the model predictions and experimental results (F^*=0.47326<$F_{critical}$ at α=0.25). At the conclusion of these time-lapse experiments, the beads were collected and analyzed via flow cytometry with the results shown in Figure 2.4b. The data shows that measurements in the device are reproducible and independent of position (NS, p=0.14 by one way ANOVA). This will ensure that measurements from different channels are comparable to facilitate the construction of standard curves and quantification of sample concentrations.

For the second validation experiment, 4 different concentrations of biocytin-AlexaFluor488 were flowed simultaneously over the bead beds at 500 nL/min for 3 hours. The beads were then washed and collected for analysis using flow cytometry. Identical conditions were simulated, and a comparison of the results is shown in Figure 2.4c. Once again, a good correlation was observed through regression analysis (R^2=0.99236) and the lack of fit sum of squares test confirmed the model is accurate (F^*=0.16<$F_{critical}$ at α=0.25). Together, the validation experiments provide statistical evidence that the mathematical model accurately predicts binding in our experimental system.

Therefore, it can be appropriately utilized to aid in optimization of assay parameters to minimize the amount of required sample volume and incubation time.

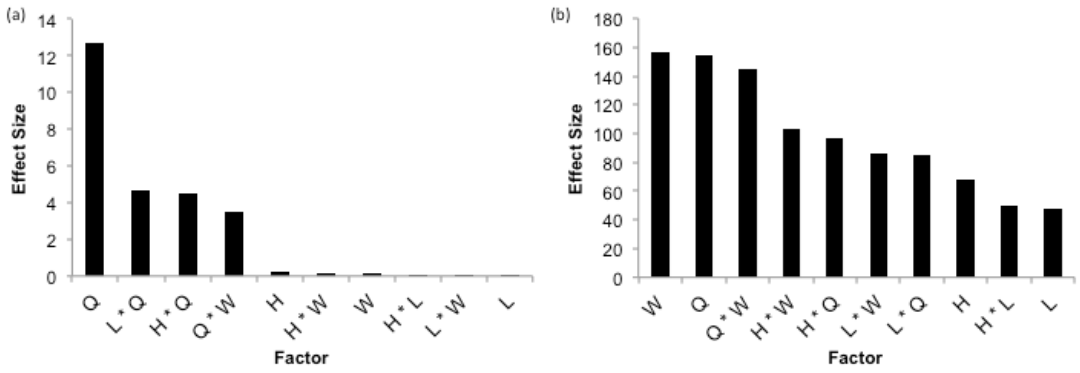

Figure 2.5: Results of DOE.

Effect of input parameters on a) required sample volume and b) incubation time required to reach the LOD. An asterisk denotes an interaction between two factors. H=Height, L=Length, Q=Flow Rate, W=Width

Exploration of Design Parameters Using DOE

With a validated mathematical model, a full factorial DOE was used to explore the effect of the design parameters. The length, width, and height of the reaction zone were varied at three levels. These parameters also determine the number of antibody-coated microbeads that are modeled. The different combinations of geometric parameters resulted in 27 different possible numbers of beads. The flow rate was modeled at 15 levels to determine when the transition occurs from the reaction to transport limited regimes. Three levels were used for all other parameters to ensure the ability to investigate possible non-linear effects.

The importance of each factor on the design objectives was determined by ranking the main factor and interaction effects. The effect sizes, which represent the strength of the relationship between the input parameter and a respective output parameter, were calculated in modeFrontier from the entire full factorial design dataset and the results are shown in Figure 2.5. An interaction effect, denoted by an asterisk, signifies that the effect of an input variable is not constant as the range of another parameter is varied. For example, if varying one input parameter when a second input parameter is at its minimum value affects the output differently than if the second input is at its maximum value, an interaction effect exists. The results of the DOE clearly demonstrate that the flow rate is the most important input parameter in determining the amount of sample volume needed, as its effect is almost three times as large as any other parameter. The only other factors that substantially affect volume are the interaction of the flow rate with each of the geometric parameters, each contributing to approximately the same extent. This can be explained by the fact that in these simulations the reaction volume (i.e. the product of length, width, and height) determines the number of microbeads and therefore antibodies that are present. However, alone each factor has almost no effect. Since only the interaction between the flow rate and the geometric parameters affects volume, this suggests that these parameters do not have an effect over the entire range of flow rates that were studied.

The most important factors in determining incubation time needed to reach the LOD are width and the flow rate. These factors alone had a very similar

effect size, with the interaction between the two having a slightly smaller effect. This can be explained by the fact that the velocity is dependent on the flow rate and cross sectional area of the channel, i.e. the product of width and height. It is the velocity, not the flow rate, which determines the local concentrations of analyte and therefore the binding rate, as can be seen in Eq. 5. Consequently, the interaction between width and height is the next most significant factor, followed closely by the height and flow rate interaction. It is logical to hypothesize that the height should affect time at the same magnitude as the width since they equally determine the velocity. However, width was varied over the largest range of any geometric parameter, thus having the largest effect on velocity and as a result, the incubation time. The interactions of the length with the width and flow rate were the next two largest effects, with the remainder of the factors impacting incubation time to a lesser extent. With these results, it is seen that the incubation time is much more sensitive to the geometry than the required sample volume.

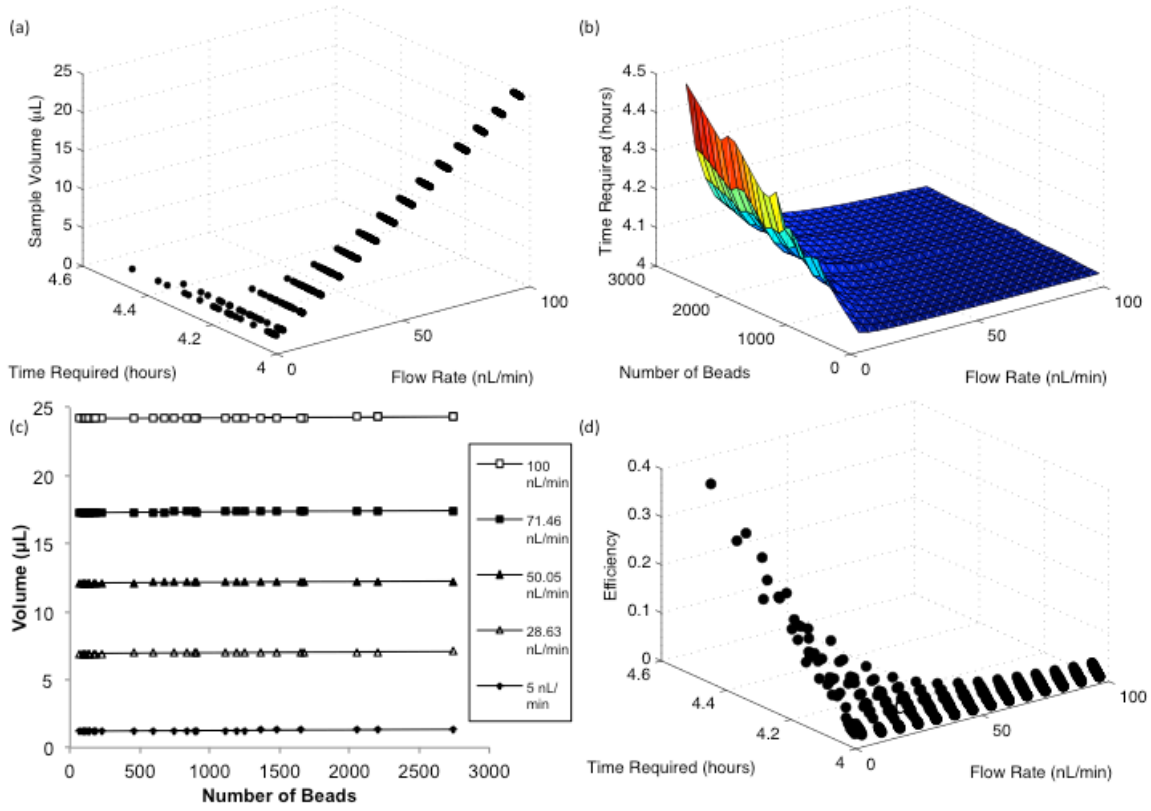

Figure 2.6: Full Factorial DOE results

a) Effect of the flow rate on the time and volume required to reach the limit of detection b) Effect of the number of beads on the time to reach LOD at different flow rates c) Effect of number of beads on the sample volume at selected flow rates d) Relationship between the flow rate, time required to reach the LOD, and the binding efficiency defined as the fraction of protein flowed through the channel that is bound

Due to the presence of interactions between design parameters revealed by the DOE, the results of the simulations were further analyzed. At higher flow rates, the amount of time required to perform the assay is relatively unchanged, regardless of the number of beads in the bed, shown in Figure 2.6a&b. As the

flow rate is decreased, the effect is greatly augmented. However, the sample volume remains essentially unaffected by the number of beads and is virtually solely dependent on the flow rate as shown in Figure 2.6c.

Since the required assay time is generally unaffected at higher flow rates, binding is not dependent on the amount of sample delivered to the reaction region. Furthermore, the efficiency of the reaction, defined as the fraction of protein flowed through the channel that binds, is very low at higher flow rates as shown in Figure 2.6d. However, at lower flow rates the number of beads has a clear effect on incubation time. Together, these results suggest the existence of different operating regimes that occur within our design space as the balance between convection, diffusion, and reaction is altered.

In order to investigate the balance between these phenomena the Peclet and Damkohler numbers were studied since these dimensionless quantities relate convection with diffusion, and reaction and convection, respectively [49]. The effect of these numbers on the product of time and volume was investigated and is shown in Figure 2.7. It is obvious that it is most advantageous to minimize the Peclet number. At higher Peclet numbers, convection occurs faster than diffusion and the reaction zone is not well mixed. However, minimizing the Peclet number is not sufficient as a concomitant increase in the Damkohler number to approximately 40 is necessary in order to minimize time and volume required for the assay. This signifies an increase in the residence time of the sample within the bed accomplished by decreasing the fluid velocity resulting in more time for the protein to bind. However, a large bead bed and slowed

convection causes the solution concentration to decrease along the length of the bed. This results in increased assay time, causing a plateauing of the effect of increasing the Damkohler number at a low Peclet number.

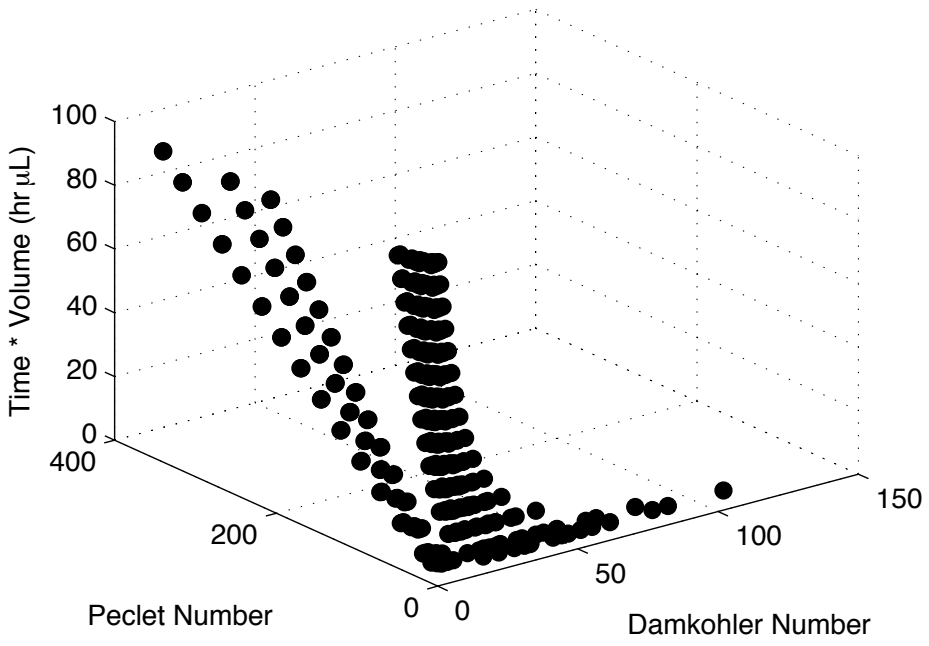

Figure 2.7: Effect of the Damkohler Number and the Peclet Number on the product of the incubation time required to reach the LOD and the necessary sample volume. Low Peclet numbers (<10) and Damkohler Numbers greater than 40 results in the minimization of the incubation time and sample volume needed to perform an assay.

These conclusions explain the results of the full factorial matrix (Figure 2.6). The increased convection at higher flow rates does not allow enough time for the reaction to occur resulting in a reaction-limited regime where the rate of binding is only determined by the affinity of the antibody for the protein. As

convection is slowed, the efficiency increases. However, a point is reached where the reaction is occurring faster than protein can be transported to the bead surface (i.e. higher Damkohler and low Peclet numbers) and the amount of time required to reach the limit of detection begins to increase. At the transition between these two regimes, the product of sample volume and reaction time are minimized. In the presented design space, this occurs when the Peclet number is less than 10 and the Damkohler number approaches 40, as shown in Figure 2.7.

Model-driven Multi-Objective Optimization

Optimization was performed using the Hybrid Algorithm in modeFrontier with the same parameter constraints as the DOE. This technique is a combination of a NSGAII algorithm and an SQP optimizer and was chosen for its ability to handle multiple objectives with continuous variables. All the simulations included in the optimization and the optimal designs of the Pareto frontier as are shown in Figure 2.8a and Figure 2.8b, respectively. In result of the trade-off between time and volume, no design combination exists that minimizes both objectives. Therefore, a large number of designs are selected as optimum as shown in Figure 2.8c. These designs encompass a large range of flow rates, but the number of beads converges to the lower range of the allowable number of beads, shown in Figure 2.8d. This corroborates the fact that a high efficiency is not an important design consideration as efficiency increases with the number of beads in the reaction region. In addition, amongst the optimal parameter combinations very little incubation time must be sacrificed to greatly reduce

sample volume. While this holds true when the number of beads is low, this trade off becomes more pronounced as the bead number is increased, as shown in Figs. 6a&b.

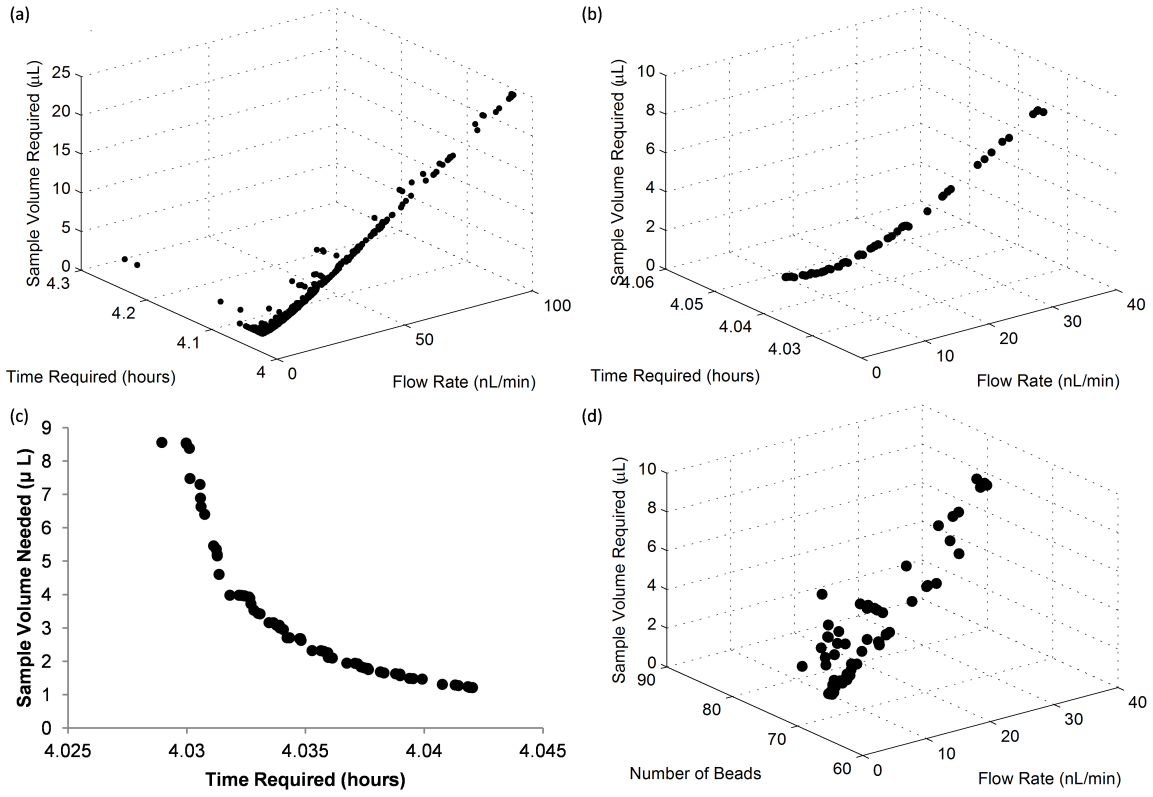

Figure 2.8: Optimization Results
a) All design points included in the optimization b) Designs selected as optimal designs. c) Trade off between design objectives of optimal designs d) Number of beads for optimal designs shown in b.

Although the optimization algorithm minimized the number of microbeads in the chosen Pareto designs (Figure 2.8d), the number of beads required for analysis is an important consideration that must be accounted for in our experimental system. The Bio-Plex 200 system used in our on-chip experiments requires a minimum of 50 beads to perform an assay. To ensure that sufficient beads are recovered from the device, it is necessary to incubate more than the

minimum number of beads to account for bead loss during the collection step. From our DOE, we concluded that the number of beads did not affect the amount of volume needed (Figure 2.6c), and only affect the time required by about 30 minutes, across the entire design space (Figure 2.6b). From an experimental standpoint, a modest increase in incubation time is a necessary trade off required to ensure sufficient bead recovery. In addition, the relatively small increase in incubation time over the large range of bead numbers tested (70 to more than 2700) we can conclude that small variations will not significantly impact the results of the assay. This is advantageous in practice, as precise control of the number of beads in each channel is difficult to achieve. Small imperfections and inconsistencies between bead traps or debris trapped in the device during fabrication may cause changes in channel resistance and therefore alter the distribution of beads. These practical concerns led us to fill the reaction zone of our device approximately halfway with beads, yielding about 900 beads per channel. With this bed size, we incubated at a flow rate of 5 nL/min for 4.5 hours, slightly longer than our computational results suggest, to mitigate the effects of possible flow instabilities produced by the syringe pump at this very low flow rate. In our device, these parameters translate to a Peclet number of 1.29 and a Damkohler Number of 34.3, which provides a good balance between sample consumption and assay time (see Figure 2.7).

Optimized Low Volume Immunoassay

To demonstrate the utility of the mathematical model and optimization platform, a low volume on-chip immunoassay was performed using a commercially available

IL-6 kit. A standard curve was constructed consisting of 7 samples. A blank condition of 0.5% BSA with no IL-6 was also run to quantify the noise floor attributed to background proteins. Sample was flowed at 5 nL/min for 4.5 hours, consuming only 1.35 µL of sample. In addition, only 4.5 µL of detection antibody was used, a greater than 10 fold reduction compared to bench-top assays, resulting in a significant decrease in cost per sample. The standard curve resembles that of a standard bench-top assay using this kit, and the fluorescence intensity of the 10 pg/mL condition was greater than the blank, shown in Figure 2.9. The measurement of the noise floor in conjunction with the clear difference observed in the fluorescence between the 25 pg/mL and 10 pg/mL samples was used to determine that 10 pg/mL is above the detection limit of the assay. While it is ideal to calculate the LOD from the standard deviation of two independents measurements of a blank sample within a single device, this approach has been used previously to determine the LOD with only one sample [50]. This allowed maximization the number of samples processed in order to demonstrate the large dynamic range of the assay, ranging from 10 to 25,699 pg/mL. Therefore, the optimization studies were successful in designing a low volume immunoassay while maintaining high sensitivity and a large dynamic range.

The computational platform presented mitigates the need for empirical assay optimization. Performing sufficient experiments to meticulously explore the design space would be completely unfeasible, even when employing a partial factorial design with only three levels. However, the complicated relationship between the design variables and objectives would most likely not be captured

without an increased number of flow rates. In addition, experimental error resulting from expected variations in device fabrication, bead packing, and syringe pump flow rates would require replicate experiments. Together, the computational platform presented is a cheaper, less laborious, and more useful approach than empirical optimization. In addition, it can be used to optimize the device for different beads, proteins, and/or antibody affinities by simply altering constants. To the best of our knowledge, this is the first report of a model describing the reaction on the surface of microbeads in a packed bed configuration within a microfluidic device. Previous reports have modeled surface based reactions [16-18] and even attempted to optimize assays [19]. However, these studies were not experimentally validated and did not perform mathematical optimization.

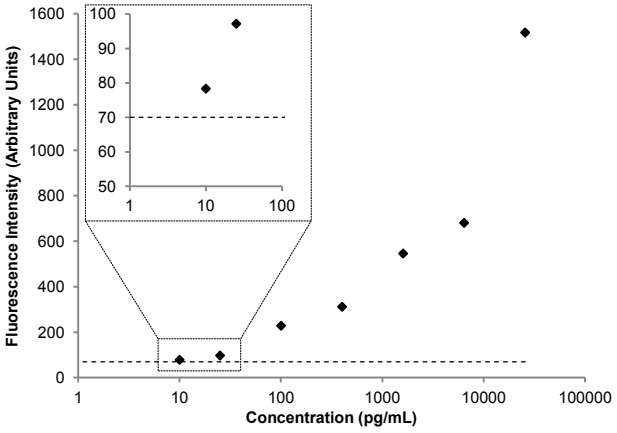

Figure 2.9: Results of low volume on chip IL6 immunoassay with optimal parameters.

The dotted line represents the noise floor of the assay, determined by measuring the fluorescence of a sample containing no IL-6

In conjunction with the optimization workflow, the device presented represents a platform technology with the ability to detect virtually any protein with an available antibody pair. In addition, it allows for the analysis of scarce samples while maintaining a high sensitivity and large dynamic range. However, the relatively long assay time (4.5 hours of sample incubation) may not be optimal for certain applications. This lengthy incubation is the result of reaction rate and cannot be increased, but a shorter incubation time is possible by sacrificing the high sensitivity of the assay. A previous report showed that a microfluidic immunoassay could be performed with an incubation time of only 20 minutes [10]. However, this assay was performed with an analyte concentration approximately four orders of magnitude greater than what was used in this study. This holds true in our system, as the desired LOD of the assay affects the required incubation time to a much higher degree than any of the input parameters explored in the DOE. For example, decreasing the assay sensitivity from 10 pg/mL to 50 pg/mL of IL-6 (358 fM to 1.79 pM) reduces the incubation time to less than 1 hour, as shown in Figure 2.10. In addition, the number of captured molecules needed to reach the limit of detection can be decreased by using quantum dots for fluorescence labeling [51] or introducing a signal amplification technique such as rolling circle amplification [52] to further decrease assay time and improve the sensitivity of this device. Furthermore, by incorporating Luminex beads the device can be expanded for multiplexing in a miniscule sample volume. This also results in a significant cost savings by drastically reducing the amount of antibodies and reagents needed. Finally,

although the current design possesses only 8 reaction zones, the design is scalable and can be easily expanded to facilitate many more samples.

Conclusions

In this work, we present a bead based microimmunoassay platform and computational assay optimization methodology which allow for a single device to be tailored to many analytes with minimal experimentation. Together, the advantages of this approach make it amendable to a variety of applications. One example is the analysis of cellular secretion profiles through in vitro studies. Typically, each time point of interest is assigned to an individual well to acquire sufficient volume for protein analysis. With this device, small volumes could be extracted at each time point, creating temporal secretion profiles using a single well. This capability will greatly reduce the amount of cells and media needed to carry out these studies. In addition, in vivo applications exist, for example analyzing scarce samples such as cerebrospinal fluid (CSF) in rodent models [53-54]. Moreover, the high-throughput, low-cost, and multiplexing capabilities of this technology also make it suitable for biomarker discovery studies [55]. Finally, this could be used in a clinical setting for the analysis of scarce clinical samples from pediatric or neonate patients [5].

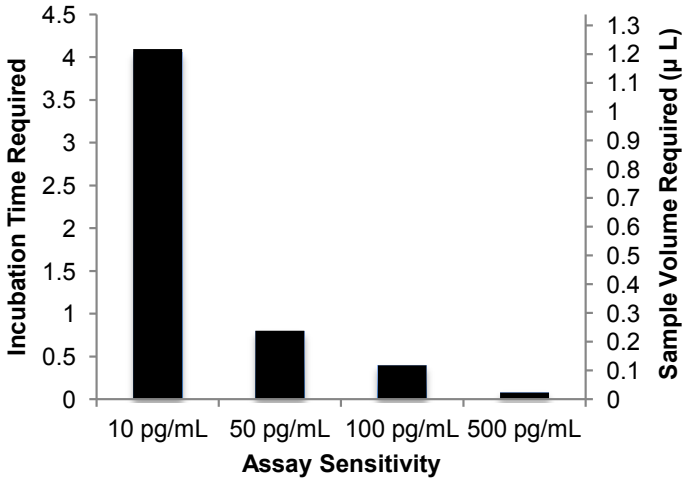

Figure 2.10: Effect of the desired assay sensitivity on the incubation time and sample volume required to perform the assay at a flow rate of 5 nL/min

Acknowledgements

This work was partially funded by the National Institute of Health Grants P41EB002503 and UH2TR000503, the National Institute of Health Rutgers Biotechnology Training Program (T32GM008339), and the National Science Foundation Integrated Science and Engineering of Stem Cells Program (DGE0801620). The authors would like to thank Dr. Sara Salahi, Dr. Kellie Anderson, and Anwesha Chaudhury for productive conversations regarding computational and optimization issues, Dana Barrasso for guidance pertaining to statistical analysis, Dr. Bhaskar Mitra for support in developing the fabrication protocols, and modeFrontier customer support for extensive troubleshooting of the optimization platform.

References

1. Diercks, A.; Ozinsky, A.; Hansen, C.; Spotts, J.; Rodriguez, D.; Aderem, A., A microfluidic device for multiplexed protein detection in nano-liter volumes. *Analytical Biochemistry* **2009,** *386* (1), 30-35.

2. Henares, T. G.; Mizutani, F.; Hisamoto, H., Current development in microfluidic immunosensing chip. *Anal. Chim. Acta* **2008,** *611* (1), 17-30.
3. Wild, D., *The immunoassay handbook*. Elsevier Ltd.: San Diego, 2005.
4. Ng, A. H. C.; Uddayasankar, U.; Wheeler, A. R., Immunoassays in microfluidic systems. *Anal. Bioanal. Chem.* **2010,** *397* (3), 991-1007.
5. Phillips, T. M., Rapid analysis of inflammatory cytokines in cerebrospinal fluid using chip-based immunoaffinity electrophoresis. *Electrophoresis* **2004,** *25* (1011), 1652-1659.
6. Bange, A.; Halsall, H.; Heineman, W., Microfluidic immunosensor systems. *Biosensors and Bioelectronics* **2005,** *20* (12), 2488-2503.
7. Derveaux, S.; Stubbe, B. G.; Braeckmans, K.; Roelant, C.; Sato, K.; Demeester, J.; Smedt, S. C., Synergism between particle-based multiplexing and microfluidics technologies may bring diagnostics closer to the patient. *Anal. Bioanal. Chem.* **2008,** *391* (7), 2453-2467.
8. Seong, G. H.; Crooks, R. M., Efficient mixing and reactions within microfluidic channels using microbead-supported catalysts. *Journal of the American Chemical Society* **2002,** *124* (45), 13360-13361.
9. Beebe, D. J.; Mensing, G. A.; Walker, G. M., Physics and Applications of Microfluidics in Biology. *Annual Review of Biomedical Engineering* **2002,** *4* (1), 261-286.
10. Sato, K.; Tokeshi, M.; Odake, T.; Kimura, H.; Ooi, T.; Nakao, M.; Kitamori, T., Integration of an immunosorbent assay system: Analysis of secretory human immunoglobulin A on polystyrene beads in a microchip. *Anal. Chem.* **2000,** *72* (6), 1144-1147.
11. Wilson, R.; Cossins, A. R.; Spiller, D. G., Encoded microcarriers for high-throughput multiplexed detection. *Angew. Chem.-Int. Edit.* **2006,** *45* (37), 6104-6117.
12. Sato, K.; Yamanaka, M.; Takahashi, H.; Tokeshi, M.; Kimura, H.; Kitamori, T., Microchip‐based immunoassay system with branching multichannels for simultaneous determination of interferon‐γ. *Electrophoresis* **2002,** *23* (5), 734-739.
13. Shin, K. S.; Lee, S. W.; Han, K. C.; Kim, S. K.; Yang, E. K.; Park, J. H.; Ju, B. K.; Kang, J. Y.; Kim, T. S., Amplification of fluorescence with packed beads to enhance the sensitivity of miniaturized detection in microfluidic chip. *Biosensors and Bioelectronics* **2007,** *22* (9), 2261-2267.
14. Kong, J.; Jiang, L.; Su, X.; Qin, J.; Du, Y.; Lin, B., Integrated microfluidic immunoassay for the rapid determination of clenbuterol. *Lab Chip* **2009,** *9* (11), 1541-1547.
15. He, H.; Yuan, Y.; Wang, W.; Chiou, N.-R.; Epstein, A. J.; Lee, L. J., Design and testing of a microfluidic biochip for cytokine enzyme-linked immunosorbent assay. *Biomicrofluidics* **2009,** *3* (2), 022401.
16. Lionello, A.; Josserand, J.; Jensen, H.; Girault, H. H., Dynamic protein adsorption in microchannels by “stop-flow” and continuous flow. *Lab Chip* **2005,** *5* (10), 1096-1103.

17. Lionello, A.; Josserand, J.; Jensen, H.; Girault, H. H., Protein adsorption in static microsystems: effect of the surface to volume ratio. *Lab Chip* **2005,** *5* (3), 254-260.
18. Winz, R.; de los Rıos Gonzalez, A.; von Lieres, E.; Schmittel, M.; Wiechert, W. In *Simulation of a micro-analytical device for adsorbing substances from a fluid*, Proceedings of the European Comsol Conference, Grenoble, 2007; pp 736-741.
19. Zimmermann, M.; Delamarche, E.; Wolf, M.; Hunziker, P., Modeling and optimization of high-sensitivity, low-volume microfluidic-based surface immunoassays. *Biomedical microdevices* **2005,** *7* (2), 99-110.
20. Houser, B., Bio-Rad's Bio-Plex(R) suspension array system, xMAP technology overview. *Archives of physiology and biochemistry* **2012,** *118* (4), 192-6.
21. Unger, M. A.; Chou, H.-P.; Thorsen, T.; Scherer, A.; Quake, S. R., Monolithic Microfabricated Valves and Pumps by Multilayer Soft Lithography. *Science* **2000,** *288* (5463), 113-116.
22. Bird, R. B.; Stewart, W. E.; Lightfoot, E. N., *Transport phenomena*. Wiley: 2006.
23. Andersson, H.; van der Wijngaart, W.; Stemme, G., Micromachined filter-chamber array with passive valves for biochemical assays on beads. *Electrophoresis* **2001,** *22* (2), 249-257.
24. Wilkes, J. O., *Fluid mechanics for chemical engineers*. Prentice Hall PTR: Upper Saddle River, 2006.
25. Squires, T. M.; Quake, S. R., Microfluidics: Fluid physics at the nanoliter scale. *Reviews of modern physics* **2005,** *77* (3), 977.
26. Dimartino, S.; Boi, C.; Sarti, G. C., A validated model for the simulation of protein purification through affinity membrane chromatography. *Journal of Chromatography A* **2011,** *1218* (13), 1677-1690.
27. Boi, C.; Dimartino, S.; Sarti, G. C., Modelling and simulation of affinity membrane adsorption. *Journal of Chromatography A* **2007,** *1162* (1), 24-33.
28. Dullien, F. A., *Porous media: fluid transport and pore structure*. Access Online via Elsevier: 1991.
29. Haynes, W. M.; Lide, D. R.; Bruno, T. J., *CRC Handbook of Chemistry and Physics 2012-2013*. CRC press: 2012.
30. Piran, U.; Riordan, W. J., Dissociation rate constant of the biotin-streptavidin complex. *Journal of Immunological Methods* **1990,** *133* (1), 141-143.
31. He, L.; Niemeyer, B., A novel correlation for protein diffusion coefficients based on molecular weight and radius of gyration. *Biotechnology progress* **2003,** *19* (2), 544-548.
32. Froment, G. F.; Bischoff, K. B.; De Wilde, J., *Chemical reactor analysis and design*. Wiley New York: 1990; Vol. 2.
33. ANSYS, Fluent 13.0-User Manual. 2010.
34. BD BD FACSCalibur Flow Cytometry System Technical Specifications. http://www.bdbiosciences.com/documents/FACSCalibur_FlowCytometry_TechSpec.pdf.

35. Lichtman, J. W.; Conchello, J.-A., Fluorescence microscopy. *Nature Methods* **2005,** *2* (12), 910-919.
36. Toumpanakis, D.; Theodoros, V., Molecular mechanisms of action of Interleukin-6 (IL-6). *Pneumon* **2007,** *20*, 154-167.
37. Montgomery, D., Design and analysis of experiments. John Wiley & Sons, New York. Design and analysis of experiments. 7th ed. John Wiley & Sons, New York: 2009.
38. ESTECO, modeFRONTIER 4 User Manual. 2013.
39. Deb, K.; Pratap, A.; Agarwal, S.; Meyarivan, T., A fast and elitist multiobjective genetic algorithm: NSGA-II. *Evolutionary Computation, IEEE Transactions on* **2002,** *6* (2), 182-197.
40. Madou, M. J., *Fundamentals of microfabrication: the science of miniaturization*. CRC: 2002.
41. Chan-Park, M. B.; Zhang, J.; Yan, Y.; Yue, C., Fabrication of large SU-8 mold with high aspect ratio microchannels by UV exposure dose reduction. *Sensors and Actuators B: Chemical* **2004,** *101* (1), 175-182.
42. Fordyce, P. M.; Diaz-Botia, C.; DeRisi, J. L.; Gomez-Sjoberg, R., Systematic characterization of feature dimensions and closing pressures for microfluidic valves produced via photoresist reflow. *Lab Chip* **2012,** *12*, 4287-4295.
43. Desai, S. P.; Freeman, D. M.; Voldman, J., Plastic masters—rigid templates for soft lithography. *Lab Chip* **2009,** *9* (11), 1631-1637.
44. Xia, Y. N.; Whitesides, G. M., Soft lithography. *Annu. Rev. Mater. Sci.* **1998,** *28*, 153-184.
45. Schneider, F.; Draheim, J.; Kamberger, R.; Wallrabe, U., Process and material properties of polydimethylsiloxane (PDMS) for Optical MEMS. *Sensors and Actuators A: Physical* **2009,** *151* (2), 95-99.
46. Bhattacharya, S.; Datta, A.; Berg, J. M.; Gangopadhyay, S., Studies on surface wettability of poly (dimethyl) siloxane (PDMS) and glass under oxygen-plasma treatment and correlation with bond strength. *Microelectromechanical Systems, Journal of* **2005,** *14* (3), 590-597.
47. Yoo, S. K.; Kim, Y. M.; Yoon, S. Y.; Kwon, H.-S.; Lee, J. H.; Yang, S., Bead Packing and Release Using Flexible Polydimethylsiloxane Membrane for Semi-Continuous Biosensing. *Artificial Organs* **2011**, no-no.
48. Sasso, L. A.; Undar, A.; Zahn, J. D., Autonomous magnetically actuated continuous flow microimmunofluorocytometry assay. *Microfluid. Nanofluid.* **2010,** *9* (2-3), 253-265.
49. Fogler, H. S., *Elements of chemical reaction engineering*. Prentice Hall PTR: Upper Saddle River, 1999.
50. Sasso, L. A.; Johnston, I. H.; Zheng, M.; Gupte, R. K.; Ündar, A.; Zahn, J. D., Automated microfluidic processing platform for multiplexed magnetic bead immunoassays. *Microfluid. Nanofluid.* **2012,** *13* (4), 603-612.
51. Medintz, I. L.; Uyeda, H. T.; Goldman, E. R.; Mattoussi, H., Quantum dot bioconjugates for imaging, labelling and sensing. *Nature materials* **2005,** *4* (6), 435-446.

52. Konry, T.; Smolina, I.; Yarmush, J. M.; Irimia, D.; Yarmush, M. L., Ultrasensitive Detection of Low‐Abundance Surface‐Marker Protein Using Isothermal Rolling Circle Amplification in a Microfluidic Nanoliter Platform. *Small* **2011,** *7* (3), 395-400.
53. Shapiro, J. S.; Stiteler, M.; Wu, G.; Price, E. A.; Simon, A. J.; Sankaranarayanan, S., Cisterna magna cannulated repeated CSF sampling rat model-effects of a gamma-secretase inhibitor on Aβ levels. *Journal of Neuroscience Methods* **2011,** *205*, 36-44.
54. Stammers, A. T.; Liu, J.; Kwon, B. K., Expression of inflammatory cytokines following acute spinal cord injury in a rodent model. *J Neurosci Res* **2012,** *90* (4), 782-790.
55. Shoemaker, L. D.; Achrol, A. S.; Sethu, P.; Steinberg, G. K.; Chang, S. D., Clinical Neuroproteomics and Biomarkers: From Basic Research to Clinical Decision Making. *Neurosurgery* **2012,** *70* (3), 518.

Chapter 3: Development and Validation of a Microfluidic Immunoassay Capable of Multiplexing Parallel Samples Using Commercially Available Reagents

Note: this Chapter will be submitted as a manuscript to *Lab on a Chip*.

Mehdi Ghodbane,[a] Elizabeth Stucky,[a] Tim J. Maguire,[a] Rene S. Schloss,[a] David Shreiber,[a] Jeffrey D. Zahn,[a] and Martin L. Yarmush[*a,b]

[a] Department of Biomedical Engineering, Rutgers, The State University of New Jersey, 599 Taylor Road, Piscataway, New Jersey 08854, USA. E-mail: yarmush@rci.rutgers.edu

[b] Center for Engineering in Medicine/Surgical Services, Massachusetts General Hospital, 51 Blossom Street, Boston, MA, 02114, USA

To be submitted to: Lab of a Chip

Introduction

The immunoassay is one of the most versatile and widely used assays. Highly selective antibody antigen interactions allow the measurement of any analyte for which specific antibodies are available. The flexibility of this technique permit the analysis of a variety of biomolecules, including cytokines, viruses, antibodies, drugs, hormones, and bacteria[1]. This has led to its utilization in a variety of applications both in the clinic and basic research[2]. In recent years,

the development of methods for multiplex analysis, i.e. the measurement of a panel of analytes within a single sample, have further improved the capabilities of the assay. Luminex has developed one of the most popular multiplexing platforms using optically encoded antibody conjugated microbeads. This technology allows for the simultaneous quantification of up to 100 proteins in a single sample[3], and microbeads pre-conjugated with antibodies specific for many different molecules are commercially available from a variety of manufacturers. Due to its broad applicability and flexibility, thousands of studies have been published utilizing this technology[4]. However, like standard immunoassays, these assays are very expensive due to the high cost of monoclonal antibodies and assay reagents and typically require at least 50 µL of volume per sample.

Due to these drawbacks, several microfluidic based multiplex immunoassays have been developed in order to reduce sample and reagent consumption while respectively decreasing cost. These devices have utilized a variety of different approaches in order to facilitate multiplexing. These include, but are not limited to, DNA encoded antibody libraries[5-7], the aforementioned Luminex microbeads[8], performing parallel single protein immunoassays in a CD format[9], patterning antibodies at known positions within microchannels[10-13], and quantum dot barcodes[14]. Together, these approaches have demonstrated the ability to perform multiplex immunoassays in microfluidic devices with low sample volumes, high sensitivity, large dynamic range, commercial reagent compatibility, and a high sample throughput. However, no single device has simultaneously exhibited all of these characteristics. In addition, most reports only demonstrate

the ability to generate standard curves while neglecting to validate quantification across the working range of the assay and/or compare results to measurements obtained from conventional immunoassays. A device overcoming these disadvantages could be utilized in a wide variety of in vitro, in vivo, and clinical applications.

In this work, we build upon previous technology to develop a device possessing all of the aforementioned advantages. We present a microfluidic multiplex immunoassay device capable of analyzing 32 samples simultaneously in small sample volume (<5 μL). The device utilizes commercially available Luminex multiplex reagents, which allows this device to be used to multiplex virtually any panel of analytes for which minimally cross-reactive specific antibodies can be generated. In addition, we test and demonstrate the accuracy of the device over a large dynamic range with sensitivity comparable to the standard benchtop assay. Finally, the utility of the device is demonstrated in an in vitro co-culture model of rat hippocampal slices and human alginate encapsulated human mesenchymal stem cells (eMSC).

Materials and Methods

Immunoassay Reagents, Spiked Sample Preparation, and Conventional Immunoassay

Bio-Plex Pro immunoassay reagents including cytokine standards, Luminex microbeads conjugated to antibodies specific to rat IL-6, TNF-α, IL-13, IL-1β, IL-10, and MCP-1, the respective biotinylated detection antibodies,

streptavidin-phycoerytrin, assay buffer, and wash buffer were used as received in both on-chip and benchtop immunoassays (Bio-Rad Laboratories, Hercules, CA). Bovine serum albumin solution (BSA) was prepared at 0.05% w/v in phosphate buffered saline (PBS) (Life Technologies, Carlsbad, CA). The lyophilized standards containing a cocktail of 24 inflammatory markers were reconstituted and diluted in BSA and media in device validation and supernatant analysis studies, respectively. For the validation study, known samples were prepared by spiking cytokine standards into BSA solution. The antibody conjugated beads and streptavidin-phycoerythrin were prepared at 34X and 100X in assay buffer, respectively. Detection antibodies were diluted 20X in detection antibody diluent. The benchtop multiplex assay was performed as per manufacturer recommendations.

Organotypic Hippocampal Slice Culture

All animal procedures were approved by the Rutgers University Institutional Animal Care and Use Committee (Piscataway, NJ). Organotypic hippocampal slice cultures (OHSC) were prepared according to established methods[15]. Briefly, Sprague-Dawley rat pups (Taconic Biosciences Inc., Rensselaer, NY) at postnatal day 8-10 were decapitated, the hippocampus rapidly dissected, sliced into 400μm sections with a McIllwain tissue chopper (Vibratome, St. Louis, MO), and immersed in ice-cold Gey's balanced salt solution (Sigma-Aldrich, St. Louis, MO) supplemented with 4.5mg/ml glucose (Sigma-Aldrich, St. Louis, MO). Slices were separated and plated onto Millicell CM culture inserts (EMD Millipore, Billerica, MA) and maintained at 37°C in 5%

CO2 for 14 days. Maintenance medium consisted of 25% heat-inactivated horse serum (Life Technologies, Carlsbad, CA), 25% Hank's balanced salt solution (HBSS) (Sigma-Aldrich, St. Louis, MO) and 50% minimum essential medium (MEM) with added Earle's salts (Sigma-Aldrich, St. Louis, MO), supplemented with 1mM glutamine (Sigma-Aldrich, St. Louis, MO) and 4.5mg/ml glucose (Sigma-Aldrich, St. Louis, MO). Medium was changed every 3 to 4 days.

Human Mesenchymal Stem Cell Culture

Human mesenchymal stem cells (MSCs) were purchased from Texas A&M at passage one and cultured as previously described[16]. Briefly, cells were cultured in MEM-α medium (Life Technologies, Carlsbad, CA), supplemented with 10% FBS (Atlanta Biologicals, Lawrenceville, GA), 1ng/ml basic fibroblast growth factor (bFGF) (Peprotech, Rocky Hill, NJ), 100 units/ml penicillin and 100µg/ml streptomycin (Life Technologies, Carlsbad, CA). Cells were plated at 5000 cells per cm2 and allowed to proliferate to 70% confluence before passaging, and were only used at passages 2 through 5. All cultures were incubated at 37°C in 5% CO2.

Alginate Microencapsulation

Alginate Poly-L-Lysine microencapsulation of MSCs was performed as previously described[17], using a 2.2% alginate (Sigma-Aldrich, St. Louis, MO) and cell solution of 4 million cells/mL. Alginate beads were generated using an electrostatic bead generator (Nisco, Zurich, Switzerland), resuspended in MEM-α (Life Technologies, Carlsbad, CA), and transferred to 25 cm2 tissue culture flasks, and used for experiments one day post-encapsulation.

LPS Injury & Co-culture

Organotypic slices cultured on transwell membrane inserts were added to 24-well plates and either cultured alone or co-cultured with eMSC at 1x105 cells/well. Maintenance medium was exchanged for serum-free medium (75% MEM with added Earle's salts, 25% HBSS, 1mM glutamine, and 4.5mg/mL glucose). Cultures were stimulated with 1μg/ml LPS (Escherichia coli 055:B5, Sigma-Aldrich, St. Louis, MO)[18-19] and media supernatants were collected at 6, 12, 24, or 48 hours and immediately frozen at -20°C. All collected supernatants were then thawed simultaneously and diluted at 1:10 in media. Diluted samples were aliquotted for on-chip and benchtop immunoassays and then frozen at -80°C until they were thawed on ice for analysis.

Device Fabrication and Operation

The device is an expanded version of our previous design[20] which allows for 32 samples to be assayed simultaneously, shown in Figure 3.1a. A single common inlet allows for the introduction of all assay reagents. Individual sample inlets are positioned upstream of bead traps. The bead traps consist of an array of small features with a width of 3 μm spaced 7 μm apart, which blocks the passage of 6.5 μm beads while allowing the passage of fluid. The pneumatic valves divert fluid flow to the proper regions of the device throughout the assay[21]. Devices were fabricated as described in our previous report[20], except that the valve seats were fabricated at a height of 30 μm and photomasks for the expanded design were used. Briefly, the bead traps were first patterned at a height of 7 um with SU-8 2007 (Microchem Corp., Newton, MA) using a reduced

exposure dose relative to the manufacturer's recommendations to improve resolution[22]. The wafer was flood exposed, hard baked, and coated with two 15 μm layers of AZ Electronic Material AZ9260 photoresist (Capitol Scientific Inc., Austin, TX). The valve seats were patterned, and then reflowed to round the channel cross-section to allow for complete valve closure. The remaining fluidic network was then fabricated at a height of 41 μm using SU-8 2025 (Microchem Corp., Newton, MA). The pneumatic channels were patterned on a separate layer, also at a height of 41 μm. The fluidic wafer is reproduced in polyurethane which was used in subsequent soft lithography steps to extend the life of the mold[23]. Poly (dimethylsiloxane) was prepared at a 10:1 pre-polymer to curing agent ratio, poured thick (3-4 mm) on the fluidic mold, and spin coated onto the pneumatic wafer. The devices were then assembled using multilayer soft lithography techniques[24]. Prior to use, devices were primed overnight submerged in deionized water under vacuum in a desiccator.

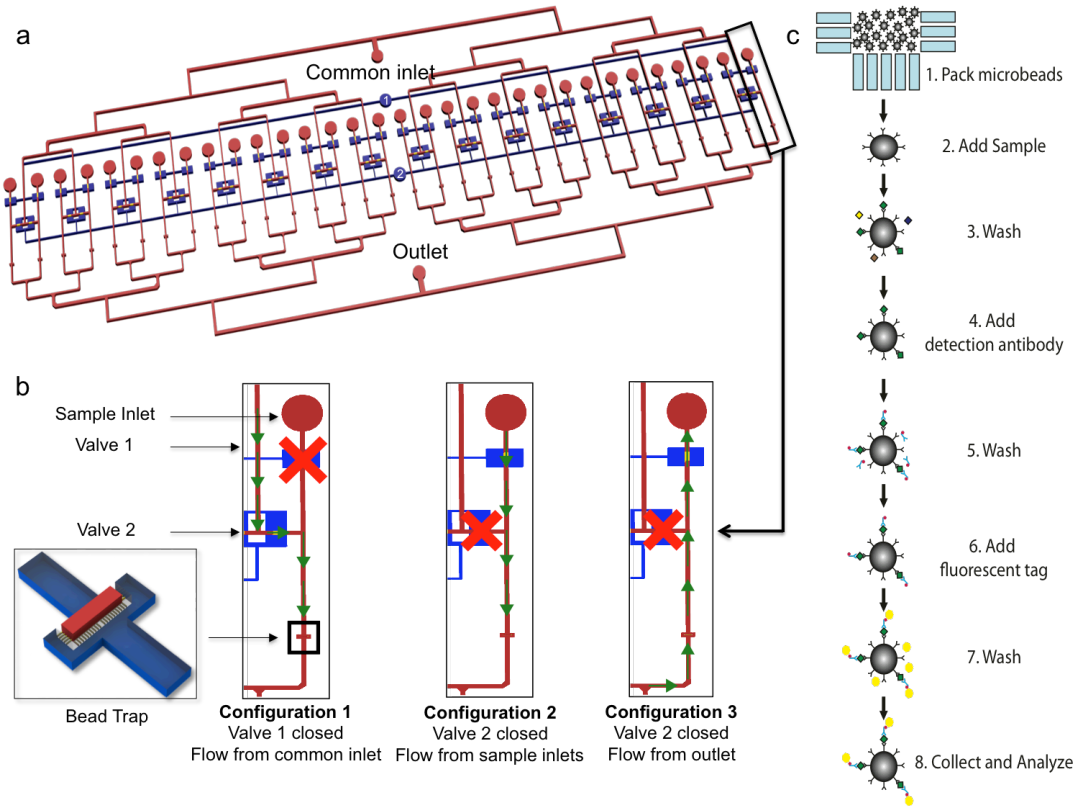

Figure 3.1: Device layout and assay principle

a) Overall schematic of the device. The blue channels represent the pneumatic control layer and the red channels and gold valve seats denote the fluidic network b) Schematic of individual channels and fluid paths during different assay steps. Configuration 1 is used during bead, wash buffer, detection antibody, and fluorescent tag introduction. Configuration 2 is used during sample incubation. Configuration 3 is used during bead collection at the completion of the assay c) Overview of the assay workflow

A Rheodyne MXP7970-000 switching valve (Idex Health & Science LLC, Oak Harbor, WA) was connected to the common inlet to allow for switching of reagent solutions without introducing bubbles into the device. Assay buffer was

flowed at 40 µL/min for 10 minutes to block non-specific binding to the channel walls with all valves open. Pneumatic valve 1 was then closed causing fluid to flow from the common inlet through the bead traps. A mixed solution of the 6 antibody conjugated microbeads was introduced at 40 µL/min for 5 minutes in order to pack the bead beds (Figure 3.1b, Configuration 1). Wash buffer was then flowed at 40 µL/min for 5 minutes to further pack the bead beds and ensure all beads were in the traps. Pneumatic valve 2 was then closed and pipette tips containing each standard or sample was inserted into the sample ports. With this valve closed, fluid is prohibited from mixing between adjacent channels must flow from the sample inlet over the packed bed of beads located directly downstream (Figure 3.1b, Configuration 2). A syringe pump was connected to the outlet and set to withdraw at 500 nL/min, corresponding to a flow rate of 15.6 nL/min/channel. Sample incubation was carried out for 4.5 hours, which was determined in our previous study to provide an assay sensitivity of 358 fM for IL6[20]. Under these conditions, 4.2 µL of sample was consumed per channel. At the conclusion of the sample incubation, pneumatic valve 2 was opened, pneumatic valve 1 closed, and the beads were washed at 40 µL/min for 5 minutes (Figure 3.1b, Configuration 1). Secondary antibodies and streptavidin-phycoerythrin were flowed at 1.6 µL/min for 30 and 10 minutes, respectively, each followed by a wash step performed for 5 minutes at 40 µL/min. At the completion of the assay, new pipette tips were inserted into the sample ports, pneumatic valve 2 was closed, and wash buffer was flowed into the common outlet (Figure 3.1b, Configuration 3). The beads were collected from the sample

inlet ports and transferred to a vacuum filter 96-well plate included with the immunoassay kit, the wash buffer was removed, and the beads were resuspended in assay buffer. The plate was then transferred to a Bio-Plex 200 equipped with Bio-Plex Manager 5.0 (Bio-Rad, Hercules CA). The assay workflow is summarized in Figure 3.1c.

Data Analysis

Bio-Plex Manager 5.0 software was used to obtain the median fluorescence intensities of the beads and calculate the sample concentrations. Normalized standard curves were generated by dividing each fluorescence reading by the intensity of the highest standard for that analyte and fitting a 5-parameter logistic regression[25] using MasterPlex ReaderFit software (Hitachi Solutions, San Bruno, CA). For the validation studies, the measured concentration of the spiked samples were compared with their expected concentrations calculated from the dilutions used to prepare the samples. For the in vitro supernatant studies, the measurements taken using the microfluidic immunoassay were compared to the concentration obtained using the conventional benchtop multiplex immunoassay. A linear regression and 95% confidence interval of the fit was constructed for the individual measurement of each sample in Matlab (Mathworks, Natick, MA) (n=10 for each of the 7 known samples in the validation studies, n=6 for the 7 samples in the in vitro supernatant studies). The confidence intervals were calculated for the linear fit itself, not to be confused with wider confidence limits for linear regressions that are to be used for the prediction of new observations[26]. For the

in vitro supernatant analysis, measurements that fell below the limit of detection (LOD) of the microfluidic immunoassay were omitted from the analysis.

Results and Discussion

Device Validation

The ability of the device to accurately quantify multiple proteins in a single sample was first evaluated. The pharmaceutical industry validates immunoassays for use in clinical, drug development, and/or biomarker discovery studies by quantifying freshly spiked samples of known concentrations[27-28]. Therefore, seven samples spiked with cytokines, eight standards at the manufacturer's recommended concentrations, and a blank sample were prepared and processed in the device. The relatively large sample capacity allowed all 16 samples/standards to be assayed simultaneously in duplicate on a single chip. The standard curves generated from this study closely resemble the sigmoidal shape obtained when performing the benchtop assay, shown in Figure 3.2. High quality standard curves for all 6 analytes were obtained, corroborated by a very high coefficient of determination and low root mean squared error ($R^2>0.99$ and RMSE<0.05 for all analytes). The noise floor, calculated by the mean plus 3 standard deviations of the fluorescence of the blank sample, is also shown on the curves. The intersection of the standard curve and the noise floor was concluded to be the limit of detection of each specific analyte. For analytes where the lower asymptote of the standard curve was higher than the noise floor (MCP-1, IL-6, TNF-α), the limit of detection was determined to be the concentration of the most dilute standard.

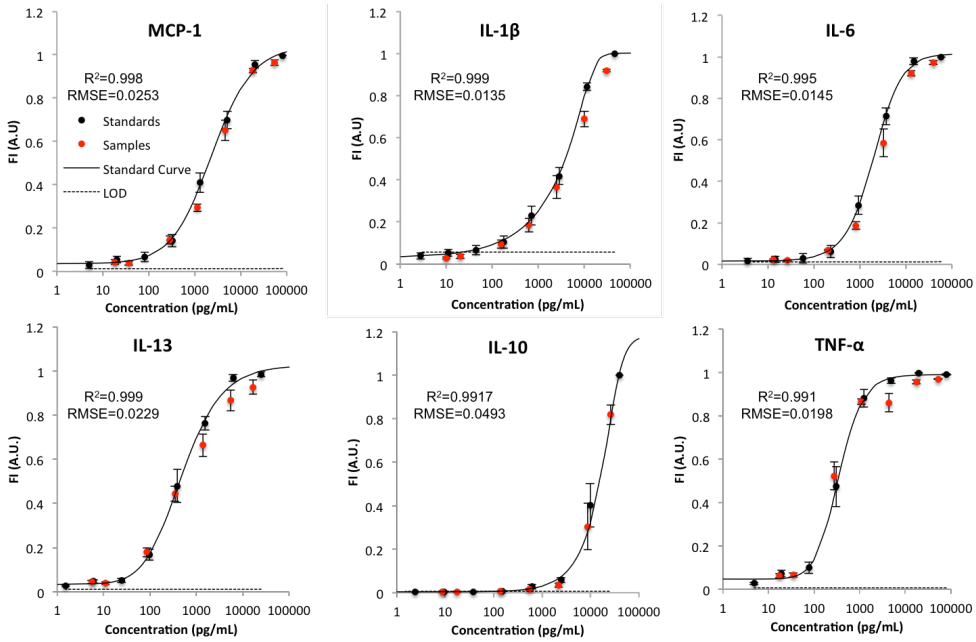

Figure 3.2: Standard curves, sample measurements, and noise floor

Fluorescence intensities of the standards (black circles) and spiked samples of known concentrations (red circles) are shown overlaid on the standard curve generated using a 5-parameter logistic curve fit (black line). The limit of detection (LOD) is represented by the dotted black line. The error bars represent ±S.E.M., n=10 for each data point. RMSE=Root Mean Squared Error

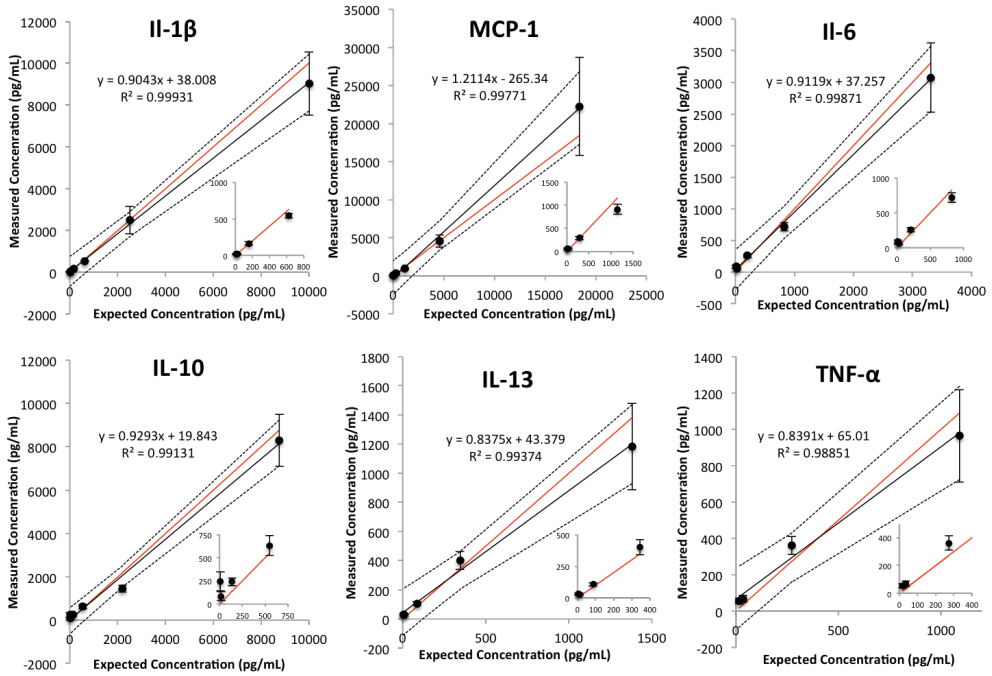

Figure 3.3: Comparison of the expected and measured concentration of the spiked samples.

A linear regression (black line), 95% confidence interval of the fit (dotted lines), and line representing a perfect agreement (red line) are shown. The error bars represent ±S.E.M., n=10 for each data point.

The fluorescence intensity of the spiked samples is plotted in respect to their expected concentrations and overlaid on the standard curves. Visual inspection reveals that the fluorescence measurements for the samples fall very close to their expected position on the standard curve. The ability of the device to quantify the concentration of the spiked samples was then evaluated. Figure 3.3 shows the comparison of the expected and measured concentrations of the samples. The 95% confidence band of the linear regression straddles the perfect

agreement between the expected and measured concentrations for all 6 analytes. In addition, the coefficient of determination of the linear regression for all six analytes was greater than 0.98. From this experiment, we defined the working range of the assay from the calculated LOD to the highest concentration in shown for each analyte in Figure 3.3. The working range of the assay for each analyte is summarized in Table 3.1.

Analyte	Limit of Detection (pg/mL)	Limit of Detection (fM)	Highest Quantified Sample (pg/mL)	Dynamic Range (Orders of Magnitude)
MCP-1	<5.0	387	18406	3.56
Il-1β	21.8	1211	10000	2.66
IL-6	<3.6	151	3310	2.96
IL-13	15.4	963	1380	1.95
IL-10	103.1	5726	8766	1.93
TNF-α	<4.8	92	1090	2.36

Table 3.1: Working range for each analyte in the multiplex assay**.**

The dynamic range was calculated by dividing the highest quantified sample by the limit of detection and taking a logarithm (base 10).

In Vitro Supernatant Quantification

With the working range of the device established, the ability of the device to quantify in vitro samples was compared to a standard benchtop immunoassay performed as per the manufacturer's protocol. Hippocampal slices extracted from neonatal rats were cultured on transwell inserts, treated with LPS, and

cultured alone or co-cultured with eMSC. The supernatants were collected, aliquotted, and analyzed by the standard multiplex immunoassay and the microdevice in parallel. The same 6 analytes were analyzed as the validation studies; however, IL-13 was not measured in the samples. In addition, IL-10 was only measured in 3 samples in the conventional assay and was below the LOD for the microfluidic assay format. A comparison of quantification with the standard and microfluidic multiplex immunoassay is shown in Figure 3.4, with the grey band denoting the 30% error allowed by the pharmaceutical industry for biomarker discovery immunoassays[27]. It is important to note that this acceptable error could affect the agreement of the data obtained from the two assay systems. Nonetheless, a good correlation exists between the bench-top and microfluidic immunoassay (R2=0.8999). However, IL-6 and TNF-α concentrations seem to be slightly under predicted, while some MCP-1 measurements were over predicted, possibly biasing the linear fit. Moreover, the regression line possesses a slope very close to 1 and the 95% confidence interval of the linear fit encompasses the perfect agreement between the two assay formats. Overall, the microdevice provides comparable sample quantification of in vitro protein concentrations as a conventional assay using commercially available reagents.

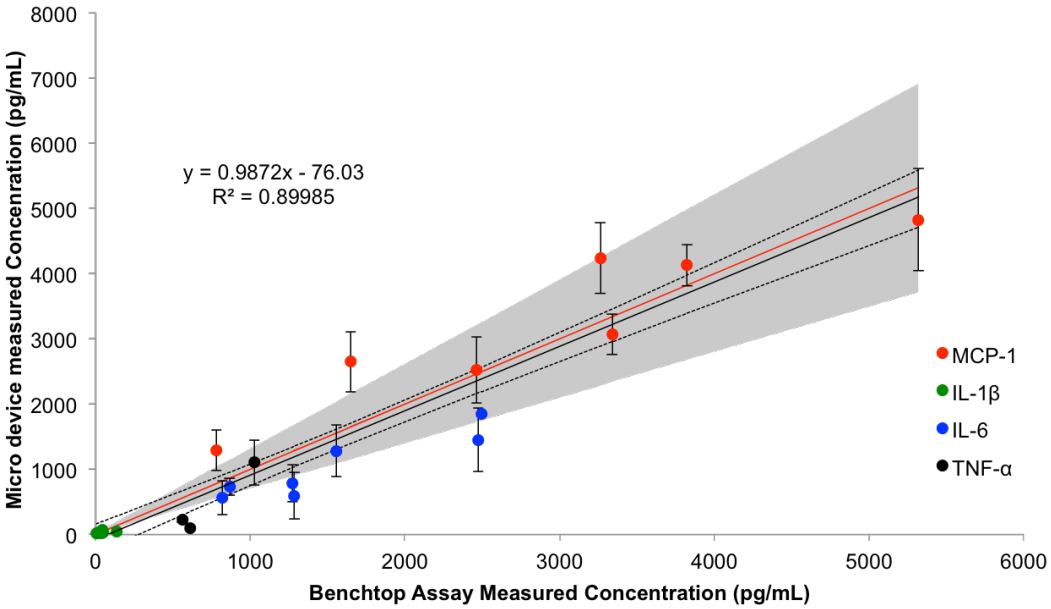

Figure 3.4: Comparison of quantification of *in vitro* supernatants Using commercially available multiplex immunoassay reagents in the conventional benchtop and microfluidic assay formats. A linear regression (black line), 95% confidence interval of the fit (dotted lines), and line representing a perfect agreement (red line) are shown. The gray shaded region represents a ±30% error accepted by the pharmaceutical industry for biomarker discovery immunoassays. The error bars represent ±S.E.M., n=6 for each data point.

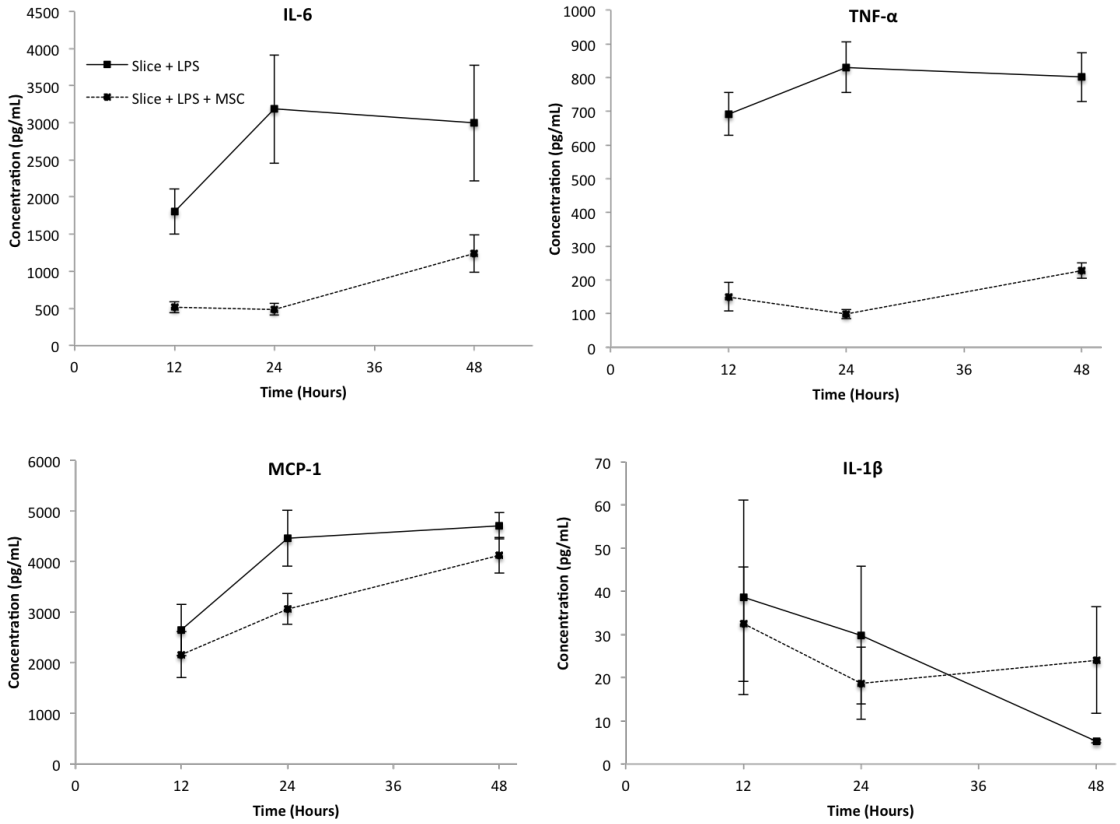

Figure 3.5: Effect of eMSC on rat hippocampal slices treated with LPS. All concentrations are shown at 10 fold dilutions. Error bars represent ± S.E.M., n=4 for TNF-a, Slice + LPS at 12 and 24 hours, n=6 for all other data points)

We then investigated the effect of eMSC on the activated hippocampal slices using our microfluidic system. The addition of LPS to the slices is known to elicit an inflammatory response resulting in cytokine secretion[29], and co-culture with mesenchymal stem cells has been shown to modulate the immune response[30]. In addition, our previous studies have shown that alginate encapsulation allows the cells to remain viable for up to 60 days while permitting

secreted proteins to diffuse through the capsule[31]. As indicated in Figure 3.5, LPS induced increased secretion of TNF-α, IL-6 and MCP-1 from the slices during the 48 hour experimental time period, while IL-1β levels decreased. We also observed that the addition of eMSC modulated cytokine levels. TNF-α and IL-6 were markedly decreased at 12, 24 and 48 hours following LPS addition. The effect on MCP-1 secretion was less pronounced, with the largest decrease observed at 24 hours. The effect on IL-1β was much smaller and in fact, a slight increase was observed in the eMSC treated slices by 48 hours. Therefore, we were able to observe cytokine specific immunomodulatory effects of eMSC on activated hippocampus slices using our microdevice. More importantly, the temporal progression of cytokine secretion was quantified.

The decrease in TNF-α secretion observed from the hippocampal slice in the presence of MSC is consistent with our studies using conventional techniques (manuscript under review). While the biological effects of eMSC on hippocampal slices are discussed in detail in this report, the differences in the cytokines measured here demonstrates the ability of this device to be used as a screening tool in in vitro systems. Furthermore, we were able to perform this analysis using only 4.2 μL of supernatant compared to the 50 μL of sample volume required in the bench-top assay. In addition, antibody conjugated microbeads consumption was reduced >13 fold (2.5 μL to 0.184 μL of each stock bead solution) and detection antibody requirement was reduced >16 fold (25 to 1.5 μL of each 1x detection antibody solution). Thus, one commercially available

kit (including 25% excess reagents) can be used to analyze 1565 samples on chip versus 96 using the benchtop assay format.

In addition to the significant reduction in required sample volume and accompanying cost savings provided by this device, the performance make it well suited for a variety of applications. The device possesses sensitivity comparable to the benchtop assay (low pg/mL concentrations) with a dynamic range of ~2-3.5 orders of magnitude. This large working range allows for multiple analytes present at different concentrations to be measured simultaneously, as shown in our in vitro supernatant analysis. This mitigates the need to optimize dilutions prior to analysis in order to avoid saturation, which is necessary when using assays with smaller dynamic range. Furthermore, the use of the Luminex multiplexing reagents allows this device to be used to measure many different analytes that are commercially available. These reagents are available for purchase pre-conjugated to capture antibodies specific for a wide variety of molecules in several species. Finally, this design allows for parallel processing of samples on a single chip. This device is an expanded version of our 8 channel device with the same basic layout[20], demonstrating scalability beyond the 32 sample capacity presented in this report. To the best of our knowledge, this is the first report simultaneously demonstrating low sample usage, high sensitivity, a large dynamic range, commercial reagent compatibility, quantification capabilities (confirmed with spiked samples and comparison to a conventional assay), and parallel sample processing. The combination of these characteristics allow for broad applications in both clinical and research settings.

For example, the analysis of in vitro culture supernatants in this study demonstrates one of the many potential applications of this device. In typical in vitro studies, one well is dedicated to each time point of interest due to the relatively high sample consumption of conventional immunoassays. In the system used here, each well contains a rat hippocampal slice, 100,000 eMSC, and 200 µL of media. Isolation of hippocampal slices requires difficult and time consuming surgery which only yields enough tissue to investigate effects at 10 time points per rat using conventional bench top methods. With lowered sample consumption, one well can be used to perform a time course study by only removing the required 4.2 µL of supernatant at each time point of interest and allowing the culture to continue. This way, the study shown here could be performed using only 2 wells rather than 7. Furthermore, the number of time points examined could be increased without requiring additional hippocampal slices, eMSC, and associated tissue culture reagents for maintaining the culture systems. These advantages demonstrate how reduced sample consumption provides additional cost and reagent savings beyond what is required to perform the assay. It is important to note that this was a relatively small study (2 conditions, 4 time points) and these advantages would be greatly amplified in larger in vitro studies.

The device could also be applied to in vivo studies. For example, analysis of cerebrospinal fluid (CSF) in rat models of central nervous system disease models has been prohibited by the small amount of available volume. This limitation has forced developmental Alzheimer's disease therapies to be studied

in larger animals, resulting in increased drug compound, veterinary costs and ethical concerns when compared to rodent models[32]. In addition, potential spinal cord injury biomarker candidates identified in a human clinical trial[33] were unable to be further explored in a rat model with controlled injury. This resulted in samples needing to be pooled from multiple animals[34] or the analysis of spinal tissue rather than CSF[35], which can not be analyzed in human patients and is therefore not directly clinically translatable.

A scaled down assay would also provide advantages in a clinical setting. The decreased cost of the assay could drastically decrease the cost of diagnostic procedures. In addition, samples from pediatric and neonatal patients that do not yield sufficient sample volumes could be analyzed[36]. Finally, the high-throughput, low volume, and low cost multiplexing characteristics of this device are perfectly suited for biomarker discovery studies[37]. Also, like most microfluidic assays, automation of this device would be fairly straightforward[38]. This could eliminate the need for highly trained technicians to perform the assay in clinical labs, reducing assay variability and the laborious workflow associated with immunoassays.

Conclusions

Herein we present a multiplex immunoassay device capable of performing 32 simultaneous multiplex immunoassays in only 4.2 µL of sample volume. This design allows for further scalability beyond a 32 sample capacity and allows for the analysis of virtually any analyte for which immunoassay antibodies are available. The device is shown to have a high sensitivity with a dynamic range of

~2-3.5 orders of magnitude depending on the analyte. Furthermore, we demonstrate the ability to quantify samples across the entire working range of the assay and compare on-chip quantification with a standard benchtop multiplex immunoassay. The type of assay validation performed in this study has been lacking in microfluidic immunoassay publications, which typically only demonstrate the ability to generate standard curves. To the best of our knowledge, no device demonstrated to date possesses the combination of the aforementioned characteristics. These capabilities allow for utilization in broad in vitro, in vivo, and clinical applications.

Acknowledgements
This work was partially funded by the National Institute of Health Grants P41EB002503 and UH2TR000503, the National Institute of Health Rutgers Biotechnology Training Program (T32GM008339), and the National Science Foundation Integrated Science and Engineering of Stem Cells Program (DGE0801620). The authors would like to thank Dr. Bhaskar Mitra and Henry Yu for support in developing the fabrication protocols.

References

1. Henares, T. G.; Mizutani, F.; Hisamoto, H., Current development in microfluidic immunosensing chip. *Anal. Chim. Acta* **2008,** *611* (1), 17-30.
2. Wild, D., *The immunoassay handbook*. Elsevier Ltd.: San Diego, 2005.
3. Dunbar, S. A., Applications of LuminexÆ xMAP(TM) technology for rapid, high-throughput multiplexed nucleic acid detection. *Clinica Chimica Acta* **2006,** *363* (1-2), 71-82.
4. Houser, B., Bio-Rad's Bio-Plex(R) suspension array system, xMAP technology overview. *Archives of physiology and biochemistry* **2012,** *118* (4), 192-6.

5. Wang, J.; Ahmad, H.; Ma, C.; Shi, Q.; Vermesh, O.; Vermesh, U.; Heath, J., A self-powered, one-step chip for rapid, quantitative and multiplexed detection of proteins from pinpricks of whole blood. *Lab Chip* **2010,** *10* (22), 3157-3162.
6. Qin, L.; Vermesh, O.; Shi, Q.; Heath, J. R., Self-powered microfluidic chips for multiplexed protein assays from whole blood. *Lab Chip* **2009,** *9* (14), 2016-2020.
7. Fan, R.; Vermesh, O.; Srivastava, A.; Yen, B. K. H.; Qin, L.; Ahmad, H.; Kwong, G. A.; Liu, C.-C.; Gould, J.; Hood, L.; Heath, J. R., Integrated barcode chips for rapid, multiplexed analysis of proteins in microliter quantities of blood. *Nature Biotechnology* **2008,** *26* (12), 1373-1378.
8. **!!! INVALID CITATION !!!**
9. Park, J.; Sunkara, V.; Kim, T.-H.; Hwang, H.; Cho, Y.-K., Lab-on-a-disc for fully integrated multiplex immunoassays. *Anal. Chem.* **2012,** *84* (5), 2133-2140.
10. Bernard, A.; Michel, B.; Delamarche, E., Micromosaic immunoassays. *Anal. Chem.* **2001,** *73* (1), 8-12.
11. Song, Y.; Zhang, Y.; Bernard, P. E.; Reuben, J. M.; Ueno, N. T.; Arlinghaus, R. B.; Zu, Y.; Qin, L., Multiplexed volumetric bar-chart chip for point-of-care diagnostics. *Nature communications* **2012,** *3*, 1283.
12. Garcia-Cordero, J. L.; Nembrini, C.; Stano, A.; Hubbell, J. A.; Maerkl, S. J., A high-throughput nanoimmunoassay chip applied to large-scale vaccine adjuvant screening. *Integrative Biology* **2013,** *5* (4), 650-658.
13. Stern, E.; Vacic, A.; Rajan, N. K.; Criscione, J. M.; Park, J.; Ilic, B. R.; Mooney, D. J.; Reed, M. A.; Fahmy, T. M., Label-free biomarker detection from whole blood. *Nature nanotechnology* **2009,** *5* (2), 138-142.
14. Klostranec, J. M.; Xiang, Q.; Farcas, G. A.; Lee, J. A.; Rhee, A.; Lafferty, E. I.; Perrault, S. D.; Kain, K. C.; Chan, W. C., Convergence of quantum dot barcodes with microfluidics and signal processing for multiplexed high-throughput infectious disease diagnostics. *Nano letters* **2007,** *7* (9), 2812-2818.
15. Stoppini, L.; Buchs, P.-A.; Muller, D., A simple method for organotypic cultures of nervous tissue. *Journal of neuroscience methods* **1991,** *37* (2), 173-182.
16. Parekkadan, B.; Van Poll, D.; Suganuma, K.; Carter, E. A.; Berthiaume, F.; Tilles, A. W.; Yarmush, M. L., Mesenchymal stem cell-derived molecules reverse fulminant hepatic failure. *PloS one* **2007,** *2* (9), e941.
17. Maguire, T.; Novik, E.; Schloss, R.; Yarmush, M., Alginate PLL microencapsulation: Effect on the differentiation of embryonic stem cells into hepatocytes. *Biotechnology and bioengineering* **2006,** *93* (3), 581-591.
18. Lieberman, A. P.; Pitha, P. M.; Shin, H. S.; Shin, M. L., Production of tumor necrosis factor and other cytokines by astrocytes stimulated with lipopolysaccharide or a neurotropic virus. *Proceedings of the National Academy of Sciences* **1989,** *86* (16), 6348-6352.
19. Chung, I. Y.; Benveniste, E. N., Tumor necrosis factor-alpha production by astrocytes. Induction by lipopolysaccharide, IFN-gamma, and IL-1 beta. *The Journal of Immunology* **1990,** *144* (8), 2999-3007.
20. Ghodbane, M.; Kulesa, A.; Yu, H. H.; Maguire, T.; Schloss, R.; Ramachandran, R.; Zahn, J. D.; Yarmush, M. L., Development of a low-volume,

highly sensitive microimmunoassay using computational fluid dynamics-driven multiobjective optimization. *Microfluid. Nanofluid.* **2014,** *In Press*.
21. Unger, M. A.; Chou, H.-P.; Thorsen, T.; Scherer, A.; Quake, S. R., Monolithic Microfabricated Valves and Pumps by Multilayer Soft Lithography. *Science* **2000,** *288* (5463), 113-116.
22. Chan-Park, M. B.; Zhang, J.; Yan, Y.; Yue, C., Fabrication of large SU-8 mold with high aspect ratio microchannels by UV exposure dose reduction. *Sensors and Actuators B: Chemical* **2004,** *101* (1), 175-182.
23. Desai, S. P.; Freeman, D. M.; Voldman, J., Plastic masters—rigid templates for soft lithography. *Lab Chip* **2009,** *9* (11), 1631-1637.
24. Fordyce, P. M.; Diaz-Botia, C.; DeRisi, J. L.; Gomez-Sjoberg, R., Systematic characterization of feature dimensions and closing pressures for microfluidic valves produced via photoresist reflow. *Lab Chip* **2012,** *12*, 4287-4295.
25. Gottschalk, P. G.; Dunn, J. R., The five-parameter logistic: a characterization and comparison with the four-parameter logistic. *Analytical biochemistry* **2005,** *343* (1), 54-65.
26. Montgomery, D. C.; Runger, G. C., Applied statistics and probability for engineers. 4 ed.; John Wiley & Sons: 2007.
27. Valentin, M.-A.; Ma, S.; Zhao, A.; Legay, F.; Avrameas, A., Validation of immunoassay for protein biomarkers: bioanalytical study plan implementation to support pre-clinical and clinical studies. *Journal of pharmaceutical and biomedical analysis* **2011,** *55* (5), 869-877.
28. Lee, J. W.; Hall, M., Method validation of protein biomarkers in support of drug development or clinical diagnosis/prognosis. *Journal of Chromatography B* **2009,** *877* (13), 1259-1271.
29. Huuskonen, J.; Suuronen, T.; Miettinen, R.; Van Groen, T.; Salminen, A., A refined in vitro model to study inflammatory responses in organotypic membrane culture of postnatal rat hippocampal slices. *J Neuroinflammation* **2005,** *2*, 25.
30. Foraker, J. E.; Oh, J. Y.; Ylostalo, J. H.; Lee, R. H.; Watanabe, J.; Prockop, D. J., Cross-talk between human mesenchymal stem/progenitor cells (MSCs) and rat hippocampal slices in LPS-stimulated cocultures: the MSCs are activated to secrete prostaglandin E2. *Journal of Neurochemistry* **2011,** *119* (5), 1052-1063.
31. Barminko, J.; Kim, J. H.; Otsuka, S.; Gray, A.; Schloss, R.; Grumet, M.; Yarmush, M. L., Encapsulated mesenchymal stromal cells for in vivo transplantation. *Biotechnology and Bioengineering* **2011**, n/a-n/a.
32. Shapiro, J. S.; Stiteler, M.; Wu, G.; Price, E. A.; Simon, A. J.; Sankaranarayanan, S., Cisterna magna cannulated repeated CSF sampling rat model-effects of a gamma-secretase inhibitor on Aβ levels. *Journal of Neuroscience Methods* **2011,** *205*, 36-44.
33. Kwon, B. K.; Casha, S.; Hurlbert, R. J.; Yong, V. W., Inflammatory and structural biomarkers in acute traumatic spinal cord injury. *Clin. Chem. Lab. Med.* **2011,** *49* (3), 425-433.

34. Lubieniecka, J. M.; Streijger, F.; Lee, J. H. T.; Stoynov, N.; Liu, J.; Mottus, R.; Pfeifer, T.; Kwon, B. K.; Coorssen, J. R.; Foster, L. J.; Grigliatti, T. A.; Tetzlaff, W., Biomarkers for Severity of Spinal Cord Injury in the Cerebrospinal Fluid of Rats. *PLoS ONE* **2011,** *6* (4), e19247.
35. Stammers, A. T.; Liu, J.; Kwon, B. K., Expression of inflammatory cytokines following acute spinal cord injury in a rodent model. *J Neurosci Res* **2012,** *90* (4), 782-790.
36. Phillips, T. M., Rapid analysis of inflammatory cytokines in cerebrospinal fluid using chip-based immunoaffinity electrophoresis. *Electrophoresis* **2004,** *25* (1011), 1652-1659.
37. Shoemaker, L. D.; Achrol, A. S.; Sethu, P.; Steinberg, G. K.; Chang, S. D., Clinical Neuroproteomics and Biomarkers: From Basic Research to Clinical Decision Making. *Neurosurgery* **2012,** *70* (3), 518.
38. Bange, A.; Halsall, H.; Heineman, W., Microfluidic immunosensor systems. *Biosensors and Bioelectronics* **2005,** *20* (12), 2488-2503.

Chapter 4: Device Fabrication and Operation Procedure

Introduction

During the development of the device, several technical issues arose that required significant troubleshooting. While many of the techniques used in this project have been reported in literature, many of the steps had to be thoroughly optimized empirically. The difficulties we encountered were most likely due to differences in processing facilities and equipment. These discrepancies required large time investments to accomplish previously reported results, which are inherently not novel. In addition, most published methods are written very succinctly, prohibiting elaboration of the critical details of fabrication and/or operating procedures. Therefore, the purpose of this chapter is to provide an in depth explanation of the fabrication and operating procedure of this device.

In addition to detailed procedures, an explanation of the critical parameters that must be carefully controlled to achieve desired results is included. Every aspect of fabrication including silicon mold manufacturing using photolithography, mold reproduction using polyurethane, and multilayer soft lithography is detailed. In addition, the operation of the device is described. This should allow for straightforward reproduction of the results presented in this dissertation with minimal optimization of the fabrication and operating procedure.

Mold Production using Photolithography

The device requires 4 separate photolithography steps. Three steps are required construct the fluidic network, consisting of the bead traps, valve seats, and the remainder of the fluidic channels. On a separate wafer, the pneumatic control layer is fabricated at a height of 41 μm. In this section, these fabrication steps are discussed along with a justification for diverging from conventional photolithographic methods[1] that were used as a starting point for the procedure.

Fluidic Layer Step 1: Bead Trap Fabrication

The first layer to be fabricated on the fluidic layer is the bead trap. The purpose of these features is to block the passage of 5.6 or 6.5 μm diameter[2-3] Luminex microbeads while allowing the passage of fluid. One concern with mechanical trapping of microbeads is the high flow resistance created by a packed bed[4]. Therefore, the bead trap was designed to minimize flow resistance. The channel width expands from 100 μm to 200 μm at the bead trap, halving the fluid velocity through the bed. Since the pressure drop is directly proportional to the velocity, this reduces the pressure drop. In addition, it allows the same number of beads to be packed in a bed of half the length, which is also directly proportional to pressure drop[5]. In addition, the channels are oriented both parallel and orthogonal to fluid flow. This approach has been shown to greatly reduce clogging of microbeads in microfluidic channels[6].

The height and width of the features contained in this layer was the next issue that required troubleshooting. These dimensions should be maximized to reduce the fluidic resistance of the features themselves[7]. However, a trade-off exists between the reproducibility and ease of the fabrication process. We first

attempted a height of 13 μm, which did not yield good results. While the aspect ratio is not unreasonably large, the tight spacing of the features makes the desired resolution difficult to acheive[8]. With poor resolution, the array of features will connect with one another and allow the passage of microbeads during device operation. To make simplify fabrication, we reduced the height of the features to 7 μm, and significantly reduced the exposure dose relative to the manufacturer's recommendation to increase resolution[9]. Furthermore, we first fabricated features at a width of 5 μm with 5 μm spacing, but found that this was too wide and the microbeads could clog the trap, as shown in Figure 4.1. We then reduced the feature width to 3 μm, which remedied this issue. Therefore, a width of 3 μm, height of 7 μm, and a spacing of 7 μm between features was used as the dimensions for the bead traps. This provides a good trade off between pressure drop and reproducible fabrication and bead trapping.

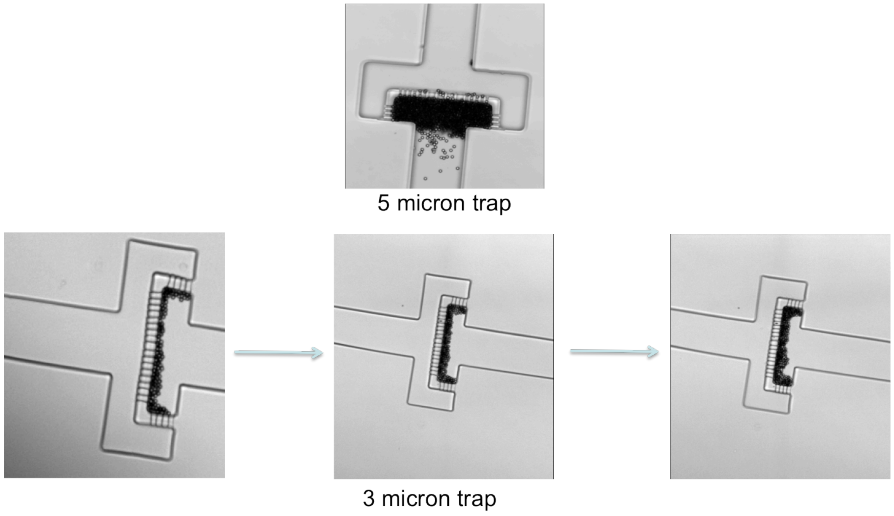

Figure 4.1: Bead trap width testing

(Top) Initial attempts using 5 μm channel width allowed some beads to pass through the trap. Reducing the channels to 3 μm wide prevents any beads from

escaping the trap. (Bottom) Images of the bead packing over time are shown, demonstrating a growing bead bed

Protocol:

A silicon wafer is first cleaned by a rinse and subsequent 10-minute soak in acetone, isopropanol (IPA), and water, in that order. The wafer is dried using filtered compressed air, then dehydrated in a convection oven at 150°C for at least 20 minutes. SU-8 2007 is then coated to a thickness of 7 μm by spinning at 4000 rotations per minute (rpm) for 30 seconds with an acceleration of 300 rpm/second. A cotton swab is dipped in SU-8 developer and the edge of the wafer is wiped to perform edge bead removal. The wafer is then placed on a hotplate at room temperature and set to 65°C. Once temperature is reached, it is baked for 2 minutes. The temperature is raised to 95°C and baked at that temperature for 3 minutes once set point is reached. At this point, the hotplate is turned off with the wafer still on it and allowed to cool for 1 hour. While wafers are usually baked on a hotplate that has already reached set point to increase throughput, this temperature ramping approach decreases interfacial stress between the wafer and photoresist. This provides better adherence to the silicon wafer and decreases the chance of delamination during development.

After soft bake, the wafer is exposed using the mask for the bead trap layer using an exposure dose. Vacuum hard contact mode and exposure energy of 45 milliJoules per centimeter squared (mJ/cm^2) is used, representing a 40% decrease in the dose recommended by the manufacturer. This reduced dose decreases diffraction and thus improves photolithographic resolution[9].

Post-exposure bake is performed using the same temperature ramping approach as the soft bake, baking for 3 and 5 minutes at 65°C and 95°C, respectively. The wafer is allowed to cool on the hot plate for 1 hour. Development is performed using SU-8 developer for 1 minute with gentle manual agitation. Harsh agitation leads to delamination of the features due to the decreased exposure dose. The wafer is then thoroughly rinsed in IPA to remove and residual developer and soluble SU-8 and dried with filtered compressed air. The wafer is examined under a metallurgical microscope to ensure sufficient development. Since the wafer was initially underexposed, it is flood exposed followed by a hard bake in a convection oven at 150°C for 20 minutes. This improves the mechanical integrity of the photoresist and prevents features from failing during subsequent molding steps. It is important to note that in our experience the exposure dose may need to be altered to produce good results. We believe this is due to the fact that temperature and humidity of our cleanroom is not tightly controlled. If the features delaminate during development or if resolution is poor, the dose should be increased or decreased, respectively.

Fluidic Layer Step 2: Valve Seat Fabrication

The valve seat layer is fabricated next. These features are located directly above the pneumatic channels and are crucial for the proper functioning of the pneumatic valves. First introduced by Unger et al., pneumatic valves have been demonstrated to be a robust method to control fluid flow in microchannels[10]. Since their inception, they have been used in a large number of microfluidic devices[11-12] making them the most popular on-chip valving technique[13]. The

valves function by taking advantage of the elastomeric properties of (poly)dimethylsiloxane (PDMS), the most common polymeric material used in the fabrication of microfluidic devices[14-15]. The valves are constructed using two microchannels separated by a thin membrane of PDMS. A schematic of these valves is shown in Figure 4.2, where the top layer contains the fluidic channels while the bottom layer consists of the pneumatic channels. These can be constructed in the reverse manner, but the actuation pressure of the valves is reduced if the control channel is on the bottom[16]. When pressure is applied to the pneumatic channel, the PDMS membrane separating the two layers expands and moves into the fluidic channel, stopping fluid flow and creating a valve.

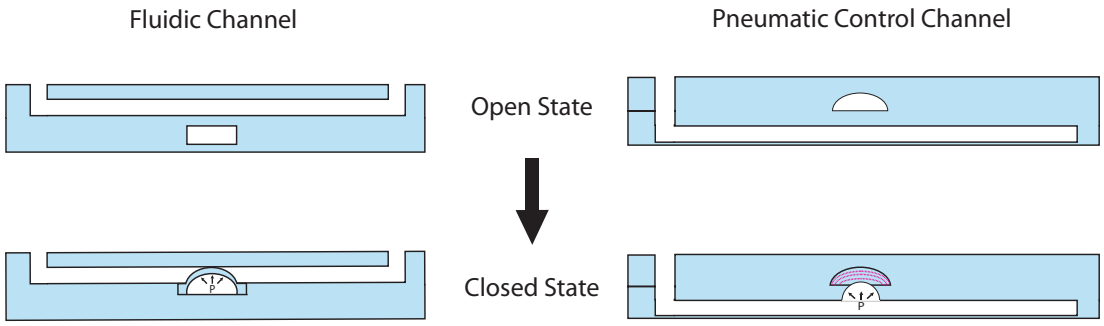

Figure 4.2: Pneumatic valve operating principle.

The pneumatic control channel is the bottom layer, and fluidic channel is the top layer. Upon pressurization of the control channels, the PDMS membrane separating the two channels expands upwards, restricting fluid flow in the fluidic channel

The caveat is that the fluidic channel must be rounded where the flow is to be halted. Otherwise, the valve will not close completely as the deflected

membrane is parabolic in shape and can not conform to the corners of the channel[17]. SU-8 is not suitable for this purpose, as it results in very straight sidewalls and rectangular channel profiles[18]. Therefore, AZ9260 is used, a positive photoresist that can be processed to obtain rounded channel profiles[19].

Protocol:

The wafer with the bead traps patterned is removed from the convection oven and coated with 30 μm of AZ9260. The layer is deposited in two separate steps. The photoresist is spun onto the wafer at 1500 rpm for 30 seconds with an acceleration of 10,000 rpm/sec. It is then immediately baked on a 110°C hotplate for 3:15 minutes. It is then removed from the hotplate, allowed to cool briefly, and a second layer is deposited using the same spin settings. Edge bead removal is performed using a cotton swab dipped in acetone and then baked on a 110°C hotplate for 3:15 minutes. The wafer is left at room temperature for at least 90 minutes in order to rehydrate the photoresist, as recommended by the manufacturer.

Once rehydrated, the wafer is aligned and exposed. An exposure dose of 1,650 mJ/cm^2 is used. However, such a high dose administered at once would cause nitrogen gas, which is released during exposure of this photoresist, to become trapped in the resin creating bubbles[20]. Therefore, the exposure dose is dispensed in 33 doses of 50 mJ/cm^2, with 10 seconds in between doses to allow for the dissipation of the nitrogen gas and cooling of the silicon wafer. Following exposure, the wafer is immediately developed in AZ400K developer (1:4 dilution) with heavy agitation for 8 minutes or until the wafer completely clears. Five

minutes into development, the developer solution is changed to remove soluble photoresist from the developer bath. The wafer is then thoroughly rinsed with deionized (DI) water. After air-drying, the wafer is baked above the glass transition temperature of the photoresist, rounding the channels[19]. This step is performed on a programmable hotplate to control the rate of the heating and cooling. The wafer is placed on a hot plate at room temperature, heats to 190°C at a rate of 10°C/hr, bakes at 190°C for 4 hours, and is cooled back to room temperature at a rate of 10°C/hr. This changes the channel profile from rectangular to round, allowing for complete valve closure. The change in cross-section was confirmed using a Dektek Profilometer, and the results are shown in Figure 4.3.

Before Reflow

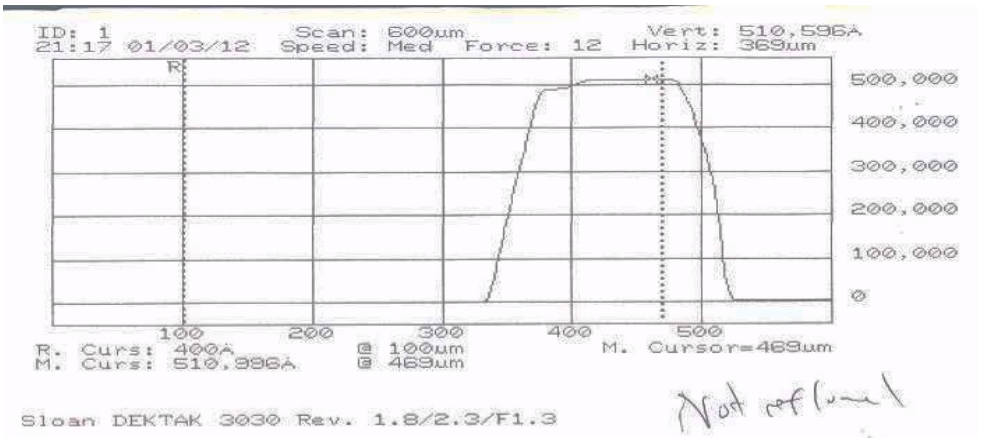

After Reflow

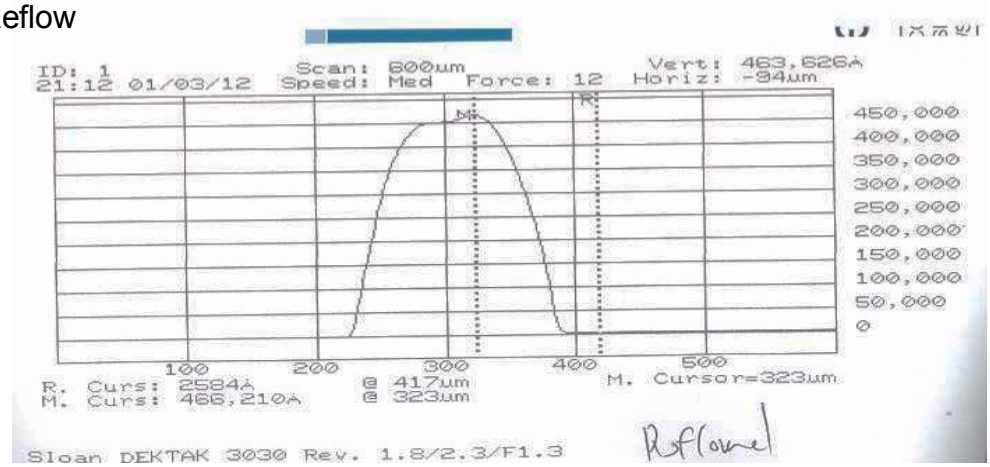

Figure 4.3: Effect of reflow on channel cross section

Comparison of cross-sections of channels fabricated using AZ9260 before (top) and after (bottom) reflow at 190C for 4 hours. Heating the resist above the glass transition temperature caused reflow and rounding of the channel wall.

Fluidic Layer Step 3: Fluidic Network Fabrication

The third step is the fluidic network, which contains the channels, sample inlets, common inlet, outlet, and bead bed regions. This step does not require high resolution and is therefore processed using the manufacturer's recommended protocol. This procedure is very straightforward.

Protocol:

The wafer with the first two layers already patterned is dehydrated for 20 minutes at 150°C in a convection oven. The wafer is coated with a 41 μm layer of SU-8 by spinning SU-8 2025 at 2000 rpm for 30 seconds with an acceleration of 300 rpm/second. The wafer is then soft baked at 65°C for 3 minutes followed by 95°C for 7 minutes. Exposure is performed using soft contact mode and a dose of 160 mJ/cm^2. Post-exposure bake is then performed at 65°C for 2 minutes followed by 95°C for 7 minutes. The wafer is developed for 6:30 minutes under heavy agitation, rinsed with IPA, and blow-dried using filtered compressed air. A final hard bake is performed 150°C for 20 minutes to complete the fabrication of the fluidic silicon mold.

Pneumatic Layer

The pneumatic, or control layer, is fabricated on a separate silicon wafer. This mold contains the pneumatic channels, which are pressurized during device operation causing the expansion of the membrane between the two layers and shutting off fluid flow. The purpose of this layer is shown in Figure 4.2.

Protocol:

A silicon wafer is first cleaned by a rinse and subsequent 10-minute soak in acetone, isopropanol (IPA), and water, in that order. The wafer is dried using filtered compressed air, then dehydrated in a convection oven at 150°C for at

least 20 minutes. This layer is then fabricated using the same procedure as the fluidic layer.

Mold Reproduction In Polyurethane

Typical microfluidic device fabrication processes use silicon wafers with patterned photoresist as molds for soft lithography[21]. This is a very simple and straightforward method for making devices, given the photolithography protocol used to fabricate the molds is fast and/or easy to carry out. However, with multilayer photolithography protocols the time required to make a silicon mold can be quite lengthy. The protocol presented above takes approximately a week to complete. This is caused by the additional processing time required by the temperature ramping, AZ9260 photoresist rehydration, and reflow steps. In addition, each attempt at high-resolution photolithography may not yield adequate features. Furthermore, errors in alignment during multilayer photolithography could ruin molds containing one or more successfully fabricated layers, causing the entire procedure to be repeated. While a successfully patterned wafer can be re-used for multiple moldings, its lifetime is finite. The interface between the silicon and the SU-8 can fail during repeated molding, and the wafer itself can crack during normal handling. Since a wafer failure could delay experiments a week or more, we sought a solution to extend the life of our silicon wafers. This would allow us to decrease the amount of time spent performing photolithography and increase experimentation.

A method originally described by Desai et al. allows for the reproduction of silicon wafers using hard plastics. Conventional soft lithography is used to create

a negative PDMS replica, with the features on the surface of the silicon wafer embedded into the PDMS surface. This is then used as a mold to make a negative polyurethane replica of the PDMS, with the features raised on the polyurethane surface identical to those on the silicon wafer, albeit with insignificant shrinkage[21]. This extends the life of the wafer because each PDMS replica is not used to make a single device, but instead creates a polyurethane mold than can then be used for many moldings. In fact, we found that the polyurethane molds have a longer life than silicon wafers. This is perhaps due to the absence of an interface between two materials, i.e. a monolithic polyurethane mold versus a silicon wafer with photoresist features adhered to the surface. In addition, polyurethane is very inexpensive compared to photolithography reagents, including photoresists, silicon wafers, and developer solutions.

Protocol:

We adapted the published method to our needs and equipment. First, the silicon wafer patterned using photolithography is treated to prevent sticking of the PDMS to the surface and facilitate mold release. The wafer is place in a vacuum desiccator and 5 µL of Trichloro(1H,1H,2H,2H-perfluorooctyl)silane (referred to as silane for the rest of this chapter) is dropped onto a glass slide adjacent to the wafer. Vacuum is applied, and the surface of the wafer is exposed to the silane vapors for 20 minutes. The wafer is then place in polystyrene petri dish, PDMS is prepared at a 10:1 of pre-polymer to curing agent, is poured onto the wafer, degassed in a vacuum desiccator for 30 minutes, and cured at 65°C for at least 4

hours. The cured PDMS is cut and removed from the wafer, which can be repeatedly used for molding until failure.

A thin layer of PDMS is coated on an empty petri dish. Before curing, the PDMS replica is placed onto the uncured PDMS with the features facing upwards. Bubbles are removed from underneath the replica using gentle pressure and the dish is cured at 65°C for 4 hours. This bonds the replica to the PDMS coated petri dish surface, which prevents the polyurethane from irreversibly bonding to the polystyrene. The assembly is then exposed to silane vapors overnight as described above. This prevents sticking of the polyurethane to the PDMS.

The polyurethane (Smooth-Cast 325 Colormatch, Smooth-On, Easton, PA) is then prepared for molding. The polymer is purchased in two parts that are mixed together at equal volumes. Once mixed, the pot life is 2.5 minutes and cure time is 10 minutes, not allowing for long working times. In addition, mixing the two parts together introduces bubbles, which will be trapped in the polymer bulk upon curing. Therefore, the polymer parts are measured and then degassed for 30 minutes. The two parts are then mixed, immediately poured over the mold, and placed in the vacuum chamber of the plasma generator. The vacuum pump is then used to decrease the chamber pressure and extract the air from the polyurethane. After 15-30 seconds under vacuum, the vacuum is released and the petri dish is removed. It is allowed to cure on a flat surface until no longer fluid, and then baked at 65°C overnight to harden the polyurethane. To remove the polyurethane from the PDMS, a band saw is used to cut around

the mold to remove the sides of the petri dish. The PDMS can then be easily removed from the hardened polyurethane by gentle prying with tweezers. Feature replication is ensured by light microscopy, and the mold is then exposed to silane vapor for 20 minutes prior to use for soft lithography.

Multilayer Soft Lithography

In our experience, soft lithography techniques are well established, robust, and straightforward when making single layer devices that do not need to withstand high pressures. Bonding can be done using either corona discharge[22] or oxygen plasma treatment[23] to obtain acceptable results. However, the device developed in this thesis required a 2-layer device able to withstand high pressures up to 45 pounds per square inch (psi) necessary to facilitate complete valve closure. In literature, the common solution to this problem is to perform bonding by varying the curing agent ratios of the PDMS layers. Two PDMS formulations are prepared, one with excess and one deficient in curing agent. The PDMS deficient in curing agent is spin coated on the pneumatic wafer. The PDMS with excess curing agent is poured thick (4-5 mm) on the fluidic layer. The thick layer is then removed from the mold, aligned to the pneumatic layer, and brought into contact. The assembly is then baked and the excess curing agent diffuses from the fluidic to the pneumatic layer, causing the interface to bond[11, 24-25].

While this method has used in several reports, we were not have able to achieve acceptable results bonding with this technique. Perhaps we did not sufficiently optimize our process. Nonetheless, we decided to use a simpler

method with which we were more familiar. We utilized both plasma oxidation and corona discharge methods which have both been characterized[26], providing a good starting point for our optimization.

Another issue we ran into was the rupture of the pneumatic valves. We found that with the 32-channel device, a small rip in the PDMS membrane between the pneumatic and fluidic layer would often appear upon initial pressurization of the pneumatic channel. The defect prohibits pressure to build up in the channels and causes cross-layer leakage, rendering the device useless. While the problem of membrane tearing has not been formally addressed, the relationship between the valve parameters and the required closing pressure has been previously studied and mathematic models have even been developed[17, 27]. Therefore, we utilized the known effects of the length, width, height, and Young's modulus of the PDMS membrane to minimize the chance of membrane rupture.

To remedy this issue, four actions were taken. First, the pneumatic layer was redesigned. In the 8-channel device, the control channel closest to the sample inlets is a straight line emanating from the pneumatic inlet. In this configuration, the valves are essentially in series. The layer was redesigned for our 32-channel device so that each pair of valve seats is connected to the pneumatic inlet in parallel. In theory, this should greatly reduce channel resistance and in effect the pressure required to initially prime the channels[7]. Second, the valve seats were fabricated at a height of 30 μm instead of the 45 μm height used in the 8-channel device. This should reduce the closing pressure

of the valve 70%, which is proportional height of the channel cubed[27]. Third, the protocol for curing the PDMS on the control layer was standardized. Typically, PDMS is mixed and then cured at 65°C for at least 4 hours. However, the Young's modulus increases significantly as the PDMS cures, almost doubling in 2 days[28]. This makes the material stiffer, increasing the requiring closing pressure[27] and in turn increasing the propensity to tearing. Finally, we varied the thickness of the PDMS membrane to find a compromise between high closing pressures and an increased risk of membrane tearing. The optimized process parameters are outlined in the protocol.

Protocol:

A polyurethane mold is used for the fluidic layer, and a silicon mold is used for the control layer. Both molds are exposed to silane vapors for 20 minutes prior to use to prevent PDMS sticking to the molds. PDMS was prepared at a 10:1 prepolymer to curing agent ratio and mixed for at least 2 minutes using a transfer pipette inserted into the chuck of a drill press (bulb side facing down). The transfer pipette is used as a mixing apparatus because it can be discarded after a single use. PDMS is then poured into the polyurethane mold 4-5 mm thick. The poured molds and the remaining PDMS are degassed for 30 minutes. The duration of this step is kept consistent to ensure reproducible viscosity of the uncured PDMS in order to produce consistent spin coated thicknesses. The polyurethane molds are removed from the desiccator and cured at 65°C for at least 4 hours. Since this layer does not contain the PDMS membranes, this cure time does not need to be tightly controlled. PDMS

is then poured and manually spread on the pneumatic channel molds by gently tilting the wafer. The wafer is then spun at 500 rpm for 15 seconds to ensure full coverage of the wafer, and then held at 1000 rpm for 30 seconds to generate the desired PDMS thickness. Spin coated molds are then cured for 3 hours. This curing time is kept constant from to avoid membrane rupture. The cured molds are kept at room temperature until bonding.

Once the fluidic (thick) layer is cured, it is removed from the polyurethane mold and punched. The punch diameter is crucial to device operation. The common inlet and outlet are punched using a 0.75 mm diameter Harris Uni-Core biopsy punch. A good seal between the device and the microbore tubing avoids leaking at the ports. The sample inlets are punched with a 1.2 mm diameter Harris Uni-Core biopsy punch. We found that this diameter punch is ideal for inserting pipette tips, ensuring a good seal and preventing the introduction of bubbles into the device. The punched devices are cleaned with scotch tape, cut to size using a razor blade, and sonicated in acetone using a bath sonicator for 15 minutes. This step removes PDMS debris in the channels and ports that can be introduced during punching. The devices are rinsed with fresh acetone followed by IPA and air dried with filtered compressed air. The cleaned devices are placed in a petri dish, features facing upwards, and further dried at 65°C overnight to remove any residual solvent dissolved in the PDMS[29].

The cured control layer, still on the pneumatic mold, and a cleaned fluidic layer are then exposure to oxygen plasma at a pressure of 700 milliTorr (mTorr) for 60 seconds at a power of 100 Watts (W). Both layers are removed from the

chamber, manually aligned under a stereomicroscope, and placed into contact. The assembly is immediately baked on a hotplate at 95°C for 5 minutes to complete the bond. The bonded assembly is then cut gently around its edges with a razor blade and removed from the control layer mold. The pneumatic inlets are punched using a 0.75 mm diameter Harris Uni-Core biopsy punch. A good seal at these inlets is critical in allowing the pressure to be transferred into the pneumatic channels. The punched device is then cleaned with scotch tape. A pre-cleaned 3-inch by 1-inch glass slide and the device are then treated with corona discharge equipped with a 4.5 inch T-tip electrode (Electro-Technic Products 12121). The electrode is passed over both the device and glass slide 4 times, the surfaces are placed into contact, and light pressure is applied to remove any bubbles trapped between the glass and PDMS. Since the PDMS is porous, entrapped bubbles move into the PDMS bulk and allow conformal contact between the glass and PDMS. The complete device is heated at 95°C for 30 minutes to complete the bond. We found that this cure time is absolutely necessary to create a bond with sufficient strength to withstand pressurization of the pneumatic channels. Fabricated devices can then be stored at room temperate in a petri dish until they are ready for use.

Device Operation

Bio-Plex Pro immunoassay reagents including cytokine standards, Luminex microbeads conjugated to antibodies specific to rat IL-6, TNF-α, IL-13, IL-1β, IL-10, and MCP-1, the respective biotinylated detection antibodies, streptavidin-phycoerytrin, assay buffer, and wash buffer are used in this protocol

(Bio-Rad Laboratories, Hercules, CA). Assay buffer and wash buffer are filtered using a 0.2 μm syringe filter prior to use.

Protocol:

The day prior to experimentation, devices are submerged in reverse osmosis purified water at a resistivity of at least 18 MegaOhms (MΩ) in a petri dish. The devices are placed in a vacuum desiccator overnight to fully prime the channels. Due to the complex architecture of the fluidic network and the dead end channels in the control layer, it is very difficult to remove all the air by simply flowing fluid in the device. In addition, high pressures are required to displace the air out of the pneumatic channels into the PDMS bulk, which we found often results in delamination of the PDMS from the glass slide.

The experimental setup is shown in Figure 4.4. The primed device is mounted onto a microscope stage equipped with an insert for glass slides. A solution of phosphate buffered saline, pH 7.4 (PBS), is prepared with a few drops of food coloring for easy visualization in the device. The solution is loaded into a 1 mL syringe fitted with a 30 gauge beveled needle inserted into tygon microbore tubing (0.01 inch inner diameter, 0.03 inch outer diameter). The needle, syringe, and tubing are primed until all bubbles have been expelled and blue PBS is present at the end of the tubing. This procedure is used to load syringes for solution introduction into the device for the remainder of the protocol. A compressed air tank with a regulator set to 60 psi is connected to a downstream precision air regulator (McMaster-Carr part number 616K22). The precision air regulator is connected to a downstream manifold equipped with male Leur-Lock

fittings with a 3-way valve located directly upstream of the fittings. The tubing is inserted into the pneumatic inlet of the device and the needle is removed from the syringe. The needle is then screwed onto a manifold attached to a pressure source. With this setup, the pressure to each Luer-Lock fitting can be turned on or off. When the valves are closed, the valve is turned so air pressurizes the blue PBS in the tubing into the downstream pneumatic channel. When the valves are opened, the 3-way vale is turned so the tubing is exposed to atmospheric pressure, releasing the pressure in the channel.

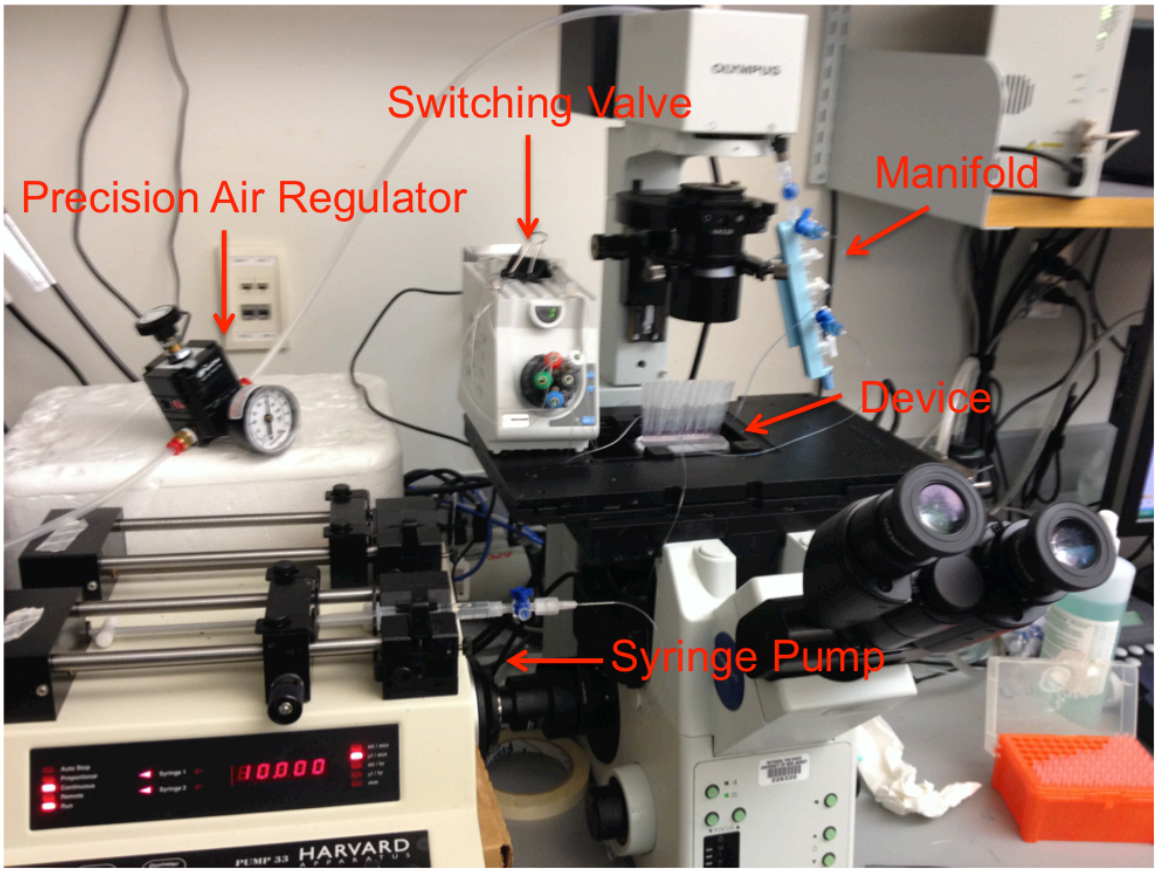

Figure 4.4: Experimental Setup.

The device is mounted on the microscope slide. The precision air regulator is connected to an upstream compressed air tank (not shown) and downstream

manifold, which transfers pressure into the pneumatic channels. The outlet of the switching valve is connected to the inlet of the device. The syringe pump is used to provide positive pressure through the switching valve and negative pressure applied to the device outlet to pull fluid from the sample inlets

The precision air regulator is set to the lowest possible setting (<5 psi) and the valve is closed to test the mechanical integrity of the pneumatic channel. The pressure is gradually increased to 35 psi while observing the valve seat using bright field microscopy. The valve is then quickly opened and closed. If no blue PBS leaks from the pneumatic to fluidic channels and the valves visually actuate, the channel is deemed to be functional. This process is repeated for the second set of pneumatic channels.

Next, the function of the valves is tested. A solution of 0.7 μm red fluorescent polystyrene beads are diluted 1:1000 in 0.5% bovine serum albumin in PBS (BSA). The diluted bead solution is then further diluted 1:100 in Bio-Plex Assay Buffer. The solution is loaded into a syringe, connected to the device outlet via microbore tubing, and flowed at 10 μL/min using a syringe pump. The particles are observed flowing through the channels using a using an Olympus IX81 inverted microscope equipped with a XM10 digital camera, an automated stage, an EXFO X-Cite 120 fluorescent light source, an RFP filter cube, and Olympus cellSens Dimension software. The pneumatic channels are pressurized, and the function of each individual valve is confirmed at the valve seat. Prior to proceeding with the experiment, no fluorescent particles should be

seen flowing through the valve seat. If flow is observed, the pressure is increased at the precision air regulator until the valve shuts. If the valve cannot be closed, the device is discarded.

Once the valve function has been confirmed, assay buffer flows at 40 µL/min through the outlet for 10 minutes. This removes fluorescent particles from the device and blocks non-specific binding to the channel walls. Meanwhile, a switching valve connected to microbore tubing is prepared. The common outlet of the switching valve and 4 inlets are connected to fittings equipped with NanoTight™ Tubing Sleeves (840 µm ID, Idex item number F-247)F and microbore tubing. Assay buffer is connected to the outlet and flowed through each inlet to remove any bubbles. The outlet of the switching valve is then connected to the inlet of the device and assay buffer is connected to inlet 1 of the switching valve. The syringe connected to the microbore tubing inserted to the device outlet is replaced with a 3-way valve. A 3 mL syringe containing 1 mL of water is connected to one Leur-Lock fitting, and the other fitting is left open to the atmosphere. The valve is set so the device is connected to the atmosphere, and assay buffer is flowed through the device inlet at 10 µL/min.

The bead solution is prepared by diluting 20 µL of each bead stock (20X) into 560 µL of assay buffer and loaded into a syringe connected to inlet 2 of the switching valve. Pneumatic valve 1 is closed and beads are flowed at 40 µL/min for 5 minutes in order to pack the bead beds. Wash buffer is loaded into a 3 mL syringe and connected to inlet 1 of the switching valve. Wash buffer is flowed at 40 µL/min for 5 minutes to further pack the bead bed and ensure all beads are in

the traps. Samples and standard are then prepared with a 1:10^5 dilution of 0.7 μm tracer particles. Pneumatic valve 2 is then closed and pipette tips containing each standard or sample is inserted into the sample ports. With this valve closed, fluid is prohibited from mixing between adjacent channels and must flow from the sample inlet over the packed bed of beads located directly downstream. The 3 mL syringe connected to the 3-way valve connected to the device outlet is then mounted on the syringe pump with the valve still set so the device is connected to the atmosphere. Both pneumatic valves are closed, and the syringe pump withdraws at 10 μL/min. The 3-way valve is turned so the device is connected to the 3 mL syringe, pneumatic valve 1 is then opened, and flow continues until tracer particles can be observed flowing into all 32 channels over the bead beds from the sample inlets. The withdrawal flow rate is then reduced to 500 nL/min, corresponding to a flow rate of 15.6 nL/min/channel, and allowed to flow for 4.5 hours, which was determined in our previous study to provide an assay sensitivity of 358 fM for IL-6[30]. Under these conditions, 4.2 μL of sample is consumed per channel. At the conclusion of the sample incubation, the 3-way valve is turned so the device is connected to the atmosphere, pneumatic valve 2 is opened, pneumatic valve 1 closed, and the beads are washed at 40 μL/min for 5 minutes.

Secondary antibody solution is prepared by diluting 25 μL of each stock (20X) secondary antibody solution into 350 μL of detection antibody diluent. The solution is loaded into a syringe and connected to inlet 3 of the switching valve. Secondary antibodies are flowed at 1.6 μL/min for 30 minutes, followed by a

wash at 40 µL/min for 5 minutes. Streptavidin-phycoerythrin is prepared by diluting 5 µL of 100X stock solution into 495 µL of assay buffer, loaded into a syringe, and connected to inlet 4 of the switching valve. Streptavidin-phycoerythrin is flowed at 1.6 µL/min for 10 minutes, and the beads are washed at 40 µL/min for 5 minutes. At the completion of the assay, new pipette tips are inserted into the sample ports, pneumatic valve 2 is closed, and 3 mL of wash buffer is flowed manually through the outlet to collect the beads. The beads are then transferred to a vacuum filter 96-well plate included with the immunoassay kit. The plate is placed on the vacuum wash manifold at and set to pressure of -1 inches of mercury (inHg) to remove the wash buffer. The beads are resuspended in 100 µL of assay buffer, triturating upon each buffer addition. The plate is sealed and agitated on a plate shaker set at the highest speed for 10 minutes. The plate is then transferred to a Bio-Plex 200 system equipped with Bio-Plex Manager 5.0 (Bio-Rad, Hercules CA).

References

1. Madou, M. J., *Fundamentals of microfabrication: the science of miniaturization*. CRC: 2002.
2. Dunbar, S. A., Applications of LuminexÆ xMAP(TM) technology for rapid, high-throughput multiplexed nucleic acid detection. *Clinica Chimica Acta* **2006,** *363* (1-2), 71-82.
3. Houser, B., Bio-Rad's Bio-Plex(R) suspension array system, xMAP technology overview. *Archives of physiology and biochemistry* **2012,** *118* (4), 192-6.
4. Derveaux, S.; Stubbe, B. G.; Braeckmans, K.; Roelant, C.; Sato, K.; Demeester, J.; Smedt, S. C., Synergism between particle-based multiplexing and microfluidics technologies may bring diagnostics closer to the patient. *Anal. Bioanal. Chem.* **2008,** *391* (7), 2453-2467.
5. Bird, R. B.; Stewart, W. E.; Lightfoot, E. N., *Transport phenomena*. Wiley: 2006.
6. Andersson, H.; van der Wijngaart, W.; Stemme, G., Micromachined filter-chamber array with passive valves for biochemical assays on beads. *Electrophoresis* **2001,** *22* (2), 249-257.

7. Oh, K. W.; Lee, K.; Ahn, B.; Furlani, E. P., Design of pressure-driven microfluidic networks using electric circuit analogy. *Lab Chip* **2012,** *12* (3), 515-545.
8. Ling, Z. G.; Lian, K.; Jian, L. In *Improved patterning quality of SU-8 microstructures by optimizing the exposure parameters*, Microlithography 2000, International Society for Optics and Photonics: 2000; pp 1019-1027.
9. Chan-Park, M. B.; Zhang, J.; Yan, Y.; Yue, C., Fabrication of large SU-8 mold with high aspect ratio microchannels by UV exposure dose reduction. *Sensors and Actuators B: Chemical* **2004,** *101* (1), 175-182.
10. Unger, M. A.; Chou, H.-P.; Thorsen, T.; Scherer, A.; Quake, S. R., Monolithic Microfabricated Valves and Pumps by Multilayer Soft Lithography. *Science* **2000,** *288* (5463), 113-116.
11. Hong, J. W.; Studer, V.; Hang, G.; Anderson, W. F.; Quake, S. R., A nanoliter-scale nucleic acid processor with parallel architecture. *Nature Biotechnology* **2004,** *22* (4), 435-439.
12. Diercks, A.; Ozinsky, A.; Hansen, C.; Spotts, J.; Rodriguez, D.; Aderem, A., A microfluidic device for multiplexed protein detection in nano-liter volumes. *Analytical Biochemistry* **2009,** *386* (1), 30-35.
13. Au, A. K.; Lai, H.; Utela, B. R.; Folch, A., Microvalves and micropumps for biomems. *Micromachines* **2011,** *2* (2), 179-220.
14. Xia, Y. N.; Whitesides, G. M., Soft lithography. *Annu. Rev. Mater. Sci.* **1998,** *28*, 153-184.
15. McDonald, J. C.; Whitesides, G. M., Poly(dimethylsiloxane) as a Material for Fabricating Microfluidic Devices. *Accounts of Chemical Research* **2002,** *35* (7), 491-499.
16. Kartalov, E.; Zhong, J.; Scherer, A.; Quake, S.; Taylor, C.; French Anderson, W., High-throughput multi-antigen microfluidic fluorescence immunoassays. *BioTechniques* **2006,** *40* (1), 85-90.
17. Studer, V.; Hang, G.; Pandolfi, A.; Ortiz, M.; French Anderson, W.; Quake, S. R., Scaling properties of a low-actuation pressure microfluidic valve. *Journal of applied physics* **2004,** *95* (1), 393-398.
18. Kuo, S. M.; Lin, C. H., The fabrication of non-spherical microlens arrays utilizing a novel SU-8 stamping method. *Journal of Micromechanics and Microengineering* **2008,** *18* (12), 125012.
19. Fordyce, P. M.; Diaz-Botia, C.; DeRisi, J. L.; Gomez-Sjoberg, R., Systematic characterization of feature dimensions and closing pressures for microfluidic valves produced via photoresist reflow. *Lab Chip* **2012,** *12*, 4287-4295.
20. Mick, J.; Gombert, A.; Blasi, B.; Muller, C. In *Maskless origination of microstructures with optical functions on large areas*, Microlithography 2005, International Society for Optics and Photonics: 2005; pp 1003-1014.
21. Duffy, D. C.; McDonald, J. C.; Schueller, O. J.; Whitesides, G. M., Rapid prototyping of microfluidic systems in poly (dimethylsiloxane). *Anal. Chem.* **1998,** *70* (23), 4974-4984.

22. Eddings, M. A.; Johnson, M. A.; Gale, B. K., Determining the optimal PDMS–PDMS bonding technique for microfluidic devices. *Journal of Micromechanics and Microengineering* **2008,** *18* (6), 067001.
23. Qin, D.; Xia, Y.; Whitesides, G. M., Soft lithography for micro-and nanoscale patterning. *Nature protocols* **2010,** *5* (3), 491-502.
24. Li, N.; Hsu, C. H.; Folch, A., Parallel mixing of photolithographically defined nanoliter volumes using elastomeric microvalve arrays. *Electrophoresis* **2005,** *26* (19), 3758-3764.
25. Berg, J.; Anderson, R.; Anaya, M.; Lahlouh, B.; Holtz, M.; Dallas, T., A two-stage discrete peristaltic micropump. *Sensors and Actuators A: Physical* **2003,** *104* (1), 6-10.
26. Bhattacharya, S.; Datta, A.; Berg, J. M.; Gangopadhyay, S., Studies on surface wettability of poly (dimethyl) siloxane (PDMS) and glass under oxygen-plasma treatment and correlation with bond strength. *Microelectromechanical Systems, Journal of* **2005,** *14* (3), 590-597.
27. Kartalov, E. P.; Scherer, A.; Quake, S. R.; Taylor, C. R.; Anderson, W. F., Experimentally validated quantitative linear model for the device physics of elastomeric microfluidic valves. *Journal of applied physics* **2007,** *101* (6), 064505-064505-4.
28. Eddington, D. T.; Crone, W. C.; Beebe, D. J. In *Development of process protocols to fine tune polydimethylsiloxane material properties*, 7th International Conference on Miniaturized Chemical and Biochemical Analysis Systems, Squaw Valley, California, USA, 2003; pp 1089-1092.
29. Lee, J. N.; Park, C.; Whitesides, G. M., Solvent compatibility of poly (dimethylsiloxane)-based microfluidic devices. *Anal. Chem.* **2003,** *75* (23), 6544-6554.
30. Ghodbane, M.; Kulesa, A.; Yu, H. H.; Maguire, T.; Schloss, R.; Ramachandran, R.; Zahn, J. D.; Yarmush, M. L., Development of a low-volume, highly sensitive microimmunoassay using computational fluid dynamics-driven multiobjective optimization. *Microfluid. Nanofluid.* **2014,** *In Press*.

Chapter 5: Dissertation Conclusions

Summary of Findings

The immunoassay is a highly sensitive and specific assay that can be used to measure a variety of analytes including proteins, small molecules, and viruses. Its excellent performance and versatility has led to widespread use in the clinic and research[1] with a global market estimated at $7.7 Billion[2]. However, limitations include long assay times, a laborious procedure, the need for highly trained operators, the high cost of reagents, and a sample requirement of 50-100 µL. In addition, only one sample can be measured per assay. This limitation further increases the cost, sample consumption, and effort required to measure multiple analytes. The demand for measuring several analytes in a sample, such as in biomarker studies[3], has prompted the development of multiplex immunoassays. A popular platform was developed by Luminex, which can theoretically quantify 100 proteins in a single sample[3-4]. However, multiplex immunoassays have the same drawbacks as standard immunoassays, with an even higher cost.

Over the last 10-15 years, several microfluidic immunoassays have been developed[5-7]. Studies have demonstrated the ability of the microscale to reduce sample and reagent consumption as well as assay time[8-9]. In addition, microfluidics is amendable to automation, which can alleviate the labor involved in performing assays, improve reproducibility, and decrease inter-assay variability[10-11]. More recently, microfluidic immunoassays have been developed

with multiplexing capabilities. However, these assays all have at least one limitation including high sample requirement, low sensitivity, small dynamic range, the requirement for specially synthesized reagents, the inability to easily change the analyte specificity, the inability to generate quantitative data, and/or low sample throughput[12-22].

Due to the limitations of previous microfluidic immunoassay technologies, no single approach is appropriate for general use in *in vitro, in vivo,* and clinical applications. Therefore, the goal of this dissertation was to develop a microfluidic multiplexing immunoassay device overcoming these limitations with the following specifications:

1. Low sample consumption (< 5 μL)
2. High sensitivity (fM)
3. Large Dynamic Range (3 orders of magnitude)
4. The ability to easily change the analytes being measured using a single device design
5. The ability to perform assays using commercially available reagents
6. The ability to produce quantitative data
7. The ability to process multiple samples simultaneously (i.e. parallel processing)

To accomplish these goals, we first designed an 8-channel device capable performing immunoassays using Luminex multiplexing antibody conjugated microbeads. Utilizing these reagents allows for analyte specificity to be easily changed using a single device design while benefiting from the demonstrated

advantages of bead based microfluidic immunoassays[8-9, 23-25]. We then developed a fabrication procedure consisting of multilayer photolithography[26], polyurethane mold reproduction[27], and multilayer soft lithography techniques[28]. Our next goal was to optimize the assay parameters to minimize the necessary sample volume. In lieu of costly, time consuming empirical optimization that may not lead to optimal parameters, we chose to complete this objective *in silico*. We developed a computational fluid dynamics (CFD) model of fluid flow, analyte diffusion, and antibody-antigen binding in a packed bed. The computational model was experimentally validated and used in conjunction with multi-objective optimization and design of experiments (DOE) techniques to minimize the sample volume and incubation time required to perform the assay. The optimized parameters were applied to an IL-6 immunoassay using Luminex multiplexing reagents. In this work, we demonstrated an assay with a sensitivity of 358 fM using only 1.35 µL of sample with an incubation time of 4.5 hours[29].

The first part of this dissertation demonstrated low sample consumption, high sensitivity, the ability to use commercially available reagents, and the ability to change the analyte specificity of the assay. However, the design criteria of parallel processing, generation of quantitative data, and a large dynamic range had yet to be achieved. In addition, to this point multiplexing was not performed on-chip. Therefore, the device design was expanded from 8 to 32 channels. Furthermore, the sample incubation step was converted from positive pressure to negative pressure driven flow. This eliminated the need to load samples into syringes, which results in a huge amount of volume being used to expel bubbles

(100+ μL). In addition, driving parallel flows using a single pressure source does not limit the sample capacity of the device to the number of available syringe pumps. Small volumes could now be loaded into pipette tips placed directly into sample inlets. The negative pressure applied to the outlet would then simultaneously pull all 32 samples over the downstream bead beds. Moreover, this approach can be scaled far beyond the sample capacity demonstrated in this work. Unfortunately, with our syringe pump we were not able to consistently generate flows using negative pressure less than 15.6 nL/min/channel. Therefore, the assays required 4.2 μL of sample instead of the 1.35 μL used in our proof-of-concept studies.

With the expanded device we multiplexed 6 analytes, IL-1b, IL-6, IL-10, IL-13, MCP-1, and TNF-a. The larger sample capacity also allowed for duplicate measurements to be performed, investigating the variability and limit of detection of the assay. The device was shown to generate high quality standard curves and have a high sensitivity. Furthermore, the quantification accuracy of the device was tested by measuring spiked samples of known concentrations, the approach used by the pharmaceutical industry to validate immunoassays[30]. A comparison of the expected and measured concentrations of the spiked samples demonstrated the quantification ability and large dynamic range of the device. A summary of the design criteria and specifications of the device are shown in Table 5.1.

Design Criteria	Device Specification
Low sample consumption (< 5 µL)	~4.2 µL used with negative pressure Demonstrated volumes as low as 1.35 µL
High sensitivity (fM)	MCP-1: 387 fM Il-b: 1211 fM Il-6: 151 fM Il-13: 963 fM IL-10: 5726 fM TNF-a: 92 fM
Large Dynamic Range (3 orders of magnitude)	MCP-1: 3.56 Il-b: 2.66 Il-6: 2.96 Il-13: 1.95 IL-10: 1.93 TNF-a: 2.36 (Values are in orders of magnitude)
The ability to easily change analytes using a single device design	Analyte specificity changed by simply using different antibody coated microbeads
The ability to perform assays using commercially available reagents.	Utilized commercially available Luminex microbeads and reagents. Multiple species and applications available
The ability to produce quantitative data	Demonstrated accuracy using spiked samples across entire range of assay and compared results to standard benchtop immunoassay
The ability to process multiple samples (i.e. parallel processing)	32 simultaneous samples with demonstrated scalability with only 2 pneumatic valves

Table 5.1: Comparison of device design criteria and demonstrated specifications

With all of our design criteria satisfied, we demonstrated the utility of the device in an *in vitro* culture system. A co-culture system of rat hippocampal slices and alginate encapsulated MSC was stimulated with lippolysaccahirde (LPS) to induce an immune response and cytokine secretion. The culture supernatants were harvested, aliquotted, and analyzed in parallel using the device and a commercially available Luminex multiplex immunoassay. A strong

agreement between the data obtained from the two assay formats was demonstrated, and immunomodulation by the MSC on the hippocampal slices was observed. Therefore, the device can be used as a screening tool using only 4.2 µL of sample volume compared to 50 µL required using conventional immunoassay techniques.

Several applications could benefit from an assay with the demonstrated specifications of the device presented in this thesis. First, temporal profiles could be generated using *in vitro* culture systems from individual wells. In addition, culture systems could be scaled down from 96 to 384 or even 1536 well plates, whose working volume is smaller than the sample size required for conventional analysis. Therefore, significant cost savings are provided from the reduced cost of the assay as well as the significant reduction in the cells, media, and experimental stimuli required in a given experimental system.

In vivo applications also exist in animal studies aiming to analyze scarce fluids. These include the study of cerebrospinal fluid (CSF) and synovial fluid in rodent models. Experiments using these animal models are low-cost, avoid ethical concerns of using larger mammals, allow for highly controlled experiments, and are well established. However, the small available volume of CSF and synovial fluid in rodents has impeded their study. Therefore, the device presented in this dissertation could be used to analyze these limited fluids, aiding in biomarker discovery and drug development studies for SCI[31-32], Parkinson's disease[33-34], Alzheimer's disease[35], rheumatoid arthritis[36], and osteoarthritis[37-39].

This device could also provide benefits in a clinical setting. First, the decreased reagent consumption compared to conventional methods could significantly decrease the cost of diagnostic procedures. In addition, low yielding samples that are difficult to obtain could be analyzed, such as CSF from pediatric and neonatal patients[40]. Finally, the ability to measure panels of proteins in a high-throughput manner at a low cost is very well suited for biomarker discovery studies[41]. Thus, the characteristics of this device enable its use in far-reaching *in vitro, in vivo,* and clinical applications.

Limitations

While the device developed in this dissertation possesses the aforementioned advantages, it also has its associated drawbacks. First, the incubation time for this assay is 4.5 hours, which may not be appropriate in certain situations. While it has been previously reported in microfluidic literature that incubation time is reduced, this was not the case in our system. This is due to the extremely low concentrations used in this study. Previous reports performing fast assays using much higher concentrations (ug/mL[9] or ng/mL[42] vs. pg/mL in our studies). At low concentrations, binding becomes increasingly reaction limited as demonstrated by our dimensionless number analysis in Chapter 2 explaining this long assay time. Regardless, this technology would not be conducive for real time monitoring in surgical settings. Other the devices have been developed for this purpose at the expense of sample consumption and parallel assay capability[43-44]. From our modeling studies, we learned that a trade-off exists between assay sensitivity and incubation time due to antibody antigen binding kinetics. We

found that decreasing the assay sensitivity from 358 fM to 1.79 pM decreases the incubation time from 4.5 hours to less than an hour[29]. However, assay time was not a priority in this dissertation and therefore a short incubation time was sacrificed in order to achieve the highest possible sensitivity. Alternatively, using a signal amplification technique such as rolling circle amplification [45], or using brighter fluorescent probes such as quantum dots [46] could reduce incubation time by reducing the number of bound molecules needed to reach the detection limit.

Another limitation of this device is that auxiliary equipment is needed, including syringe pumps, a pressure source for pneumatic valves, and a Bio-Plex analyzer or flow cytometer. This would prevent this device from being used in resource-limited settings or in the field for environmental monitoring purposes. While previous devices for these purposes exist, none have been demonstrated with the limit of detection shown here[47].

Furthermore, this device requires the beads to be removed from the device prior to interrogation. This additional assay step could be avoided by on-chip detection. Previous devices utilizing Luminex beads have been developed performing analysis both on-chip and off-chip. Off-chip detection preserves the dynamic range and sensitivity of the Luminex reagents[12]. Conversely, optical detection on-chip results in a greatly reduced dynamic range[20]. Therefore, we chose to collect the beads and interrogate them off-chip. One possible way to avoid this issue would be to integrate the beads within the device with microfluidic flow cytometer[48-49]. However, this would require the packed beds of beads to be released and focused into the detection region individually. While

this is possible, the resulting device design would be much more complicated and the footprint would be much larger.

Future Directions

This dissertation describes a proof-of-concept low-volume microfluidic multiplex immunoassay. However, several aspects of the device and operating procedure would need to be further optimized prior in order to transform this technology into a feasible commercial device. First, the fabrication procedure would need to be improved. While fabricating devices using PDMS is useful for rapid prototyping[50], it creates several issues. First, the process is very time consuming and relatively low throughput. Each inlet has to be punched manually, requiring 36 punches per device. This process introduces debris into the inlet, and a slight punch misalignment of only a few microns creates pressure difference between channels resulting in uneven flow rates. In addition, alignment of the pneumatic layer to the fluidic channels is performed manually under a stereomicroscope. Only one device can be aligned at a time, and misalignment results in a non-functional device. In addition, PDMS is a relatively expensive polymer and soft lithography is not a scalable manufacturing process. To make the device commercially viable, fabrication would need to be performed by injection molding using hard plastics. This approach would greatly reduce the cost of each device, improve throughput, and decrease variability[51]. We also believe that device-to-device variability is responsible for much of the variance in our data, which could be reduced with uniform devices. However, the resolution of the bead traps is an obstacle that must be overcome in order to use injection

molding. In addition, the pneumatic valves could no longer be used since the plastic would be a rigid thermoplastic and not a flexible elastomer. Thus, the device would have to be slightly redesigned while maintaining the assay parameters and operating principles.

Second, only the sample incubation step was optimized in our modeling study. The secondary antibody and streptavidin-phycoerythrin incubations were performed for the same duration as the benchtop assay. It is possible that optimizing the flow rate and incubation time of these steps could decrease the assay time and even improve the sensitivity and dynamic range of the device. However, this would not be trivial to model using our computational platform, and therefore would need to be performed empirically. Furthermore, the manufacturer's recommended standard concentrations were used in these experiments. Since the working range of the microfluidic assay differs from that of the benchtop assay, it may be advantageous to alter the standard concentrations. It would be logical to include more standards in the linear range of the 5-parameter logistic fit[52]. This may increase the quantification accuracy of the device.

Finally, a more precise method of generating fluid flow must be developed. We believe that applying negative pressure to the inlet should still be the approach taken, but the use of a syringe pump to generate the vacuum is not ideal. We demonstrated that only 1.35 μL of sample was required in our 8-channel device; however, these experiments were done using a syringe pump to drive the flow for each sample under positive pressure. Once we began using a

single negative pressure source in our 32-channel device, we were unable to generate consistent flow rates less than 15.6 nl/min/channel. This resulted in an increase of sample consumption to 4.2 µL. Therefore, a pumping method that could consistently generate smaller flow rates is necessary to further reduce the required sample volume.

Our vision for a commercially viable version of this device would be similar to the principle of the Agilent Bioanalyzer 2100 system[53]. The devices would be disposable, produced by injection molding using an inexpensive thermoplastic. Potentially, microbeads specific for the anlaytes of interest could be pre-loaded in the devices and sold as a consumable for the assay platform. A user could simply pipette samples into the sample ports and insert the device into an apparatus containing a pumping mechanism, assay reagents, fluidics, and potentially even optics. The apparatus could be automated to perform all the assay steps, collect and read the beads, and output the experimental results onto a computer. This would provide a fully automated, cheap, low-volume, highly reproducible multiplex immunoassay that could be broadly used in *in vitro, in vivo,* and clinical settings.

References

1. Wild, D., *The immunoassay handbook*. Elsevier Ltd.: San Diego, 2005.
2. Report Reveals Growth Opportunities in the Immunoassay Market. http://www.genengnews.com/gen-news-highlights/report-reveals-growth-opportunities-in-the-immunoassay-market/81243609/?kwrd=In%20Vitro%20Diagnostics.
3. Light, M.; Minor, K. H.; DeWitt, P.; Jasper, K. H.; Davies, S. J. A., Multiplex array proteomics detects increased MMP-8 in CSF after spinal cord injury. *Journal of Neuroinflammation* **2012,** *9* (1), 122.
4. Houser, B., Bio-Rad's Bio-Plex(R) suspension array system, xMAP technology overview. *Archives of physiology and biochemistry* **2012,** *118* (4), 192-6.

5. Ng, A. H. C.; Uddayasankar, U.; Wheeler, A. R., Immunoassays in microfluidic systems. *Anal. Bioanal. Chem.* **2010,** *397* (3), 991-1007.
6. Henares, T. G.; Mizutani, F.; Hisamoto, H., Current development in microfluidic immunosensing chip. *Anal. Chim. Acta* **2008,** *611* (1), 17-30.
7. Kong, J.; Jiang, L.; Su, X.; Qin, J.; Du, Y.; Lin, B., Integrated microfluidic immunoassay for the rapid determination of clenbuterol. *Lab Chip* **2009,** *9* (11), 1541-1547.
8. Sato, K.; Yamanaka, M.; Takahashi, H.; Tokeshi, M.; Kimura, H.; Kitamori, T., Microchip‐based immunoassay system with branching multichannels for simultaneous determination of interferon‐γ. *Electrophoresis* **2002,** *23* (5), 734-739.
9. Sato, K.; Tokeshi, M.; Odake, T.; Kimura, H.; Ooi, T.; Nakao, M.; Kitamori, T., Integration of an immunosorbent assay system: Analysis of secretory human immunoglobulin A on polystyrene beads in a microchip. *Anal. Chem.* **2000,** *72* (6), 1144-1147.
10. Derveaux, S.; Stubbe, B. G.; Braeckmans, K.; Roelant, C.; Sato, K.; Demeester, J.; De Smedt, S. C., Synergism between particle-based multiplexing and microfluidics technologies may bring diagnostics closer to the patient. *Anal. Bioanal. Chem.* **2008,** *391* (7), 2453-2467.
11. Bange, A.; Halsall, H. B.; Heineman, W. R., Microfluidic immunosensor systems. *Biosens. Bioelectron.* **2005,** *20* (12), 2488-2503.
12. Yu, X.; Hartmann, M.; Wang, Q.; Poetz, O.; Schneiderhan-Marra, N.; Stoll, D.; Kazmaier, C.; Joos, T. O., µFBI: A Microfluidic Bead-Based Immunoassay for Multiplexed Detection of Proteins from a µL Sample Volume. *PLoS ONE* **2010,** *5* (10), e13125.
13. White, R. J.; Kallewaard, H. M.; Hsieh, W.; Patterson, A. S.; Kasehagen, J. B.; Cash, K. J.; Uzawa, T.; Soh, H. T.; Plaxco, K. W., Wash-free, electrochemical platform for the quantitative, multiplexed detection of specific antibodies. *Anal. Chem.* **2012,** *84* (2), 1098-1103.
14. Wang, J.; Ahmad, H.; Ma, C.; Shi, Q.; Vermesh, O.; Vermesh, U.; Heath, J., A self-powered, one-step chip for rapid, quantitative and multiplexed detection of proteins from pinpricks of whole blood. *Lab Chip* **2010,** *10* (22), 3157-3162.
15. Stern, E.; Vacic, A.; Rajan, N. K.; Criscione, J. M.; Park, J.; Ilic, B. R.; Mooney, D. J.; Reed, M. A.; Fahmy, T. M., Label-free biomarker detection from whole blood. *Nature nanotechnology* **2009,** *5* (2), 138-142.
16. Qin, L.; Vermesh, O.; Shi, Q.; Heath, J. R., Self-powered microfluidic chips for multiplexed protein assays from whole blood. *Lab Chip* **2009,** *9* (14), 2016-2020.
17. Park, J.; Sunkara, V.; Kim, T.-H.; Hwang, H.; Cho, Y.-K., Lab-on-a-disc for fully integrated multiplex immunoassays. *Anal. Chem.* **2012,** *84* (5), 2133-2140.
18. Garcia-Cordero, J. L.; Nembrini, C.; Stano, A.; Hubbell, J. A.; Maerkl, S. J., A high-throughput nanoimmunoassay chip applied to large-scale vaccine adjuvant screening. *Integrative Biology* **2013,** *5* (4), 650-658.
19. Fan, R.; Vermesh, O.; Srivastava, A.; Yen, B. K. H.; Qin, L.; Ahmad, H.; Kwong, G. A.; Liu, C.-C.; Gould, J.; Hood, L.; Heath, J. R., Integrated barcode

chips for rapid, multiplexed analysis of proteins in microliter quantities of blood. *Nature Biotechnology* **2008,** *26* (12), 1373-1378.
20. Diercks, A.; Ozinsky, A.; Hansen, C.; Spotts, J.; Rodriguez, D.; Aderem, A., A microfluidic device for multiplexed protein detection in nano-liter volumes. *Analytical Biochemistry* **2009,** *386* (1), 30-35.
21. Chin, C. D.; Laksanasopin, T.; Cheung, Y. K.; Steinmiller, D.; Linder, V.; Parsa, H.; Wang, J.; Moore, H.; Rouse, R.; Umviligihozo, G., Microfluidics-based diagnostics of infectious diseases in the developing world. *Nature medicine* **2011,** *17* (8), 1015-1019.
22. Bernard, A.; Michel, B.; Delamarche, E., Micromosaic immunoassays. *Anal. Chem.* **2001,** *73* (1), 8-12.
23. Wilson, R.; Cossins, A. R.; Spiller, D. G., Encoded microcarriers for high-throughput multiplexed detection. *Angew. Chem.-Int. Edit.* **2006,** *45* (37), 6104-6117.
24. Shin, K. S.; Lee, S. W.; Han, K. C.; Kim, S. K.; Yang, E. K.; Park, J. H.; Ju, B. K.; Kang, J. Y.; Kim, T. S., Amplification of fluorescence with packed beads to enhance the sensitivity of miniaturized detection in microfluidic chip. *Biosensors and Bioelectronics* **2007,** *22* (9), 2261-2267.
25. Derveaux, S.; Stubbe, B. G.; Braeckmans, K.; Roelant, C.; Sato, K.; Demeester, J.; Smedt, S. C., Synergism between particle-based multiplexing and microfluidics technologies may bring diagnostics closer to the patient. *Anal. Bioanal. Chem.* **2008,** *391* (7), 2453-2467.
26. Madou, M. J., *Fundamentals of microfabrication: the science of miniaturization*. CRC: 2002.
27. Desai, S. P.; Freeman, D. M.; Voldman, J., Plastic masters—rigid templates for soft lithography. *Lab Chip* **2009,** *9* (11), 1631-1637.
28. Unger, M. A.; Chou, H.-P.; Thorsen, T.; Scherer, A.; Quake, S. R., Monolithic Microfabricated Valves and Pumps by Multilayer Soft Lithography. *Science* **2000,** *288* (5463), 113-116.
29. Ghodbane, M.; Kulesa, A.; Yu, H. H.; Maguire, T.; Schloss, R.; Ramachandran, R.; Zahn, J. D.; Yarmush, M. L., Development of a low-volume, highly sensitive microimmunoassay using computational fluid dynamics-driven multiobjective optimization. *Microfluid. Nanofluid.* **2014,** *In Press*.
30. Valentin, M.-A.; Ma, S.; Zhao, A.; Legay, F.; Avrameas, A., Validation of immunoassay for protein biomarkers: bioanalytical study plan implementation to support pre-clinical and clinical studies. *Journal of pharmaceutical and biomedical analysis* **2011,** *55* (5), 869-877.
31. Stammers, A. T.; Liu, J.; Kwon, B. K., Expression of inflammatory cytokines following acute spinal cord injury in a rodent model. *J Neurosci Res* **2012,** *90* (4), 782-790.
32. Lubieniecka, J. M.; Streijger, F.; Lee, J. H. T.; Stoynov, N.; Liu, J.; Mottus, R.; Pfeifer, T.; Kwon, B. K.; Coorssen, J. R.; Foster, L. J.; Grigliatti, T. A.; Tetzlaff, W., Biomarkers for Severity of Spinal Cord Injury in the Cerebrospinal Fluid of Rats. *PLoS ONE* **2011,** *6* (4), e19247.
33. LeWitt, P., Recent advances in CSF biomarkers for Parkinson's disease. *Parkinsonism & Related Disorders* **2012,** *18*, S49-S51.

34. Eller, M.; Williams, D. R., Biological fluid biomarkers in neurodegenerative parkinsonism. *Nature Reviews Neurology* **2009,** *5* (10), 561-570.
35. Shapiro, J. S.; Stiteler, M.; Wu, G.; Price, E. A.; Simon, A. J.; Sankaranarayanan, S., Cisterna magna cannulated repeated CSF sampling rat model-effects of a gamma-secretase inhibitor on Aβ levels. *Journal of Neuroscience Methods* **2011,** *205*, 36-44.
36. Barton, N. J.; Stevens, D. A.; Hughes, J. P.; Rossi, A. G.; Chessell, I. P.; Reeve, A. J.; McQueen, D. S., Demonstration of a novel technique to quantitatively assess inflammatory mediators and cells in rat knee joints. *J Inflamm (Lond)* **2007,** *4*, 13.
37. Seifer, D. R.; Furman, B. D.; Guilak, F.; Olson, S. A.; Brooks III, S. C.; Kraus, V. B., Novel synovial fluid recovery method allows for quantification of a marker of arthritis in mice. *Osteoarthritis and Cartilage* **2008,** *16* (12), 1532-1538.
38. Knox, P.; Levick, J.; McDonald, J., Synovial fluid-its mass, macromolecular content and pressure in major limb joints of the rabbit. *Experimental Physiology* **1988,** *73* (1), 33-45.
39. Kahle, P.; Saal, J.; Schaudt, K.; Zacher, J.; Fritz, P.; Pawelec, G., Determination of cytokines in synovial fluids: correlation with diagnosis and histomorphological characteristics of synovial tissue. *Annals of the rheumatic diseases* **1992,** *51* (6), 731-734.
40. Phillips, T. M., Rapid analysis of inflammatory cytokines in cerebrospinal fluid using chip-based immunoaffinity electrophoresis. *Electrophoresis* **2004,** *25* (1011), 1652-1659.
41. Shoemaker, L. D.; Achrol, A. S.; Sethu, P.; Steinberg, G. K.; Chang, S. D., Clinical Neuroproteomics and Biomarkers: From Basic Research to Clinical Decision Making. *Neurosurgery* **2012,** *70* (3), 518.
42. Gervais, L.; Delamarche, E., Toward one-step point-of-care immunodiagnostics using capillary-driven microfluidics and PDMS substrates. *Lab Chip* **2009,** *9* (23), 3330-3337.
43. Sasso, L. A.; Undar, A.; Zahn, J. D., Autonomous magnetically actuated continuous flow microimmunofluorocytometry assay. *Microfluid. Nanofluid.* **2010,** *9* (2-3), 253-265.
44. Sasso, L. A.; Johnston, I. H.; Zheng, M.; Gupte, R. K.; Ündar, A.; Zahn, J. D., Automated microfluidic processing platform for multiplexed magnetic bead immunoassays. *Microfluid. Nanofluid.* **2012,** *13* (4), 603-612.
45. Konry, T.; Smolina, I.; Yarmush, J. M.; Irimia, D.; Yarmush, M. L., Ultrasensitive Detection of Low‐Abundance Surface‐Marker Protein Using Isothermal Rolling Circle Amplification in a Microfluidic Nanoliter Platform. *Small* **2011,** *7* (3), 395-400.
46. Medintz, I. L.; Uyeda, H. T.; Goldman, E. R.; Mattoussi, H., Quantum dot bioconjugates for imaging, labelling and sensing. *Nature materials* **2005,** *4* (6), 435-446.
47. Gordon, J.; Michel, G., Discerning trends in multiplex immunoassay technology with potential for resource-limited settings. *Clinical chemistry* **2012,** *58* (4), 690-698.

48. Tung, Y. C.; Zhang, M.; Lin, C. T.; Kurabayashi, K.; Skerlos, S. J., PDMS-based opto-fluidic micro flow cytometer with two-color, multi-angle fluorescence detection capability using PIN photodiodes. *Sens. Actuator B-Chem.* **2004,** *98* (2-3), 356-367.
49. Chung, T. D.; Kim, H. C., Recent advances in miniaturized microfluidic flow cytometry for clinical use. *Electrophoresis* **2007,** *28* (24), 4511-4520.
50. Duffy, D. C.; McDonald, J. C.; Schueller, O. J.; Whitesides, G. M., Rapid prototyping of microfluidic systems in poly (dimethylsiloxane). *Anal. Chem.* **1998,** *70* (23), 4974-4984.
51. Beebe, D. J.; Mensing, G. A.; Walker, G. M., Physics and Applications of Microfluidics in Biology. *Annual Review of Biomedical Engineering* **2002,** *4* (1), 261-286.
52. Gottschalk, P. G.; Dunn, J. R., The five-parameter logistic: a characterization and comparison with the four-parameter logistic. *Analytical biochemistry* **2005,** *343* (1), 54-65.
53. 2100 Bioanalyzer Instruments. http://www.genomics.agilent.com/en/Bioanalyzer-System/2100-Bioanalyzer-Instruments/?cid=AG-PT-106&tabId=AG-PR-1001 (accessed November 5).